University of Texas Rio Grande Valley
ScholarWorks @ UTRGV

Theses and Dissertations

8-1-2024

A Thermo-Mechanical Analysis of the Well-Structure Integrity in Enhanced Geothermal Systems Using Numerical Simulation

John Alfred Ganal Acevedo
The University of Texas Rio Grande Valley

Follow this and additional works at: https://scholarworks.utrgv.edu/etd

 Part of the Civil Engineering Commons

Recommended Citation

Acevedo, John Alfred Ganal, "A Thermo-Mechanical Analysis of the Well-Structure Integrity in Enhanced Geothermal Systems Using Numerical Simulation" (2024). *Theses and Dissertations*. 1554.
https://scholarworks.utrgv.edu/etd/1554

This Thesis is brought to you for free and open access by ScholarWorks @ UTRGV. It has been accepted for inclusion in Theses and Dissertations by an authorized administrator of ScholarWorks @ UTRGV. For more information, please contact justin.white@utrgv.edu, william.flores01@utrgv.edu.

A THERMO-MECHANICAL ANALYSIS OF THE WELL-STRUCTURE INTEGRITY IN ENHANCED GEOTHERMAL SYSTEMS USING NUMERICAL SIMULATION

A Thesis

By

JOHN ALFRED GANAL ACEVEDO

Submitted in partial fulfillment of the

Requirements for the Degree of

MASTER OF SCIENCE

Major Subject: Civil Engineering

The University of Texas Rio Grande Valley

August 2024

A THERMO-MECHANICAL ANALYSIS OF THE WELL-STRUCTURE INTEGRITY IN ENHANCED GEOTHERMAL SYSTEMS USING NUMERICAL SIMULATION

A Thesis

by

JOHN ALFRED GANAL ACEVEDO

COMMITTEE MEMBERS

Dr. Philip Park
Committee Co-chair

Dr. Chu-Lin Cheng
Committee Co-chair

Dr. Jinwoo An
Committee member

August 2024

Copyright 2024 John Alfred Ganal Acevedo

All Rights Reserved

ABSTRACT

Acevedo, John Alfred G., A Thermo-Mechanical Analysis Of The Well-Structure Integrity In Enhanced Geothermal Systems Using Numerical Simulation. Master of Science (MS), August 2024, 96 pp., 68 figures, 6 tables, 92 references.

This thesis will investigate the well structure integrity of enhanced geothermal systems. Enhanced geothermal system is a type of renewable energy generation that utilizes heat from a rock reservoir deep within the Earth's subsurface delivered by circulating working fluids through kilometers-long well structures. However, due to the surrounding environment and harsh operating conditions, the well structures are vulnerable to deterioration and cracking, which can lead to structural failure of wells and reduced energy efficiency. The study seeks to gain a better understanding of the vulnerability of the well structure. A finite element model of a well structure was developed, and heat transfer analysis was conducted. Through the analysis, the stress and strain distributions over the metal pipes and concrete casings were obtained. The results show that stress/strain risers occur at the metal-concrete interface and the corners of the well structure. The findings of this research are expected to contribute to increasing the efficiency of enhanced geothermal systems.

DEDICATION

Thank you to my friends and family who have supported me during the entire duration of my studies. My mom, Elezabel Acevedo, my dad, Mariano Acevedo, my sister, Joanne Acevedo, my friends, Jeremy Domingo, Jeb Cirujales, Trent Pintor, Emily Trevino, Jensine Cabo, Arthur Cabo, Alexa Flores, Paola Garcia, Joshua Ebreo, Joshua Sibala, Jeremiah Gali, Philip Baldado, Lois Baldado, Nate Sacurom, Katrina Sacurom, Ryan Lavilla, Joshua Ebreo, Lara Astom, Hugo Zazueta, Shane (Micah) Dunlap III, Adelina Uy, Ayema Qureshi, Eddie Consulgarcia, Stephen Pagayon, Daniel Gomez, Vladimir Herrera, Hanxing Kuang, and everyone else that I've come across through in my life, I wouldn't have made it this far without you all.

ACKNOWLEDGMENTS

I remain grateful to Dr. Philip Park, the co-chair of my thesis committee, for all his mentoring and advice throughout my research, and for introducing me to Dr. Chu-Lin Cheng, who brought me into this research project. Additionally, I would also like to express my gratitude to Dr. Jinwoo An, my thesis committee member. I am thankful for their contribution and patience during this entire process.

I would also like to thank Arlene Campos and Dr. Jungsook Ho for helping provide a space for me to work in. I would also like to thank Dr. Lianshan Lin and the people of Oak Ridge National Laboratory for their generous hospitality and insights into my research. I would also like to thank the United States Department of Energy and the National Science Foundation for their contributions to the project. I would also like to thank Hugo Zazueta again, for accompanying me during my master's program and research.

TABLE OF CONTENTS

LIST OF FIGURES

LIST OF TABLES

CHAPTER I

INTRODUCTION

Renewable energy, also referred to as clean or green energy, is often used to describe a form of energy that can replenish itself naturally without being depleted within a considerably "short time scale" i.e., solar, wind, hydropower, etc. This is opposed to non-renewable energy sources such as oil and gas, which take longer times to replenish and are also considerably bad for the environment. Typically, Geothermal Energy is often described as thermal energy contained within the Earth's subsurface. The heat in the Earth's subsurface is often generated through geological processes to the point in which the heat is often considered "inexhaustible," and is categorized as a type of renewable energy (Ang et al., 2022; Barbier, 2002; Stober & Bucher, 2013). Nonrenewable forms of energy have been the primary source of power generation, which has caused detrimental effects on the environment due to greenhouse gas emissions. In recent decades, the desire for cleaner energy has become prominent, however, due to initial costs and limited accessibility/availability, renewable energy has yet to become a sustainable and reliable source of energy. As research continues to develop in finding more efficient harvesting methods, the push for finding an easily accessible continues to be the next step in helping the environment.

Background

Enhanced Geothermal Systems (EGS) is a developing renewable energy generation system currently being studied by various countries to find alternative energy sources, It was initially conceptualized in the early 1970s (Potter et al., 1974). While the definition and operating

considerations to classify EGS vary with authors and countries, the majority describe the conventional systems as having a minimum of two wells – injection, and extraction wells

(Breede et al., 2013; Moska et al., 2021; Zarrouk & McLean, 2019; Zhiliang et al., 2018). The well-structures are separated by a desired distance and will run into the subsurface to what is referred to as the Hot Rock Zone/Hot Dry Rock (HRZ) or a Hot Wet Rock (HWR) (Hogarth & Holl, 2017; Moska et al., 2021; Zhiliang et al., 2018). This region is a virtually non-permeable rock material with temperatures typically exceeding 150° C which can be seen 3-to-10 km below the surface. In an HRZ, the heat reservoir is expected to be nearly dry, containing little to no fluids, and in the HWZ fluids can be seen within the target area (Hogarth & Holl, 2017; Zheng et al., 2022; Zhiliang et al., 2018). If there are no pre-existing natural fractures within the rock, a series of fracture processes such as hydro-fracturing or hydro-shearing creates a network that allows the passage of a geothermal fluid (Moska et al., 2021).

Understanding the effects of the external environment acting on EGS would help increase the system's longevity while simultaneously improving the energy harvesting efficiency. EGS is a promising upcoming renewable energy resource that can be implemented almost anywhere around the world with proper understanding. Investigation of the well structure integrity is one step towards that goal.

Research Objectives

This study aims to understand the stress/strain distributions that may cause damage of EGS well-structures through thermo-mechanical numerical simulations considering subsurface material, working geothermal fluid, and the surrounding environment. The specific goals of this research are:

1. To determine locations of stress/strain concentrations throughout the structure
2. The effects of temperature and a thermal gradient on the integrity of the structure
3. The effects of internal working fluid pressure on the integrity of the structure
4. The effects of external earth pressure on the integrity of the structure

Methodology

To accomplish the objectives, a numerical simulation model was developed using a commercial finite element analysis software, ABAQUS. Finite element analysis (FEA) is a type of numerical method that can be used to predict or analyze how an assembly or part will behave under various conditions. ABAQUS was the chosen program due to the software's ability to do a coupled thermodynamic-mechanical analysis while also giving detailed values for the results over time. The model design choices and input parameters were collected from several case studies, research articles, and standard specifications such as the American Petroleum Institute, American Society of Mechanical Engineers, New Zealand Standard Code, NORSOK, and International Standard Organization guidelines, and handbooks published by the U.S. Department of Energy.

CHAPTER II

LITERATURE REVIEW

To gain an understanding of enhanced geothermal systems of where the current knowledge gap is in this state of technology, a comprehensive literature review was conducted. This was accomplished by looking at past and ongoing projects in various countries and looking for any research related to the scope of work. The following section provides a brief explanation of different types of geothermal energy harvesting systems, followed by the system of an EGS structure, including various parameters that affect the overall system. Additionally, a description of some major EGS projects that have been implemented is concluded with a brief summarization of some structural failure occurrences that had occurred for certain EGS projects.

Introduction

As previously mentioned geothermal systems have no consensus on their definition or classification as geothermal systems are complex in their way due to their design, well testing, and environmental conditions (Zarrouk & McLean, 2019). As explained in Laloui and Loria's chapter on Energy and Geotechnologies, geothermal energy is the natural thermal energy within the Earth's subsurface. While the classifications are entirely dependent on the country or author, most shallow geothermal systems have depths of no more than 400 m, with any geothermal systems exceeding that depth being labeled as deep geothermal systems, respectively (Laloui & Rotta Loria, 2020).

Types of Geothermal Energy Harvesting Systems

There are various ways to classify geothermal systems, such as open-loop or closed-loop systems, two-phase systems, shallow or deep, and conventional, or non-conventional systems.

In an open loop, it typically takes advantage of hot or cold groundwater and is pumped into a heat exchanger, which converts the varying temperature into electricity but is subsequently returned to the aquifer it was collected from, in most cases, closed loops which combine the injection and extraction well into one singular well, relying on thermal conduction of the surrounding environment to heat the fluid, eliminating seismic, scaling, and environmental concerns (Budiono et al., 2022; Muela Maya et al., 2018; Yuan et al., 2021).

The primary focus of this paper is on deep/non-conventional geothermal systems, which can also be separated by supercritical or magmatic geothermal systems. The conventional enhanced geothermal systems, are all uniform in the idea that they are exposed to high-pressure and high-temperature (HPHT) environments (Breede et al., 2013; Sakuma et al., 2021). Like shallow geothermal systems, the consensus on where the boundaries are between these classifications is typically at the discretion of the author or country. Most enhanced geothermal systems have a minimum reservoir temperature of 150 or 200 °C, however, any exceeding 400°C typically fall within the supercritical category, similarly the magmatic enhanced geothermal systems typically exceed 400°C and are exposed to or near magma (Kruszewski & Wittig, 2018; Sakuma et al., 2021; Sugama & Pyatina, 2022).

In the Enhanced Geothermal System, the temperature and pressure that the working fluid is exposed to may result in a two-phase flow. The fluid endures a phase change, due to flash

evaporation from the pressure reduction when exposed to a certain temperature, which means that below that flash point, the fluid remains as a liquid, and a vapor when above it (Akbar et al., 2016). Depending on the circumstances they can be considered as steam/vapor-dominated or liquid-dominated hydrothermal systems, in which the extracted fluid is either strictly a vapor or liquid, or a majority of either, which is usually classified at the discretion of how the author interprets the term (Kaya et al., 2011; Verma, 1997).

If the EGS system is connected to a power plant which would convert the heat into electricity, and is typically known to be a binary system (Breede et al., 2013). As neatly summarized by Breede, there is the Organic Rankine Cycle (ORC) and the Kalina Cycle. In an ORC, the low-temperature heat from the reservoir is converted into a form of mechanical energy, which can then be used to produce electrical energy using organic substances, but are mainly applicable to reservoirs with low-to-medium temperatures (90 °C to 150 °C) (Breede et al., 2013; Hijriawan et al., 2019; Madhlopa, 2022). A Kalina Cycle uses a mixture of Ammonia and water as a steam that turns mechanical energy into electricity at a better rate than ORC, however, this mixture tends to be corrosive and harmful to humans (Dincer & Demir, 2018; Madhlopa, 2022).

Enhanced Geothermal System Structure

As previously mentioned, when designing a conventional enhanced geothermal system, a minimum of two wells is required, and since Enhanced Geothermal Systems were initially based on the oil and gas industry, the structure design follows a similar idea, which can be seen in Figure 1. The basic design of the structure can be seen as telescopic, where the diameter of each subsequent casing decreases with depth. The casing consists of a layer of metal casing, which the geofluid goes through, surrounded by a layer of concrete, to act as a layer of insulation to separate

the metal tubing and the geomaterial environment. When it comes to designing the actual structure, it is seen as a "bottom-up" process. The length of the well is determined by the location of the production well (Finger & Blankenship, 2012; Zealand, 2015). However, the profile of the structure is determined by drilling or geological considerations (Finger & Blankenship, 2012; Thórhallsson et al., 2014). The casing program is important in determining the longevity of the structure, where the casing setting depth, number of casing strings, weight, material, connection type, and well-completion details are provided. The casing program serves a multitude of purposes including but not limited to protecting groundwater contamination, prevention of casing deformation, protection of corrosion, detail on access to the reservoir, and deformation prevention (Finger & Blankenship, 2012; Kruszewski & Wittig, 2018; Tayactac & Manuel, 2022; Teodoriu, 2013; Thórhallsson et al., 2014). While the number of casing strings may vary between projects, along with varying thickness and material selection, in each casing program, there is a surface casing, conductor casing, anchor casing, intermediate casing, and production casing, with the additional option of a slotted liner (Finger & Blankenship, 2012). Each casing string, excluding the slotted liner, is cemented from the shoe casing to the surface as a means to prevent corrosion, prevent cross-contamination of fluids, and help control thermal expansion (Finger & Blankenship, 2012; Kruszewski & Wittig, 2018). This can be seen in various projects around the world and is considered standard practice. An additional benefit is the reduced costs in material, as drilling and well construction are a major contributor to cost, and having optimized casing strings can help mitigate excessive costs (Sveinbjornsson & Thorhallsson, 2014).

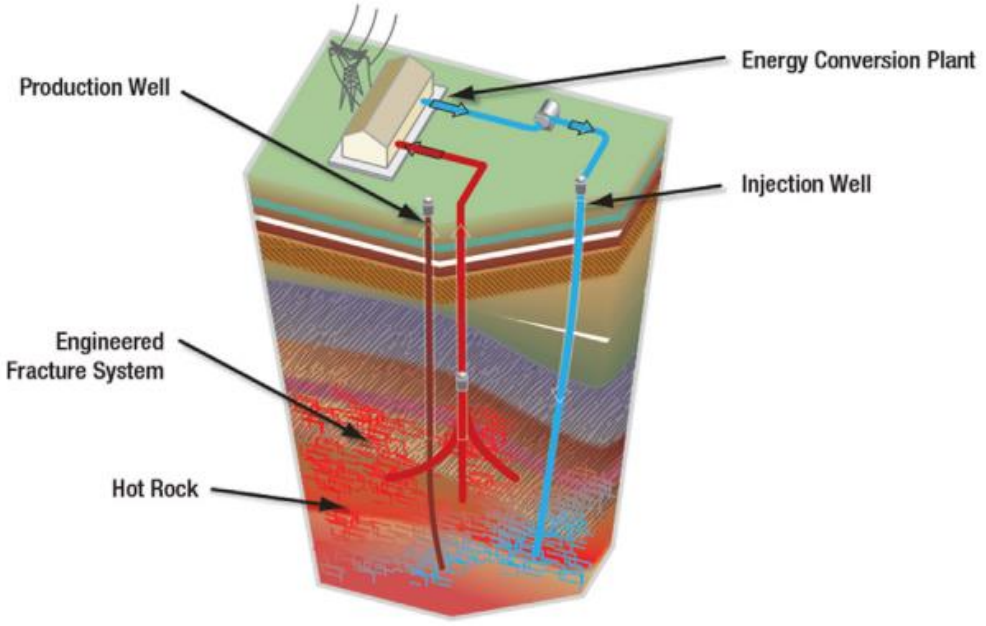

Figure 1: A Concept art of Enhanced Geothermal Systems (Olasolo et al., 2016)

The fracture network creates the pathway connecting the well system, created by either a series of hydro-fracturing or hydro-shearing, against the hot rock zone, following a similar process that is used by the oil and gas industry (Moska et al., 2021). Hydro-fracturing is a process in which new or pre-existing tensile fractures are opened when a fluid is injected at a pressure higher than the minimum principal stress (Gischig & Preisig, 2015; Moska et al., 2021). Hydro-shearing is a process in which water is injected at a moderate pressure below the target area's minimum principal stress, allowing existing fractures to dilate and slip. This process should result in the fracture surfaces remaining propped, and an increased permeability, all without the usage of proppants (Cladouhos et al., 2016; Gischig & Preisig, 2015).

The geothermal fluid depending on the design of the well or environment can be of different such as water, carbon dioxide, or natural brine. In this system, the geothermal fluid, often referred to as the "working fluid," is injected into the injection well deep into the ground, passing

through the HRZ towards the extraction well. The heat gathered from the hot rock reservoir is harvested by the plant, and the fluid is typically re-injected into the system (Breede et al., 2013; Moska et al., 2021; Olasolo et al., 2016; Zheng et al., 2021; Zhiliang et al., 2018).

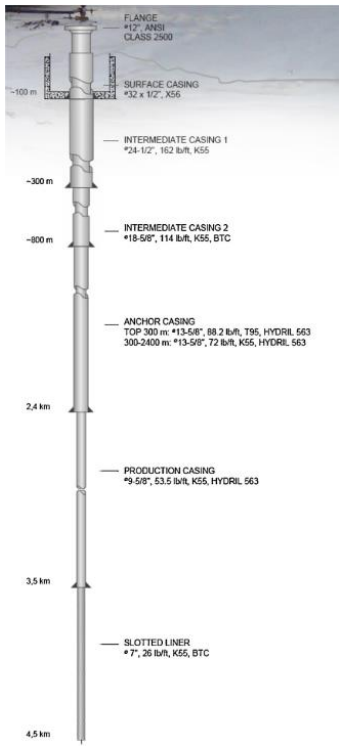

Figure 2: Original Schematic Design of IDDP-1 (Pálsson et al., 2014)

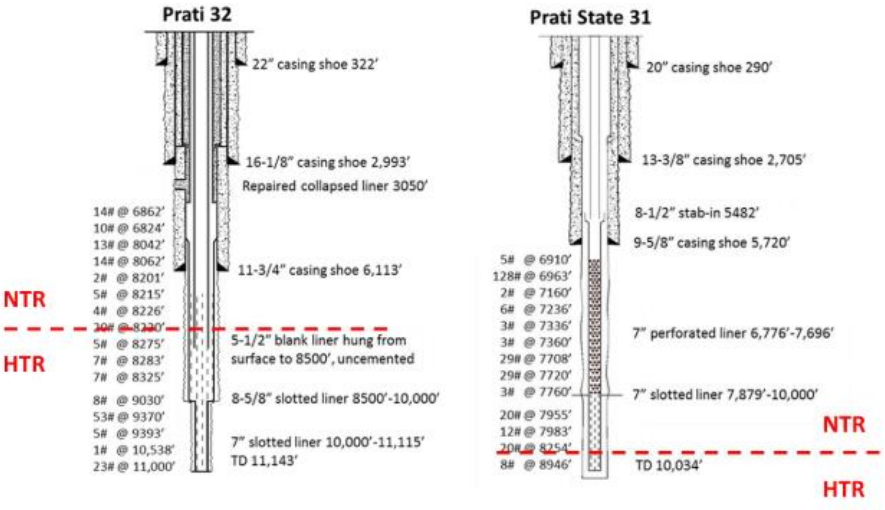

Figure 3: Not-to-scale schematic of the Geysers EGS well PS-32 and PS-31 (Hartline et al., 2019)

Enhanced Geothermal Projects

With a better understanding of the Enhanced Geothermal System, a comprehensive study of previous and ongoing projects was conducted to gain a better understanding of the progress made, and current gaps of knowledge that are currently being or need to be investigated.

Northwestern Geysers Project

The Northwestern Geysers EGS Project, located near Middletown, California was a demonstration project to determine the feasibility of a deep high-temperature reservoir (HTR). This demonstration project was funded by the US Department of Energy Geothermal Technology Office, the Calpine Geysers Power Company in a collaborative effort in conjunction with Lawrence Berkeley National Laboratory. Originally, the demonstration area was part of a steam field, operating from 1988 to 1996, but was abandoned in 2000 until it was reopened and deepened in 2010. With a temperature gradient of 182 °C/km, this geothermal project site had both a high-temperature reservoir (HTR) measuring roughly 400 °C, and a normal temperature reservoir (NTR) of approximately 240 °C (Garcia et al., 2016; Hartline et al., 2019; Rutqvist et al., 2016). The goal of the project was to determine if the HTR permeability could be stimulated by fracture reactivation if water was injected into the zone at a low flow rate and pressure. Additionally, since the geothermal field had previously been known to have corrosive hydrogen chloride gasses and some non-compressible gasses that were also responsible for the cease of production well drilling in the 1980s, the intention was to re-open and re-complete two wells, Prati State 31 & Prati 32 (PS-31 & PS-32 respectively), where Prati 32 will serve as the injection well with the latter serving as the extraction. Eventually, a third well was reopened Prati 25 (PS-25) to serve as a monitoring well for steam production. The entirety of the demonstration was separated into three separate

phases: pre-stimulation, reservoir stimulation, and the long-term data collection, monitoring, and reporting phase. With a low-rate injection of around 400 gpm, the reactivation of existing fractures had shown an increased presence of micro-seismic activities since the start of the demonstration project but had also shown that the fracture zones, which were thought to be random, are subdivided into intersecting zones that will continue to increase the reservoir volume. The project was a success as the resulting geological models and simulations seemed to have lined up with the data that was gathered during the eight years of service.

Desert Peaks Project

The Desert Peaks EGS Project, located in the Desert Peaks geothermal field in Nevada, was initially started in 2002, and was in operation between 2010-2013, intending to establish a 2-5 MW EGS stand-alone binary power plant (Benato et al., 2016; Zemach et al., 2013; Zeng et al., 2013). Well 27-15 initially started drilling and reached a depth of 1771 m but was plugged at approximately 1067 m in 2010 to do "shallow" stimulation testing. In 2012, the well was reopened to its original depth of 1771 m, where the well from 914 m to 1771 m was an "open hole" (Zemach et al., 2013). The project was able to produce 9-13 MW of power with an average of about 10 MW of energy (Benato et al., 2016; Zemach et al., 2013).

Brady Hot Springs Project

The Brady Hot Springs Geothermal Project is located in Brady's geothermal field in Churchill County, Nevada, near the previously mentioned Desert Peaks geothermal project, which sought to improve the permeability of an already existing non-productive well (Akerley et al., 2019). Well 15-12 has been active since 1992 and has an approximate reservoir temperature of 175°C-205°C with a combined flash and binary power plant. The Brady Hot Springs project followed a similar simulation plan to Desert Peaks due to their success on the previously mentioned project. It was considered a success in its own respective right producing roughly 2-3 MWe in enhancing the fracture network but had been less than what was expected (Akerley et al., 2019; Liu, 2020).

Newberry Volcano Project

The Newberry Volcano EGS Project is a United States feasibility project, located in central Oregon. The geothermal site had been investigated and explored since the 1970s but was eventually chosen as a site to demonstrate EGS technologies in 2010. Following the completion of the well 55-29, initial well simulations began in 2012, but had been halted temporarily due to problems with the casing. In 2014, the well had undergone re-simulation allowing a significant amount of rock stimulation where both the permeability and volume of the reservoir were successfully enhanced. The project was separated into three separate phases but never made it to phase three due to funding by the DOE ending in 2015 (Cladouhos et al., 2016).

Icelandic Deep Drilling Project

The Icelandic Deep Drilling Project is a series of research and development projects to determine the economic feasibility of implementing enhanced geothermal systems at supercritical conditions, which have reservoirs that exceed 400°C (Stefánsson et al., 2021). Separated into three separate projects, the first of which, IDDP-1, is located at the Krafla geothermal field in Iceland. This project was initiated in 2008 and was intentionally designed to go approximately 4-5 km deep into the subsurface, however, during the drilling program the design of the project was readjusted when indications of magma at a depth of 2096 m below the surface (Kaldal et al., 2016; Pálsson et al., 2014). After the readjustments were made to the well structure, rather than doing the simulations in the reservoir initially intended, the simulations were conducted above the encountered rhyolitic magmatic chamber, making it the first magma-EGS project in the world. Despite the project never being connected to the power grid, the expected power generation was nearly 36 Mw of electricity, the project had frequent temporary shut-ins for repairs but later had to be abandoned due to the master valve malfunction after two years of operation (Axelsson et al., 2014; Friðleifsson et al., 2021; Kaldal et al., 2016).

Following the conclusion of the first well in the Icelandic Deep Drilling Project, the second well project followed shortly after. Contrary to the first well, IDDP-2 was accepted as part of the MEET H2020 Project DEEPEGS (Deployment of Deep Enhanced Geothermal Systems for Sustainable Energy Business) which started drilling in 2016 and was completed in 2017 (Lamy-Chappuis et al., 2023; Stefánsson et al., 2021). Located in Reykjanes geothermal field in Iceland, rather than drilling a new well, an old well (RN-15) was reopened and deepened reaching around 4659 m with temperatures exceeding 500 °C (Friðleifsson et al., 2020; Friðleifsson et al., 2021; Lamy-Chappuis et al., 2023; Stefánsson et al., 2021). The project was successful in showing that

it was possible to drill into supercritical geothermal reservoirs, however, in terms of production rates, it was difficult to express whether or not it produced significant flow rates for energy production (Lamy-Chappuis et al., 2023).

At the time that this paper is being written, IDDP-3 is currently in the planning phase to drill at the Hellisheidi geothermal field, to the author's knowledge, but one goal is to test various metal alloys with this new well (Friðleifsson et al., 2020; Friðleifsson et al., 2021; MacDonald & Grauman, 2019).

Deep Heat Mining - Basel Project

As part of the Deep Heat Mining Project located near Basel, Switzerland, construction of a deep enhanced geothermal reservoir was attempted in 2006. With the injection well reaching approximately 5 km beneath the surface, after a few days in simulation, the project was temporarily halted when an event magnitude of 2.6 was detected. Officially, no temperature was measured for the reservoir, to the author's knowledge, but approximate temperatures were given near the bottom of the well of 200°C (Liu, 2020; Stober et al., 2022). Shortly after the injection fluid was temporarily shut off, a 3.4-magnitude earthquake occurred in the surrounding area. After this event, three more earthquakes that had a magnitude exceeding three were detected within the next month and a half (Häring et al., 2008; Stober et al., 2022). The project was then suspended again until the project was officially shut down in 2009 after concerns of inducing more earthquakes (Häring et al., 2008).

Soults-sous-Forêts Project

The Soults-sous- Forêts project, located in the Upper Rhine Graben (URG) in France, near the Germany-France border, with the main goal to reopen and enhance the natural permeability of pre-existing fractures of the crystalline basement and was part of the MEET H2020 Project that wanted to improve geothermal energy development in Europe (Baujard et al., 2021; Koelbel & Genter, 2017; Ledésert et al., 2021). The geothermal site is known to have a large heat harvesting potential with a thermal gradient potential of 100°C/km due to the convection loops throughout the region (Baujard et al., 2021). The project initially began in 1984, where drilling started in 1987 with frequent circulation and stimulation tests and observations until 2007, when crystalline rock and the natural fracture system became the focus, but would slowly transition from a research facility to producing commercial electricity from an Organic Rankine Cycle in 2016 (Baujard et al., 2021). There are three wells in operation each with a depth exceeding 5 km, named GPK-3 and GPK-4 for the injection wells, and GPK-2 serves as the extraction well (Baujard et al., 2021; Ledésert et al., 2021). A notable finding was allowing the reinjection of the fluid from 70°C to 40°C to allow a high energy production, at the cost of an increased scaling phenomenon, requesting further inspection on the influence of microparameters (Ledésert et al., 2021).

Groß Schönebeck Project

The Groß Schönebeck located on the Upper Rhine Graben (URG) in the North German Basin which started in 2001, was the first in-situ geothermal laboratory to improve technology to enhance the permeability using different hydraulic fracturing methods (Blöcher et al., 2016; Breede et al., 2013; Frick et al., 2011; Moska et al., 2021). The first well, GrSk 3/90, was originally completed in 1990 as a gas exploration well but was reopened and deepened to approximately

4309 m in 2000, with an initial reservoir temperature of approximately 149°C (Blöcher et al., 2016; Frick et al., 2011; Huenges et al., 2007; Moska et al., 2021). In 2006, the production well was drilled reaching a depth of approximately 4400 m (Blöcher et al., 2016; Frick et al., 2011). Various methods were used to improve the hydraulic performance in the reservoir which did improve initially, but the productivity index showed a non-linear decrease over 2 years between 2011 to 2013 possibly due to the presence of scaling or mineral clogging, compartmentalization of the hydraulic fluid in the fracture, two-phase flow, the sustainability of induced fractures (Blöcher et al., 2016).

Habanero Pilot Project

The Habanero Pilot Project, located in the Cooper Basin on top of the Habenero fault in Australia was the first EGS project in the country to generate power. Initially started in 2000, the first well, Habanero 1, was drilled in 2003 with an approximate depth of 4300 m towards a bed of Innamincka granite, followed by five other wells over the next 11 years (Hogarth & Holl, 2017). Initially, Habanero 1 was going to be connected to Habanero 3 when designing the pilot binary, single-flash power plant, however, Habanero 3 had suffered a blowout, resulting in the well being cemented and sealed. This resulted in redesigning Habanero 4 before it was drilled in 2012. With an approximate reservoir temperature of 200°C, Habanero 1 would serve as the injection well, and Habanero 4, as the extraction well (Hogarth & Holl, 2017; Mills & Humphreys, 2013). While the project was successful in generating electricity, the project was unable to satisfy economic measures and had to be abandoned (Hogarth & Holl, 2017).

Kakkonda Project

Serving as part of the New Energy and Industrial Technology Development Organization, NEDO, this project was located in the Kakkonda geothermal field in Japan in the early 1990s. WD-1 was part of the resources survey that started in 1994, passing the Kakkonda granite at a depth of 2860 m, and reaching a total depth of approximately 3729 m in 1995. However, when drilling below 3600 m, a high content of H_2S, a dangerous corrosive gas, had returned with the drilling mud, which was one of the primary reasons that the drilling operations stopped along with difficulty in drilling further (Ikeuchi et al., 1998; Kasai et al., 2000). Although temperatures had exceeded 300°C, there were no productive fractures available that could be used to produce a geothermal plant for electricity(Ikeuchi et al., 1998; Kasai et al., 2000; Suzuki et al., 2022). However, proposed future projects, such as the Japan Beyond-Brittle Project, hope to use the experience gained to produce electricity from supercritical/ultra-high-temperature geothermal reservoirs in the future (Muraoka et al., 2014; Suzuki et al., 2022).

After analyzing existing projects, it was noted that each project was unique due to the subsurface conditions. Below in Table 1 is information regarding the target reservoir and subsurface profile and properties that could be found in the public domain to summarize one of the various ways in which certain EGS projects differed from one another.

Table 1: EGS projects and their subsurface profile properties

Project	Subsurface Profile	Reservoir Rock Type	Thermal Gradient	Approximate Reservoir Temperature
The Geysers[1]	Cap Rock Graywacke Hornfels Felsite	Hornfels	182°C/km	275°C
Desert Peaks[2]	Basalt Rhyolite tuffs Basaltic dikes Rhyolite flows Altered tuff Hem mudst Calc mudst Metatuff+Dolomudst Shale Diorite Phyllite Hornfels Hornblend diabase	Altered Tuff, Hem mudst, Hornblend Diabase	N/A	220°C
Deep Heat Mining Project – Basel[3]	Oligocene Sannoisian Malm Dogger Liassic Keuper Muschelkalk Buntsst Rotliegend Crystalline Basement	Crystalline Basement	4.1°C/100m (Sedimentary Section) 2.7°C/100m (Crystalline basement)	190°C
Soults-sous-Forêts[4]	Sedimentary cover Poryphic granite Highly fractured granite High biotite content granite Two-mica granite	Poryphic Granite, Two-mica granite	90°C/km (0-1400 m depth) 30°C/km (1400 m-onwards)	180-210°C
Habanero Project[5]	Sedimentary Innamincka granite	Innamincka Granite	31°C/km	248.5
Icelandic Deep Drilling Project – I[6]	N/A	Rhyolitic Melt Magmatic Chamber	100°C/km	~340°C
Icelandic Deep Drilling Project – II[7]	Quartz Epidote Actinolite	Sheeted Dike Complex	250°C/km (0-1 km depth) 15°C/km (3 km–onwards)	>500°C
Groß Schönebeck[8]	Hannover Formation Elebe Alternatinf Sequence Elbe Base Sandstone Havel Doundation Volcanic Rocks	Volcanic Rock	N/A	149°C

1. (Garcia et al., 2016; Hartline et al., 2019; Rutqvist et al., 2016)
2. (Lutz et al., 2009; Zemach et al., 2013; Zeng et al., 2013)
3. (Häring et al., 2008; Stober et al., 2022)
4. (Baujard et al., 2021; Ledésert et al., 2021; Zeng et al., 2013)
5. (Xu et al., 2016)
6. (Axelsson et al., 2014; Thórhallsson et al., 2014)
7. (Lamy-Chappuis et al., 2023; Stefánsson et al., 2021)
8. (Moska et al., 2021)

Materials for Enhanced Geothermal Systems

In the following section, information gathered on the various materials used in the industry, or recommendations given based on research or physical simulation is provided.

Metal Casing

In geothermal wells, each casing contains a metal casing and a cement sheath. For a long time, most standards, such as the NZS 2403:2015, had given recommendations on the material selection of the metal casing, however, it only had recommendation selections to services up to 350 °C, and as seen in the previous sections, some EGS projects have reservoir temperatures that exceed that value, and with no established international standard on EGS well design, the selection of materials have been through experience on previous projects (Kruszewski & Wittig, 2018; Zealand, 2015).

Since geothermal well design originated from the oil and gas industry, the material selection is also based on the same idea, mainly in using carbon steel alloys from the API 5CT (Casing and Tubing) or API 5L (Lining) Standards, but still require some level of corrosion resistance, which is also noted in other standards such as NACE MR1075/ISO 15156 (API, 2018, 2019; Carter & Cramer, 1992; Finger & Blankenship, 2012; Wood, 2017). Carbon steel alloys are alloys with a composition of mostly iron and carbon, with low-carbon steels containing up to 0.25% by weight of carbon. Typically the higher the Carbon content, the higher the strength, and low-carbon steels, having more ferrite, have relatively low strength and high formability(Krauss, 2017). However, using Carbon steels has shown, that when exposed to geothermal brine, corrosion has led to low serviceability and relatively short service life (Karlsdottir et al., 2015; Thorbjornsson et al., 2020; Wood, 2017). When exposed to corrosion, carbon steel is likely to experience failure,

but due to its low cost and ease of availability, the alloy is often used with corrosion-resistant materials as a coating to help mitigate the issue (Gruben et al., 2021; Karlsdottir et al., 2015; MacDonald & Grauman, 2018).

As a result, various other alloys are currently being investigated as alternatives, such as stainless steel, nickel-based alloys, and titanium which offer more corrosion resistance than carbon steel alloys (Carter & Cramer, 1992; Gruben et al., 2021; MacDonald & Grauman, 2018, 2019). Titanium alloys, are mainly limited by their availably and cost but offer the most corrosion resistance, and while papers from Thomas (2003), have shown that is a promising material, along with Nickel alloys that were able to maintain strength at elevated temperatures better than Carbon steels, and should be looked into more in further research efforts (Gruben et al., 2021; Karlsdottir et al., 2015; MacDonald & Grauman, 2018, 2019).

Cement Sheath

A growing concern for the longevity of the geothermal system has been the strength and durability of the well. The conventional material used in well construction is typically a Class G Cement with some additives such as silica flour, and various other materials depending on the subsurface environment (Silva & Milestone, 2018b). Class G cement is one of the six different cement classes created by the American Petroleum Institute (API) in the early 1950s for specific usage in well cement. While in most projects it is common to refer to the American Society for Testing Methods (ASTM) and their eight types of cement types, it was determined the ASTM standards were considered insufficient in the oil and gas industry and needed to be expanded upon since the conditions of the environment were considered too different (Calvert & Smith, 1990). Of those six cements, it should be noted that classes A through C are most similar in composition to

Types I through III from ASTM standards (Wolterbeek & Hangx, 2023). The API which was the first committee, developed in 1937, had been studying the effects of cement in the downhole condition, following the realization, the API Spec. 10 standards were created by ASTM Portland Cement standards, and when the geothermal industry expanded from the O&G industry, they also followed similar standards(Calvert & Smith, 1990; Smith, 2023). While the well structure design and materials originate from the oil and gas industry (O&G) since the environment is relatively similar, the interactions between the two types are vastly different from one another (Kurnia et al., 2022; Smith, 2023). The API Spec. 10A also became an international standard followed by various other countries and may list it as ISO 10426-1.

While Class G cements have both prescriptive and performance requirements, several cases of EGS feasibility and demonstration projects have shown that in some scenarios some overlying issues need to be addressed. Due to the overall heat environment and risk of corrosion, some projects experienced casing failures due to corrosion, and poor construction implementation due to the slurry's behavior during the drilling process (Stefánsson et al., 2021; Xu et al., 2018). While Class G cement has proven to be a good cement for conventional geothermal projects and in the O&G industry, additional research needs to be conducted for the case of Enhanced Geothermal Projects as some supercritical conditions similar to that of projects in Iceland (magmatic EGS, condition exceeding 400 °C) may require a more durable material, whether it be changes or additives used in a Class G cement, or a whole new slurry mixture design overall (Pyatina & Sugama, 2018; Sakuma et al., 2021; Stefánsson et al., 2021; Sugama & Pyatina, 2022; Thorbjornsson et al., 2020).

As previously mentioned, the cements in geothermal well cements, which are derived from oil and gas wells, were based on API specifications, as the elevated temperatures and pressures

caused different hydration reactions. As explained by Silva and Milestone, the cement sheath exposed to the hydrothermal conditions of the subsurface, will cause the material to experience a gradual loss in compressive strength and increased permeability often referred to in literature as "strength retrogression," which was first documented by in the early 1950s (Kalousek & Adams; Silva & Milestone, 2018a; Swayze, 1954). To combat the effects of strength retrogression to better improve the quality of the structure at these downhole conditions, supplementary cementitious materials were investigated as a result (Iverson et al., 2010). A common solution used in most well structures was the inclusion of approximately 30-45% silica (silica flour, sand, or colloidal silica, but mainly silica flour), which could help encourage silica-rich cement phases (Pernites & Santra, 2016). However, current literature and research also suggest that the addition of silica may not be enough considering the strength regression at more elevated temperatures (Pang et al., 2021; Pyatina & Sugama, 2018). While studies do suggest in researching other possible additives or materials to use in construction, the numerical simulation will focus first on Class G cement, as there is information available on the material properties of some samples used in geothermal projects, and if time permits investigate other materials and their respective properties.

Factors Influencing Geothermal Systems

The success of geothermal systems is heavily dependent on the environmental conditions on the project site where the wells are implemented. In terms of casing design important factors to consider are the corrosion resistance, strength retrogression, depth of the well, the internal temperature of the fluid, the fluid chemistry, thermal gradient, reservoir temperature, material availability, buckling, torsion, zonal isolation, et al (Iverson et al., 2010; Teodoriu, 2013).

Even when considering the entire system, for geothermal systems, like EGS, that have multiple wells, knowledge of the reservoir and its properties is essential for the success of the

project. Additionally, along with the number of wells being used, it is also important to consider the distances and fracture pathways between the two wells, which can include factors such as permeability, chemistry of the material, density of the network, number of open and closed pathways, etc. (Gischig & Preisig, 2015). After the events of the Basel Project, mentioned later, it became prominent that seismic activity needed to be closely monitored, and would become an additional focus for other EGS projects that followed its construction (Liu, 2020).

Damages and Failures in Well Structures

In some of the major EGS projects that were previously mentioned, projects had either come to a halt due to lack of funding such as the Habanero and Newberry projects, or due to environmental concerns like the Basel-1 Project, but a common occurrence that happened in a majority of the EGS projects was damage or structural failure within the casing, and in some cases had resulted in the abandonment of the project entirely. Failures in casings are a common problem in all geothermal systems, as they are vulnerable to fatigue from drilling, running the casing, internal pressure, temperature variation, thermal cycling, corrosion, buckling, etc. (Gruben et al., 2021; Kaldal et al., 2016; Marbun et al., 2020; Teodoriu, 2013)

In the IDDP-1 project, during the drilling, which had been problematic due to the early encounter with the rhyolite magma, resulting in multiple loss circulation zones throughout the well, a failed coring attempt, and a stuck pipe, had even encountered issues during the stimulation process (Pálsson et al., 2014). As previously mentioned, there was a time in which, there was a failure in the master valves that caused a pause in testing, at the same time, due to the varying thermal stresses, excessive scaling, and corrosion in the casing material that led to a collapse in the casing material in two sections of the well, with suggestions that even more failures were

present (MacDonald & Grauman, 2019; Thorbjornsson et al., 2020). The scaling phenomena is a continuous problem and had also been shown in the Soultz-sous-Forêts, which usually would be countered with inhibitors, but under several material tests, they noticed that while titanium alloys had the least amount of corrosion, all alloys had shown some level of scaling (Ledésert et al., 2021).

The second IDDP project, IDDP-2, was also experiencing large difficulties during the drilling process. After a certain depth range, there were frequent stuck pipe incidents, hole instability, and some fluid loss, however, they were able to determine that a reverse circulation method for drilling and cementing is an effective method for deep wells (Friðleifsson et al., 2020; Stefánsson et al., 2021). The project had also experienced severe corrosion due to oxidation, and the cold water being mixed with the brine fluids, showing casing damage throughout the well. There was difficulty in investigating the damage below the 2.3 km depth for safety concerns, so only logging data from before the casing damage is available, and any temperature and fluid conditions can only be determined by investigating core samples that were gathered (Friðleifsson et al., 2021).

While the Geysers Project was often considered a success, during Phase III (Long-term stimulation observation), in which there was a loss of potential data as a corrosion-induced leak occurred at the near-surface casing in PS-31, a series of various corrosion-resistant materials were tested to be used in the casing to help bring the well back online, in which 2507 Super Duplex was eventually chosen. However, after returning to a service state, a blockage was also discovered because of not running a drill to the bottom after installing the alloy liner, which wouldn’t be cleaned out until later, resulting in no data of PS-31 during Phase III (Hartline et al., 2019).

For the convenience of the reader, the table below mentions some of the key findings and lessons learned from previous EGS projects that will affect the material selection for simulation and the reasoning behind some of the research questions about the author's scope of work.

Table 2: Lessons learned from EGS feasibility and demonstration projects

Project	Location of Project	Lessons Learned	Source
The Geysers	California, United States	2507 Super Duplex is a useful corrosive-resistant material It is possible to simulate reservoir models that are accurate to physical simulation	(Garcia et al., 2016; Hartline et al., 2019; Rutqvist et al., 2016)
Desert Peaks	Nevada, United States	It is possible to reopen and extend the life of unproductive wells using developing technologies Possible to use tracers to measure fluid flow paths	(Akerley et al., 2019; Zemach et al., 2013)
Brady Geothermal Field	Nevada, United States	While chemical stimulation can help improve fracture propagation, the efficiency of the chemicals used will vary	(Akerley et al., 2019)
Newberry Volcano	Oregon, United States	It is possible to create separate zones for fluid flow from one well	(Cladouhos et al., 2016)
Icelandic Deep Drilling Project – I	Krafla, Iceland	Drilling and Casing efficiency is limited to the state of technology Chemical and physical reactions occur between the casing, concrete, and surrounding geomaterial High-Temperature Hydrogen Attack (HTHA) can happen in Iceland's geothermal fields Thermal stress, corrosion, and excessive scaling can cause failure	(Kaldal et al., 2016; Thorbjornsson et al., 2020; Thórhallsson et al., 2014)
Icelandic Deep Drilling Project - II	Reykjanes, Iceland	The cementing process encounters fewer issues when cementing from the bottom up Thermal stress behavior and corrosion on the casing caused the failure Difficult to map all locations of failures	(Stefánsson et al., 2021)
Soultz-Sous-Foretz MEET H2020 Project	Upper Rhine Graben, France	Salination from geothermal fluids, and hydrogen sulfide presence causes corrosion Temperature of fluid during injection can affect the permeability of the fracture network	(Ledésert et al., 2021)
GroB Schonbeck	Saxony, Germany	Using chemicals to help propagate and keep fractures open increases production, but will need a constant injection of chemicals, otherwise will decrease over time	(Blöcher et al., 2016)
Habanero Project	Cooper Basin, Australia	Not all geothermal reservoirs are dry-rock Fractures that have a high slip likelihood are better for fracture networks Not all fractures in a network are open, and only those open fractures can be stimulated	(Hogarth & Holl, 2017)
Basel Project	Basel, Switzerland	Too much fluid flow pressure can induce seismic activity	(Häring et al., 2008)
Kakkonda Project	Kakkonda, Japan	Drilling into supercritical temperatures is possible, but technologies are limited in efficiency While wasn't found initially, there may be a reservoir to support an EGS Project	(Ikeuchi et al., 1998; Suzuki et al., 2022)

CHAPTER III

METHODOLOGY AND NUMERICAL MODEL DEVELOPMENT

In the following chapter, a detailed description of the software used and how it works is provided. Additional information regarding the model setup, the reasoning, along with design choices, loading conditions, and operating parameters are provided.

Introduction

While there are many research articles on numerical simulation based on the hot rock reservoir and general material behaviors under high pressure and high-temperature environments, there is a large gap of knowledge on well structure integrity under different volatile and operating conditions for different materials for enhanced geothermal structures. To help contribute to filling in this knowledge gap, and complete the desired research objectives, a numerical model will be developed to run a thermal-mechanical analysis. ABAQUS/CAE Finite Element Analysis was the chosen program to develop the model as the standard/explicit license was available. ABAQUS CAE is a Computer-Aided Engineering Finite Element Analysis program that allows users to design and analyze models under different loading and boundary conditions.

ABAQUS Analysis

To run the desired analysis on ABAQUS there is a procedure to ensure that the simulation is running as intended. Firstly, since ABAQUS is a unitless system, it is important to choose the units beforehand, in this case, the standard SI units, also referred to as kg-meters-seconds (kms) by other Finite Element Analysis users, were chosen. With an established unit system then each of the individual parts is drawn. Each part must be assigned as a material that the user shall define and be aware of what properties are necessary to run their desired analysis, i.e. including density, thermal conductivity, et al., when running a transient thermal analysis. This will be explained in further detail later in the following section. The parts can then be assembled into a single assembly part or model. Steps can now be defined in the model, where ABAQUS will give different options based on the material properties listed, this is where the coupled analysis is defined, and where the step time and time increment definitions are applied, allowing one to specify the desired outputs for their analysis such as stress or strain. This is further explained in the next section. It is important to establish any possible interactions that the parts have. Interactions are the module that establishes any analysis constraints that might exist in the module, such as mechanical and thermal interactions between regions or parts. This is followed by the load module where loading conditions boundary conditions, and various fields can be assigned in the model. To determine the results of the desired analysis, a mesh must be developed to specify where the calculations will be conducted within the model. If a region is of particular interest, then one can design a finer mesh. Finally, a job is created and submitted, that will help manage and analyze the model.

To best understand how the surrounding subsurface conditions and the fluid affect the structure, it is best to consider using a dynamic coupled thermal-displacement or thermal-stress explicit analysis. This type of analysis, and one of the reasons ABAQUS was the chosen program

for this investigation is that the thermal and mechanical solutions in the simulation are greatly affecting one another and must be completed together at each increment. For this coupled temperature-displacement analysis, time and its relation to the loading conditions are vital to the behavior of the structure.

For ABAQUS to solve a nonlinear analysis, the total load is often broken into smaller increments so that the equations used are stable and can obtain an accurate solution. For dynamic explicit types of analysis, the number of increments tends to be high, meaning that the step increment time is extremely small so that the solution can be stable. It should be noted that the real-world time and increment and step time are not the same. The increment time can be affected by the size of the element and the level of fineness of the mesh.

Once the assembly is constructed, and all loading conditions and interactions that the model might have been applied, it is important to design a mesh for the model. This is started by applying seeds along the edges of the parts. The seeds help give an idea of where the nodes will be placed, which is the location of where the equations in the analysis are used. Depending on how the seeds are placed, will determine how the element shape is described, which connects the nodes and tells the node the type of analysis, creating the mesh. If a region in a model is important for the investigation, it is possible to design the seeds in a way that will create a finer mesh across the area of interest. However, depending on how coarse or fine a mesh is, can drastically affect the time it takes to complete a simulation, where the more course it is, the faster the results will be, but you will obtain less accurate results. The case is the same for the opposite, a finer mesh will result in a more accurate result but will take a longer time to run.

Fully Coupled Thermal-Stress Analysis

In ABAQUS Explicit, the heat transfer equations follow the explicit forward-difference method for the time integration rule. Where the temperature of the node at the current increment solves the equations based on the previous increments of temperature values. The temperature increment rule is as follows:

$$\theta^N_{(i+1)} = \theta^N_{(i)} + \Delta t_{(i+1)} \dot{\theta}^N_{(i)}, \quad \text{(Equ. 1)}$$

In this equation (Equ. 1) θ^N, represents the temperature of the node N, i represents the increment during an explicit time increment step. $\theta^{\cdot N}$ represents the known values based on the previous increment, and are computed using the equation:

$$\dot{\theta}^N_{(i)} = (C^{NJ})^{-1}(P^J_{(i)} - F^J_{(i)}), \quad \text{(Equ. 2)}$$

C^{NJ} is known as the lumped capacitance matrix, which is a model used that reduces a thermal system to several discrete "lumps," where the temperature difference is assumed to be negligible inside each lump. This is useful in simplifying complex differential heat equations. P^J is known as the applied nodal source vector, and F^J is referred to as the internal flux vector. This integration method is considered explicit as there are no equations that need to be used if the lumped capacitance matrix is used.

The mechanical stress solutions are simultaneously calculated and are obtained using a central-difference integration explicit rule, which will use a lumped mass matrix.

$$\dot{u}^N_{(i+\frac{1}{2})} = \dot{u}^N_{(i-\frac{1}{2})} + \frac{\Delta t_{(i+1)} + \Delta t_{(i)}}{2} \ddot{u}^N_{(i)} \quad \text{(Equ. 3)}$$

$$u^N_{(i+1)} = u^N_{(i)} + \Delta t_{(i+1)} \dot{u}^N_{(i+\frac{1}{2})} \quad \text{(Equ. 4)}$$

u^N, is the degree of freedom, rotational or displacement, and the subscript, i, like in the previous equation denotes the increment. $u^{\cdot N}$ and $u^{\cdot\cdot N}$ also represent known values derived from the previous increment, and make use of the equation:

$$\ddot{u}^N_{(i)} = (M^{NJ})^{-1}(P^J_{(i)} - I^J_{(i)} \quad \text{(Equ. 5)}$$

From this equation, M^{NJ} is the mass matrix, P^J is the applied load vector, and I^J is the internal force vector. The lumped mass matrix is desired as the inverse of the matrix is simple to compute, and the explicit method does not require iterations or a tangent stiffness matrix. However, it is required that all nodal mass or inertia have activated or nonzero value degrees of freedom unless there is a constraint applied to it.

For both types of analysis to run properly some material properties need to be defined, such as thermal conductivity, coefficient of thermal expansion, specific heat, density, poisons ratio, elasticity, and the plasticity of the objects used. The values that are primarily being examined in this document are the Von Mises Stress and the strain of the assembly.

The von Mises yield criterion is often used in material science and engineering fields and suggests that the yielding of a material begins when the second deviatoric stress invariant, also known as J_2, reaches a critical value referred to as k. Despite a material experiencing principal stress not failing under load, the combination of the stresses the material experiences can still cause yielding. Essentially, if the Von Mises Stress of a material under a loading condition is greater than or equal to the material's yield limit the same material undergoing simple tension will yield.

Therefore, the equivalent stress of the material needs to be compared to the yield stress of the material. ABAQUS defines this equation as:

$$q = \sqrt{\frac{3}{2}(\mathbf{S} : \mathbf{S})}$$ (Equ. 6)

Where S is known as the deviatoric stress, the shear stress present in a material, and is defined as:

$$\mathbf{S} = \boldsymbol{\sigma} + p\,\mathbf{I}$$ (Equ. 7)

p is defined as the equivalent pressure stress, and I is the identity matrix. p is calculated by ABAQUS in the following equation.

$$p = -\frac{1}{3}\mathrm{trace}\,(\boldsymbol{\sigma})$$ (Equ. 8)

In the explicit model, Logarithmic strain is the default output. The logarithmic strain provides the measure of the final strain when the deformation takes place in each increment, meaning it considers the influence the strain path has on the material. ABAQUS considers this equation in numerical simulations.

$$\boldsymbol{\varepsilon}^L = \ln \mathbf{V} = \sum_{i=1}^{3} \ln \lambda_i \; \mathbf{n}_i \, \mathbf{n}_i{}^T$$ (Equ. 9)

V is the left stretch tensor, λ is the principal stresses of the material, and n refers to the principal stretch directions of the configuration at that instance of time. With all these equations, the stress and strain are calculated at each node for the model.

Developing the Numerical Model

As the number of calculations at each node takes considerable time in an explicit model, to save computational time and resources, a simplified axisymmetric model was developed. Like

real-world geothermal well projects, this geothermal well will contain multiple casing strings. This model will be composed of three, an inner, middle, and outer string, to represent the production, intermediate, and surface casing respectively. The production casing is the innermost string that is used to deliver the fluid toward the target reservoir. The intermediate casing is described as any casing string that is between the production casing and the outermost casing. The surface casing is meant for zonal isolation, a barrier to ensure separation from the subsurface and fluid. In this case, the surface casing is primarily designed to protect groundwater sources. Likewise, the cement sheath will also surround each casing from the surface toward the bottom of the casing string. Each real-scale project, mentioned in the previous chapters, has different operating parameters and boundary conditions that are unique to the drilling location. In the case of this simplified model, the model was scaled in terms of its depth, going only one meter into the subsurface to save time per test simulation, however, the thickness of each casing was kept as the original lengths. Due to the change in the overall length, all boundary conditions and loading conditions were scaled to correspond with the length of the well structure. To better visualize the model for the reader, Figure 4 below shows the simplified axisymmetric model, where the green-colored material is the cement sheath, and the beige color is the metal casing. Additionally, the table below provides some of the dimensions used for the model based on a well design used by Kaldal et al. (2015), however, rather than 12 mm or 0.472 inches, 10 mm was used for the thickness of the metal casings. Mainly for simplicity in modeling, but it should be noted that in terms of casing production for pipes, many thicknesses are determined by the project's chosen handbook or guidelines and are sold commercially in terms of the inner radius, with different choices for the thickness of the pipe, which will depend on the circumstances of the project.

Table 3: Dimensions used to design the metal sheath parts for the assembly

Metal Casing	Inner Radius (Inner wall to center of well) [m]	Thickness [m]	Depth [m]
Production String (Inner)	0.08	0.01	1
Intermediate String (Middle)	0.11	0.01	0.5
Surface String (Outer)	0.16	0.01	0.25

Table 4: Dimensions used for the cement sheath parts on the assembly

Cement Sheath	Inner Radius (Inner wall to center of well) [m]	Thickness [m]	Depth [m]
Production String (Inner)	0.09	0.02	1
Intermediate String (Middle)	0.12	0.04	0.5
Surface String (Outer)	0.17	0.05	0.25

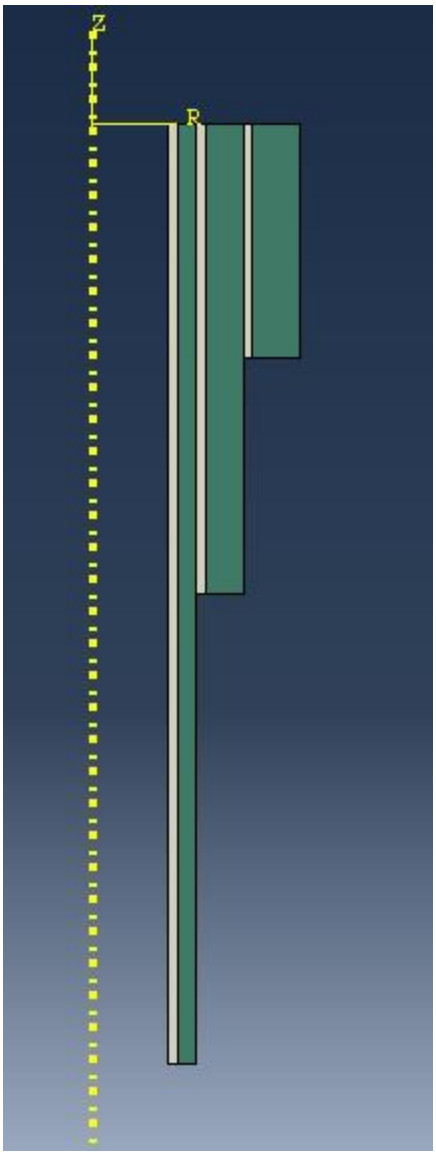

Figure 4: The simplified axisymmetric model used for numerical simulation

In the previously mentioned chapter, various factors can cause the structure to fail, which can be seen around the time that the fluid is being introduced or reintroduced into the structure, repeated shut off, and can be caused by either thermal cycling, corrosion of the material, etc. For this numerical model, the moment in time that is being investigated is shortly after the fluid is introduced into the structure after the well has already been given time to reach thermal equilibrium after being built.

The chosen materials for this project were Class G cement for the cement sheath and Grade 29 Titanium for the metal casing. Class G cement has already been established as one of the main building materials for the well structure throughout many countries, and while there is currently research being conducted on how to improve the quality of the cement sheath, it was considered suitable for this model. Grade 29 Titanium is not considered a frequently used material in geothermal projects, mostly due to cost and availability. However, the commonly used materials that have been shown in Enhanced Geothermal Systems, such as Duplex steels or API 5L pipes, may not be suitable, and there have been some suggestions to investigate other materials due to casings failing due to corrosion, mineral clogging, etc. Titanium as previously mentioned is extremely corrosion-resistant and was ultimately chosen as the representative material for this model, mainly due to its promise as a future building material. Additionally, there was more detailed information on the material properties in commercial production for its behaviors under high pressure and temperature situations. Information regarding the material properties gathered used in the numerical model from Company (2000); Kaldal et al. (2015) can be seen in the table below.

Table 5: Properties for the metal casing and cement sheath used in numerical model development

	Density [kg/m^3]	Young's Modulus [GPa]	Expansion [1/°C]	Yield Strength [MPa]	Poissons Ratio	Specific Heat [J/kg°C]	Thermal Conductivity [W/m°C]]
Titanium	4.43	114	9.2e-6: 0-100°C 9.5e-6: 0-315°C 10.1e-6: 0-538°C 10.4e-6: 0-648°C 10.8e-6: 0-816°C	759: 20°C 712: 93°C 640: 149°C 587: 204°C 532: 260°C	0.32	565	7.3
Class G Cement	1600	2.40	10e-6	-	0.15	880	0.81

After assembling the model and assigning the material to each of their corresponding parts, the desired analysis type needs to be established. This paper is investigating the thermal-mechanical response under the subsurface loading conditions; hence a coupled temperature-displacement dynamic analysis was chosen. This allows ABAQUS to view the structure's behavior and response to thermal and mechanical loading simultaneously, rather than assigning two separate steps, allowing a relatively more accurate representation of the real-world projects. To closely simulate that of a real-scale project, several boundary conditions were applied. First, the entirety outside of the well was given an encastre boundary condition to represent the surrounding geomaterial, restricting the movement of the well structure by constraining all active structural degrees of freedom for the surfaces that are in contact with the geomaterial.

As previously mentioned, all project conditions are unique to the location, and since the project was scaled in terms of its depth, a linear expression was given instead to represent the well body temperature. Firstly, the boundary condition intended to represent the Earth’s subsurface temperature was considered and applied along the structure’s contacting surfaces of the well that would be interacting with the subsurface. Since this is considered a simplified model, the initial temperature at the start of the well or the surface temperature was assigned as 20 °C and increased linearly until reaching 200°C at the bottom of the well. Additionally, the well structure itself was given an overall body temperature that would be the same as the Earth's thermal gradient boundary to simulate if the well had already reached thermal equilibrium sometime after the structure was built.

Furthermore, an additional expression was applied to the structure to represent the confining pressure due to the geomaterial in the subsurface. The lateral earth pressure load was applied as a linearly increasing distributed load along the well depth. As previously mentioned,

due to the uniqueness of each geothermal project, the surrounding geomaterial and layers apply varying amounts of pressure against the well, along with varying thermal gradients due to the geographical location, it would be difficult to select a project that would best represent all EGS projects, while it is understood that these behaviors are mostly nonlinear, to simplify the model, all expressions were considered linear and the subsurface is a homogeneous geo-material. The lateral earth pressure would be given as 13.5 MPa based on a similar earth pressure in the Krafla geothermal field in Iceland mentioned in a conference paper by Milsch et al. (2010). Mostly since the well design choices previously mentioned were chosen from a well in geothermal fields near that region, and information availability. Additionally, the fluid would be given a constant uniform pressure of 35 MPa similarly used in the Habanero project documented by Mills and Humphreys (2013). Like the earth pressure loading condition, this value was chosen mainly due to information accessibility.

To determine the effects of the fluid temperature on the well structure, a test was initially performed in which there was no fluid present in the system. This will provide a baseline to compare during the parametric study, in which the boundary conditions that will represent the fluid will change. Due to the numerical model being developed asymmetrically, the standard/explicit ABAQUS license does not allow modeling a fluid, without using the additional coupled fluid domain (CFD) license add-ons or the use of third-party programs. Instead, to closely simulate the fluid flow of the structure, a uniform distributed load was applied along the production casing where the fluid would contact the well structure as if the fluid is being introduced through a pump, like some EGS feasibility projects. Additionally, the fluid wall would also be assigned a temperature depending on the type of test that was being conducted. These values will be investigated and compared as part of the study. Due to the high temperature and pressure

conditions that the fluid will be undergoing, the fluid is typically in a state of two-phase flow. Since the velocity of the fluid throughout the casing is unknown, the temperature of the fluid along the depth is also considered to be unknown as well. As the brine or working fluid travels, the initial heat from both the pipe and the structure varies greatly, resulting in a thermal transient state for the structure. The velocity of the pipe is unknown, the possibility for the fluid to gather some heat from the structure or the structure to lose heat to reach a steady state is likely to occur, which can cause thermal stresses throughout the well. Five different boundary conditions were investigated to represent the fluid along the pipe wall. The first considered that the fluid traveled so fast that the initial temperature of the fluid, 20°C, remained uniform during its travel to the HRZ. The next scenario suggests that some heat radiating from the well had transferred to the fluid along the depth, in which the maximum temperature of the fluid before reaching the HRZ was 40°C. Like the well-body temperature, earth temperature, and pressure, the rate at which the temperature increased was linear. While having a properly modeled fluid that could show the heat transfer would be more accurate, this study is more focused on the thermal stress effect on the structure, and this knowledge gap can provide future opportunities for study. The remaining scenarios followed a similar linear expression, but the maximum temperature increased by increments of 20°C. Therefore, the minimum temperature, which is at the top of the well, where the surface is located is 20°C. The maximum temperature of the fluid, near the target reservoir, is 20, 40, 60, 80, and 100°C. An image showing the initial temperature of the well structure can be seen below in Figure 5. With the thermal load, several periods were considered until the thermal equilibrium of the object. The model would be considered to have transferred from its transient state to a steady state when the temperature within the structure had gone through no change after a period. Under

each thermal loading condition considered, the test was conducted until the steady state of the structure was determined.

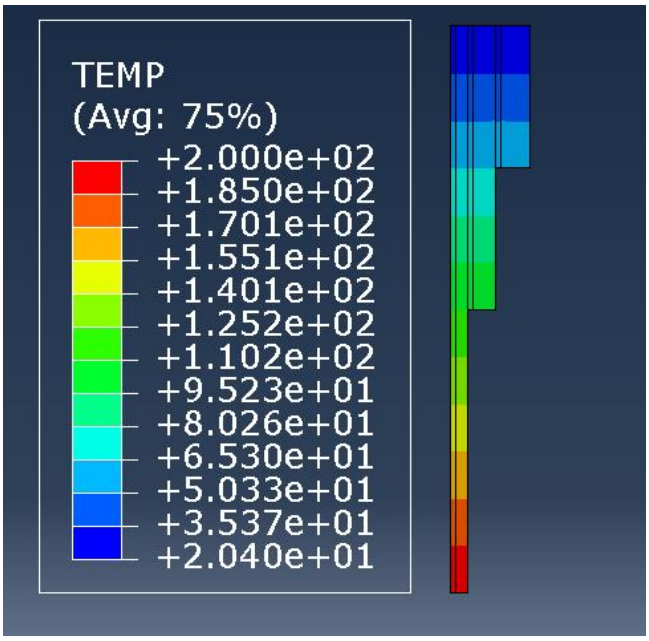

Figure 5: Modeled structure with an initial temperature condition

In each string, casing, and cement section, each contacting layer of material was given a tie constraint along with a physical contact property to physically tie the materials together. This way the material surfaces are defined to be in contact with one another and won't improperly have the mesh and material deform through each other.

The analysis used to conduct the study was an explicit dynamic coupled temperature-displacement analysis. While this is known to increase simulation time significantly, the behavior of the structure would be considered more realistic in comparison to separating the thermal and mechanical analysis into two separate steps, as the thermal and pressure loads can affect one another. Therefore the element type used was the CAX4RT, which is the designated name for an explicit coupled temperature-displacement analysis element for axisymmetric models.

The mesh used in the simulation was a structured mesh, that corresponds to the element type needed for explicit coupled temperature-displacement analysis. The mesh type determines how the shapes of the elements will be drawn, which can be either quadratic or triangular, they can also be structured or free, which will determine the geometric pattern. Depending on how the model is drawn, the mesh type is usually drawn at the discretion of the user. In this model, a quadratic structured mesh was chosen, which attempts to keep the quadratic shape in a neatly organized manner. To save simulation time a finer mesh was given at areas of interest, such as the bottom of the well which has a higher pressure and temperature load relative to the conditions near the surface. With all the conditions listed, the job was ready to be submitted, the table below summarizes the model's setup after defining the material properties.

Table 6: Parameters used for the numerical analysis model

Step	Coupled Temp-Displacement, Explicit
Boundary and Loading Conditions	Encastre
	Initial well body temperature: 20-200°C
	Earth temperature: 20-200°C
	Fluid pressure: 13.5 MPa
	Lateral Earth pressure: 35 MPa
	Case 1: No Fluid Temperature Case 2: 20°C uniform temperature Case 3: 20-40°C Fluid Case 4: 20-60°C Case 5: 20-80°C Case 6: 20-100°C
Interactions	General Surface-to-Surface Contact
Element Type	CAX4RT: Coupled axisymmetric 4-node displacement and temperature element
Mesh Type	Quad-dominated structured mesh

CHAPTER IV

RESULTS AND DISCUSSIONS

Using different fluid temperatures, finding the amount of time to reach thermal equilibrium or steady state throughout the structure needed to be determined. The uniform temperature of 20°C relative to the other scenarios has a larger temperature differentiation and was able to find a complete total steady state under three hours. The remaining test cases were able to reach a steady state relatively quickly. Thermal equilibrium in the structure was achieved at a higher rate the closer the fluid temperature was to the surrounding well body's temperature. Figures 6 and 7 (a.-d.) below show the transition from transient state to steady state throughout the entire well structure for the cases when the fluid temperature is a constant 20°C and when the fluid temperature is increasing linearly from 20 to 100°C.

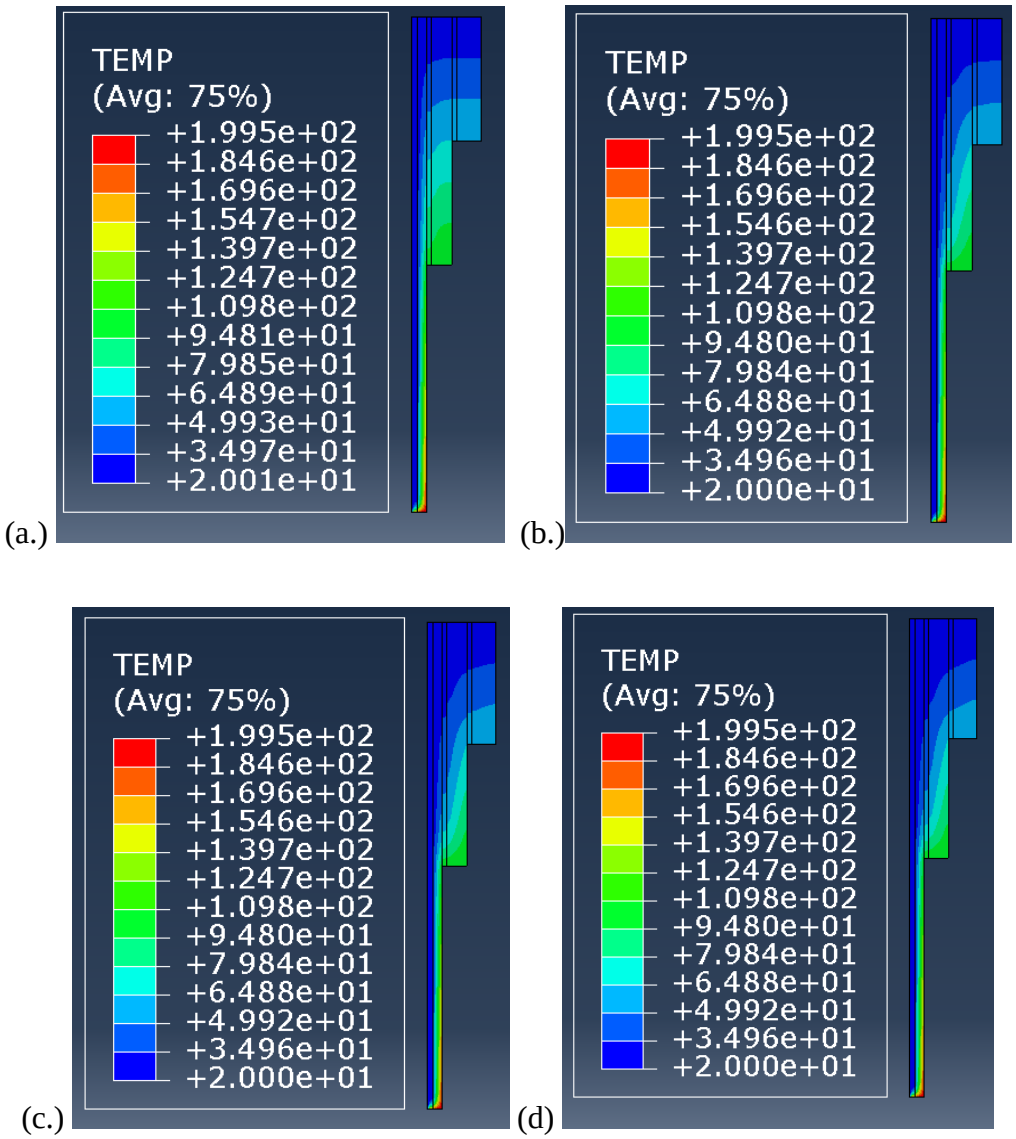

Figure 6: The numerical model approaching steady state at times: 18 minutes, 45 minutes, 1 hour and 30 minutes, and 3 hours respectively when the fluid temperature is 20 °C

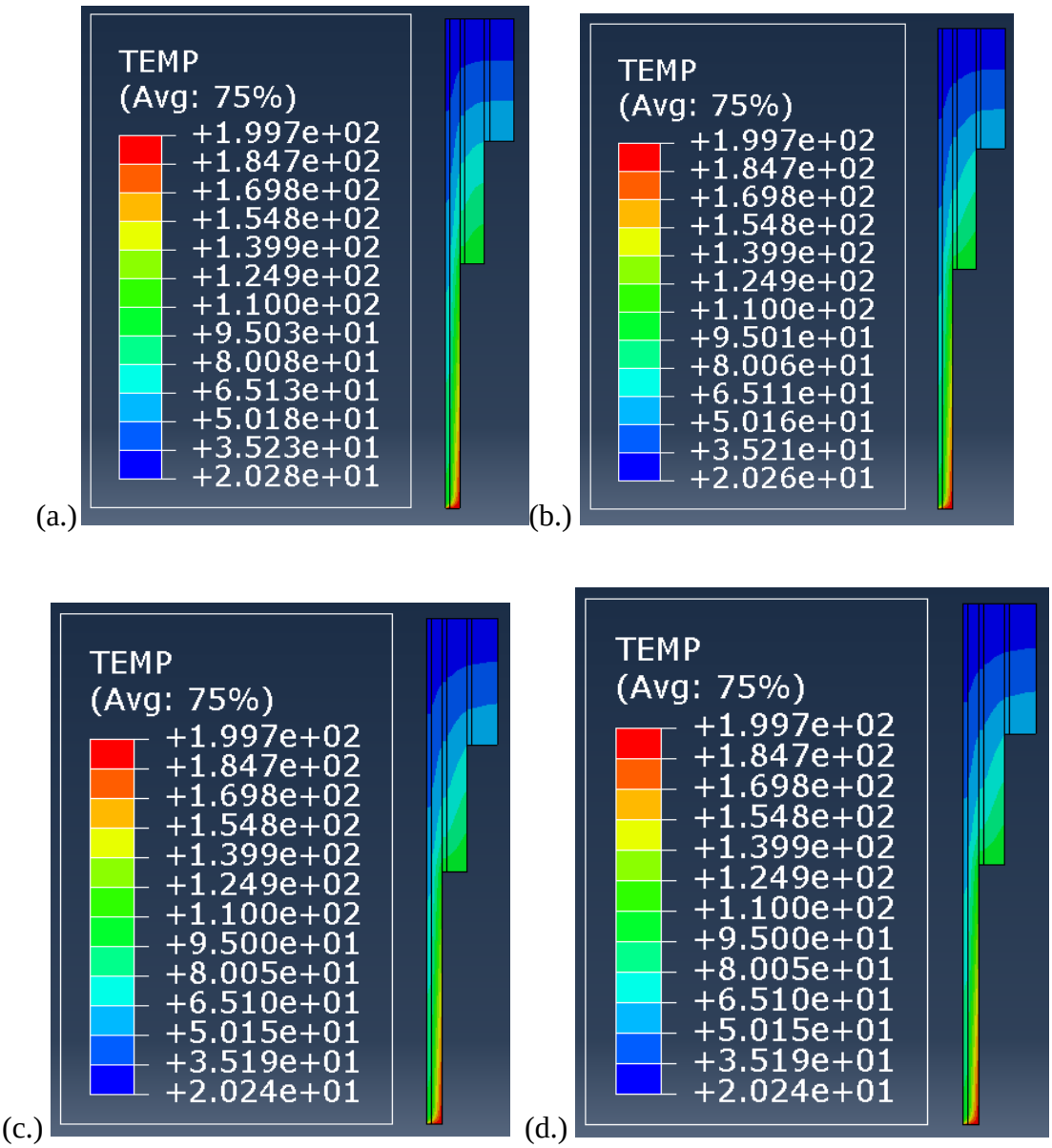

Figure 7: The numerical model approaching steady state at times: 18 minutes, 45 minutes, 1 hour 30 minutes, and 3 hours respectively when the fluid temperature increases from 20-100°C along the depth

Once a steady state for the entire structure was achieved, an analysis was performed to determine the Von Mises stress, and the Maximum In-Plane strain was gathered and inspected. Inspecting the model, the largest areas of stress and strain concentrations were along the shoes of the casings at the end of a casing string, i.e. the bottom where the outer casing program was completed, which can be seen in Figures 11, 12, and 13. Three paths were drawn that would be

used to plot the stress and strain across the well, which can be seen in the figures below. The first path goes along the edge of the shoe at the very bottom of the well that is in contact with the target reservoir and will be referred to as the HRZ path. In the remainder of the paper, the outer casing string ends and transitions to where the middle casing string is exposed to the subsurface will be referred to as the Inner-Middle-Outer (IMO) Transition. Additionally, the path where the middle casing string ends and transitions to the inner casing string will be referred to as the Inner-Middle (IM) Transition path so that referencing will be easier for the reader's convenience. For better visualization, these paths are drawn in the series of figures below, and a path showing the pipe wall that interacts with the fluid was added.

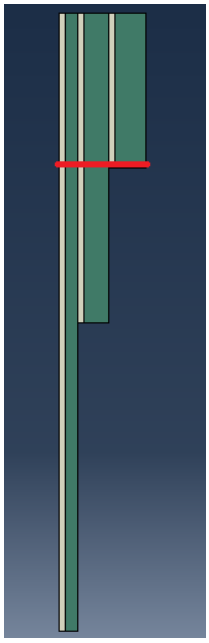

Figure 8: Inner-Middle-Outer Transition path highlighted in red on the well structure

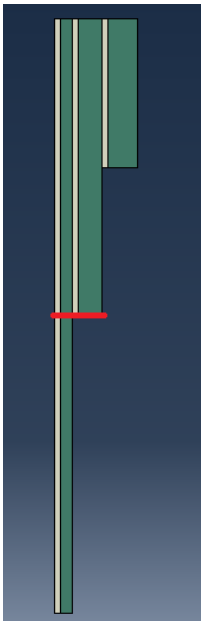

Figure 9: Inner-Middle Transition path highlighted in red on the well structure

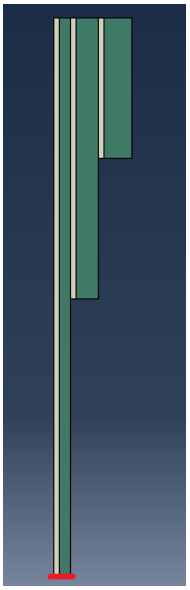

Figure 10: HRZ path highlighted in red on the well structure

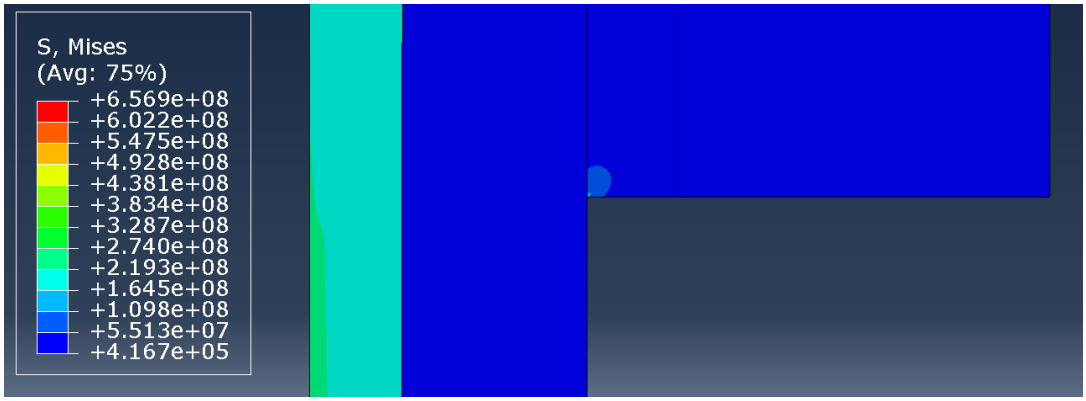

Figure 11: Stress concentration at the bottom of the metal casing at the inner-middle transition area at t = 3 hours, when fluid temperature is at 20°C

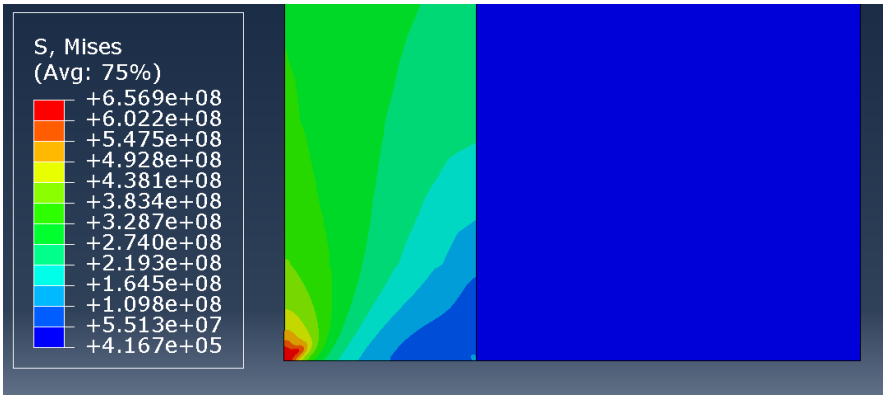

Figure 12: Stress concentration at the bottom of the innermost casing string, at time = 3 hours, when the fluid temperature is at 20°C

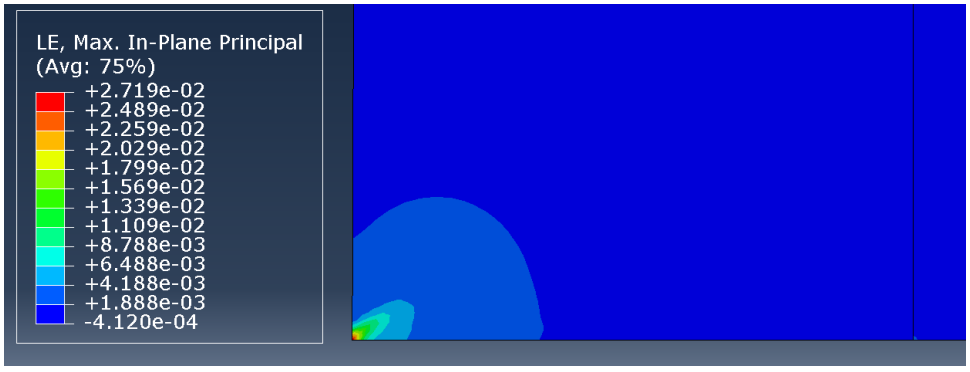

Figure 13: Strain concentration at the bottom of the innermost casing string, at time = 3 hours, when the fluid temperature is 20°C

Each of the different paths along either the depth of the well or thickness of the well was investigated in terms of their stress and strain with respect to time and compared with each of the different fluid temperature conditions.

Fluid Wall

The fluid wall is the surface of the well that is in contact with the working fluid, is part of the innermost casing, and is often referred to as the production casing. This can be seen in Figure 14. In this model, the fluid wall is the area where the loading conditions used to represent the fluid were applied. When looking at the temperature along the depth in the figures below, the fluid temperature steadily increased, until the very bottom of the well, where the fluid temperature and the well body temperature vastly differed from each other.

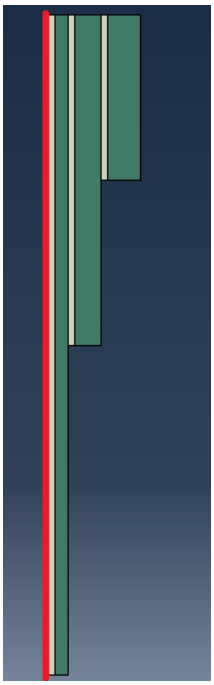

Figure 14: Fluid wall path in the numerical model highlighted in red

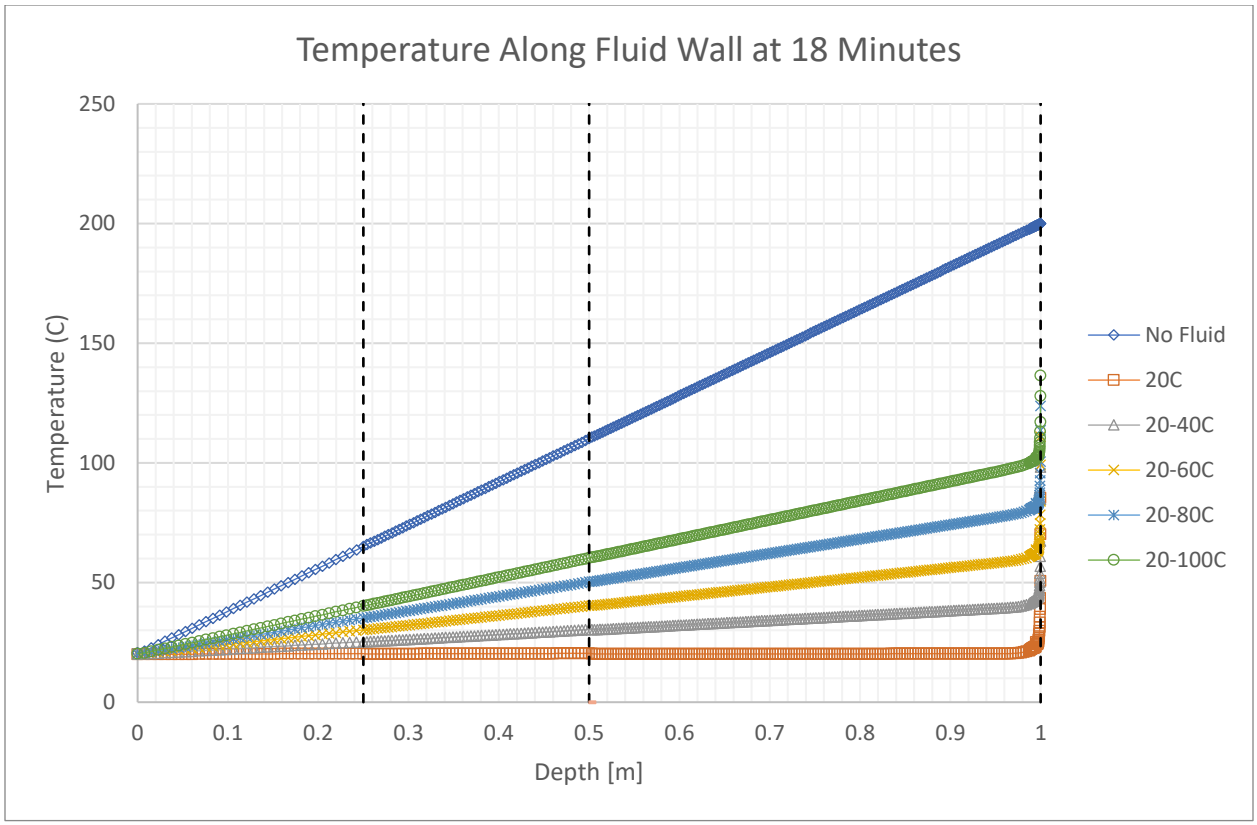

Figure 15: Temperature along the fluid wall path at 18 minutes

The temperature along the well does increase as depth increases, which is seen in Figure 15. However, the path is located directly on the boundary condition, the path itself shows little change over time, which can be supported by Figures 16 and 17 below. The bottom two figures demonstrate that no matter the fluid temperature condition, the temperature varies minimally over time. However, this is only along the surface of the fluid wall, within the well structure, this trend is not the same and will be explained further in the paper.

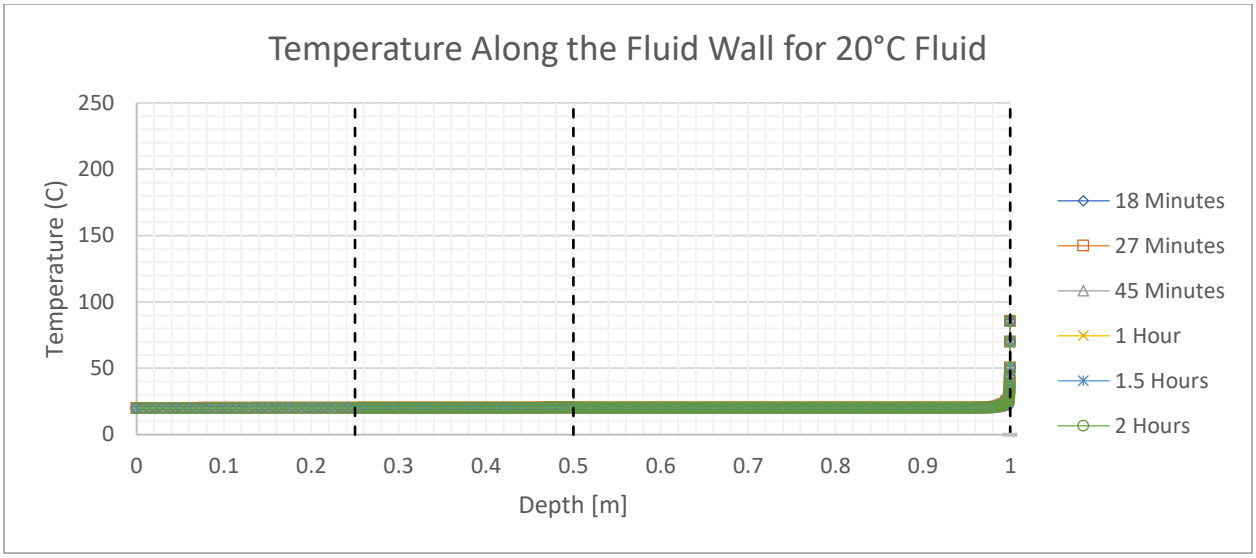

Figure 16: Temperature along the fluid wall with 20°C working fluid temperature over time

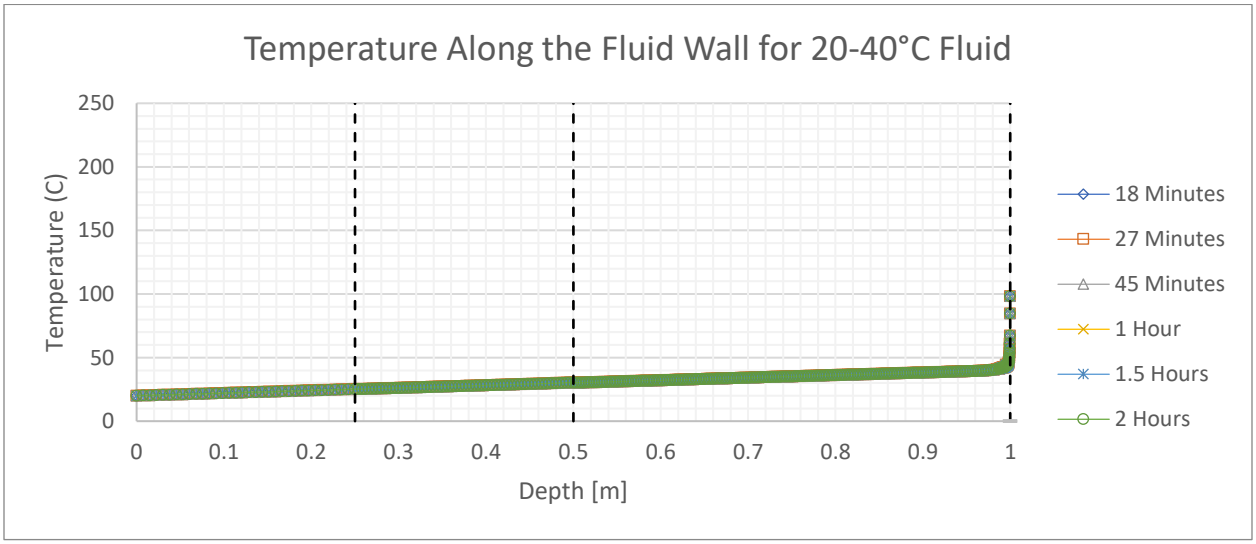

Figure 17: Temperature along the fluid wall with 20-40°C working fluid temperature over time

Once the temperature of the well was plotted, additional graphs were made to understand the behavior of the fluid wall. Firstly, when it comes to investigating the strain of the fluid wall, as seen in Figures 18, 19. 20, and 21, while the temperature of the fluid wall remains relatively constant over time, the strain throughout the entire structure seems to fluctuate around zero until reaching near the bottom of the well at the HRZ.

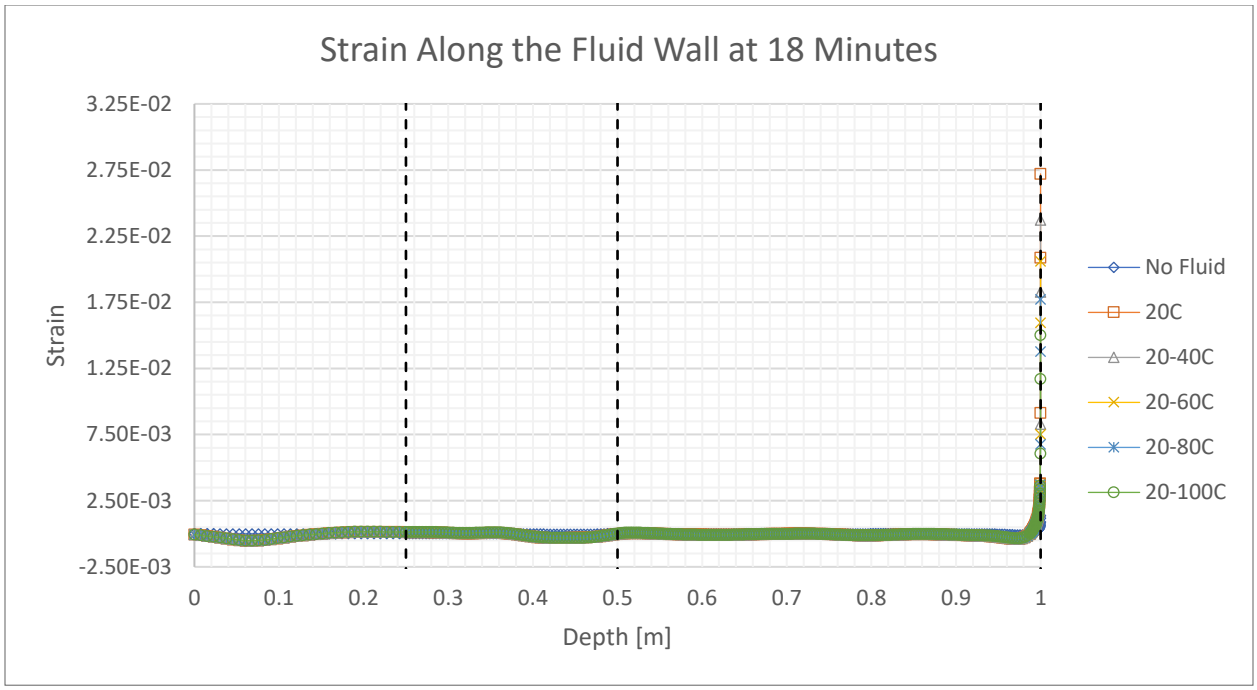

Figure 18: Strain along the Fluid Wall at 18 Minutes

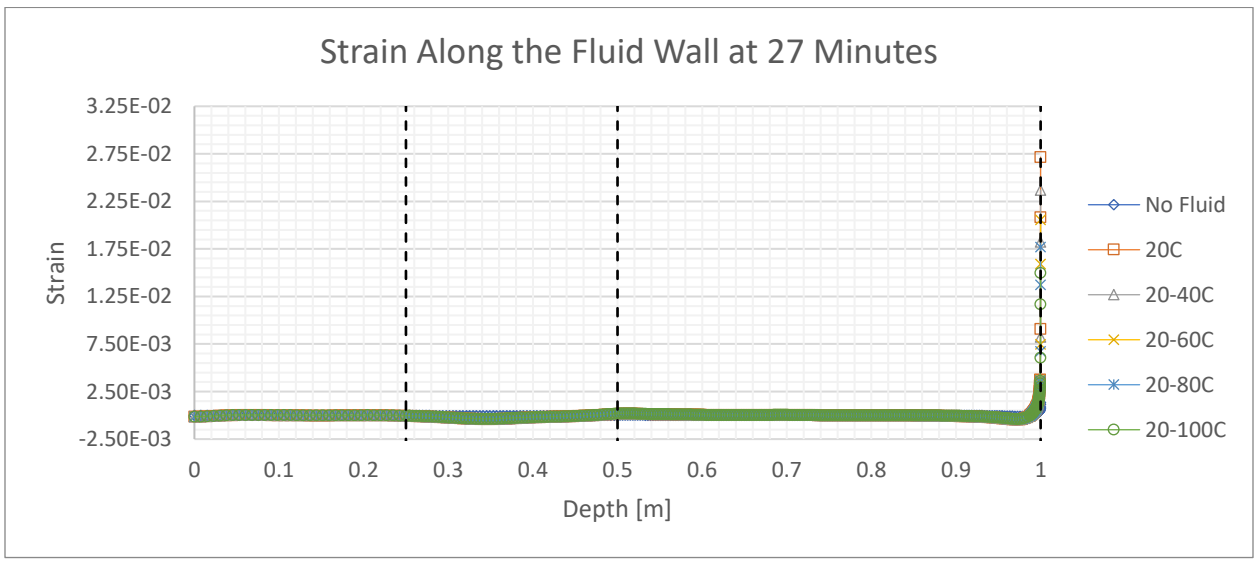

Figure 19: Strain along the Fluid Wall at 27 Minutes

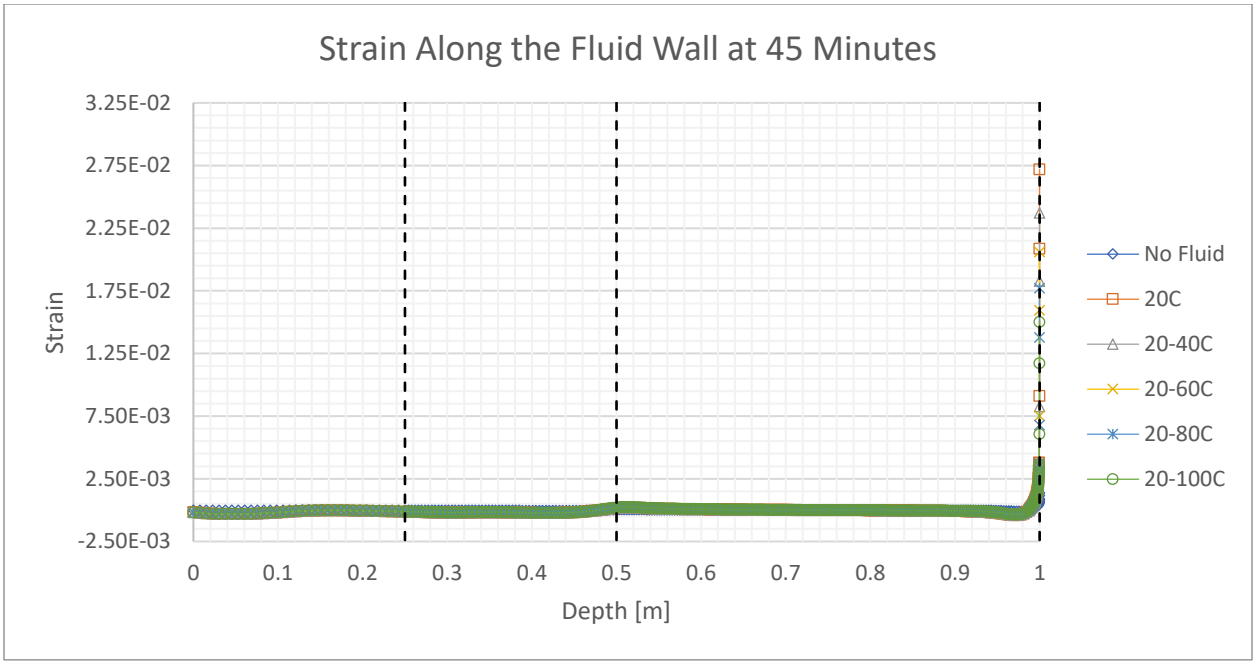

Figure 20: Strain along the Fluid Wall at 45 Minutes

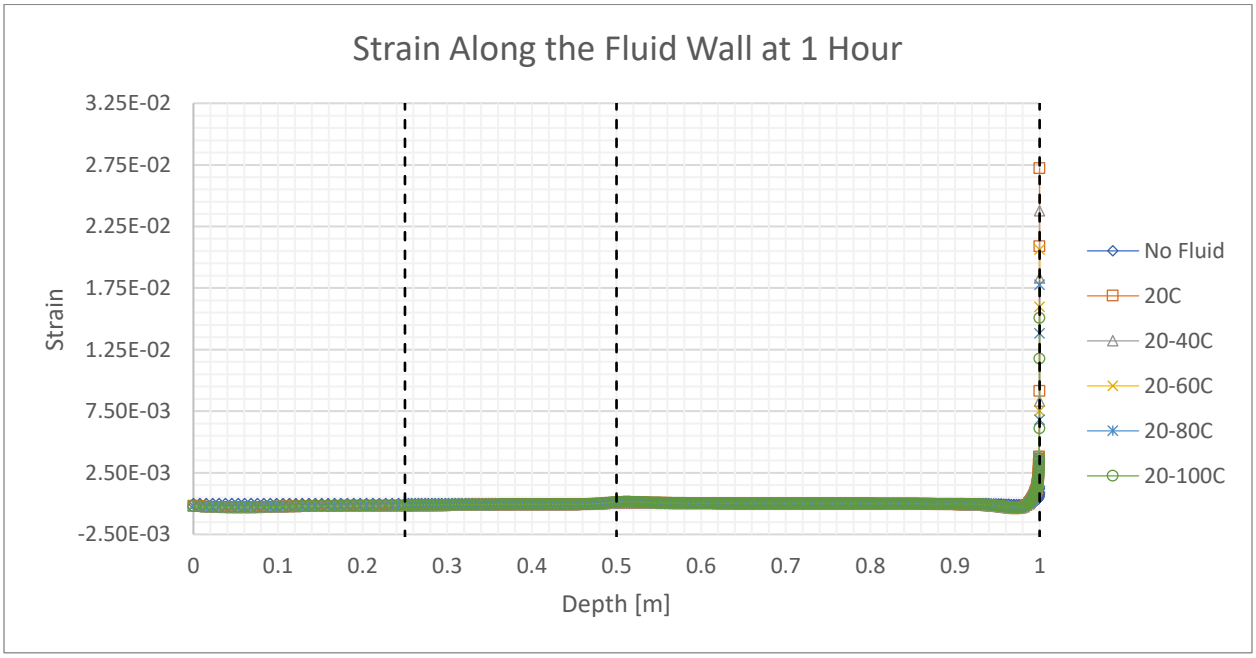

Figure 21: Strain along the Fluid Wall at 1 Hour

As previously mentioned, the strain tended to fluctuate around zero over time for most of the length of the well, however, at the bottom where the strain increases, the larger the temperature difference that existed the higher the final peak was at the bottom of the well. It should be noted

that the no fluid condition does suggest that the earth pressure does give strain to the structure, however, in comparison to the thermal loading, the temperature difference, whether the fluid is 20°C or 100°C, has a significantly larger impact on the structure than the surrounding geomaterial does. This is further supported when looking at the stress as seen in the following figures below.

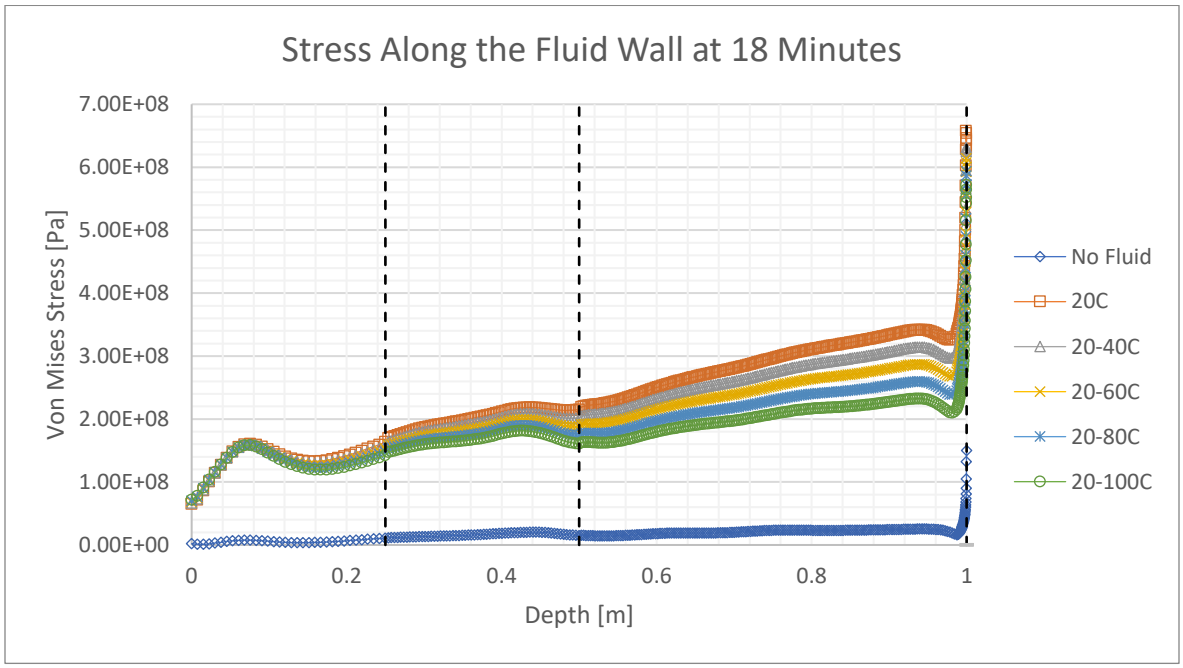

Figure 22: Stress along the fluid wall path at 18 Minutes

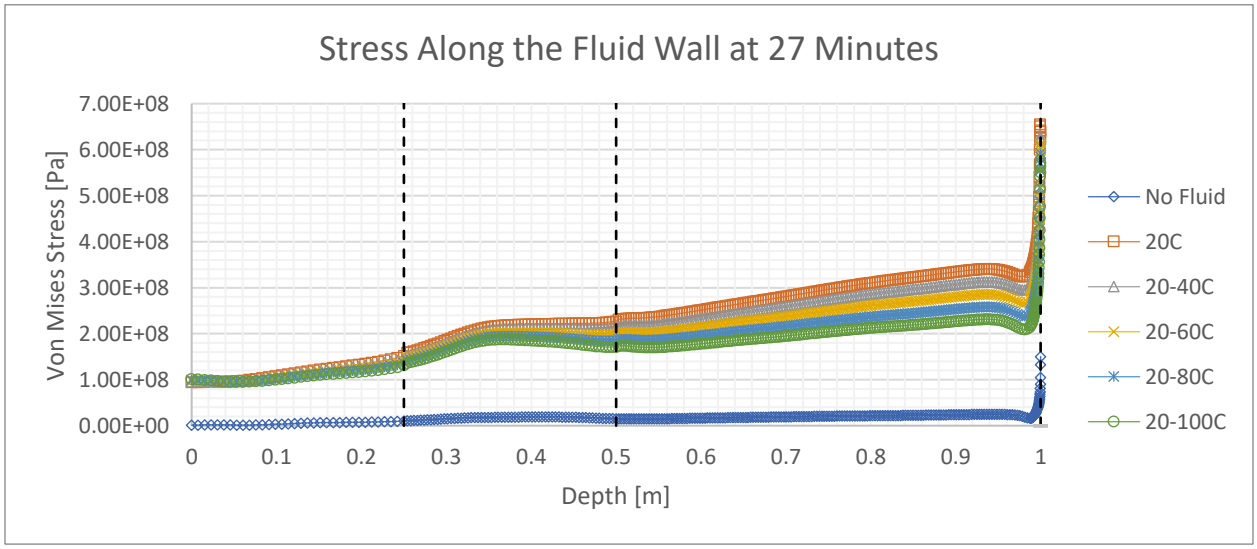

Figure 23: Stress along the fluid wall path at 27 minutes

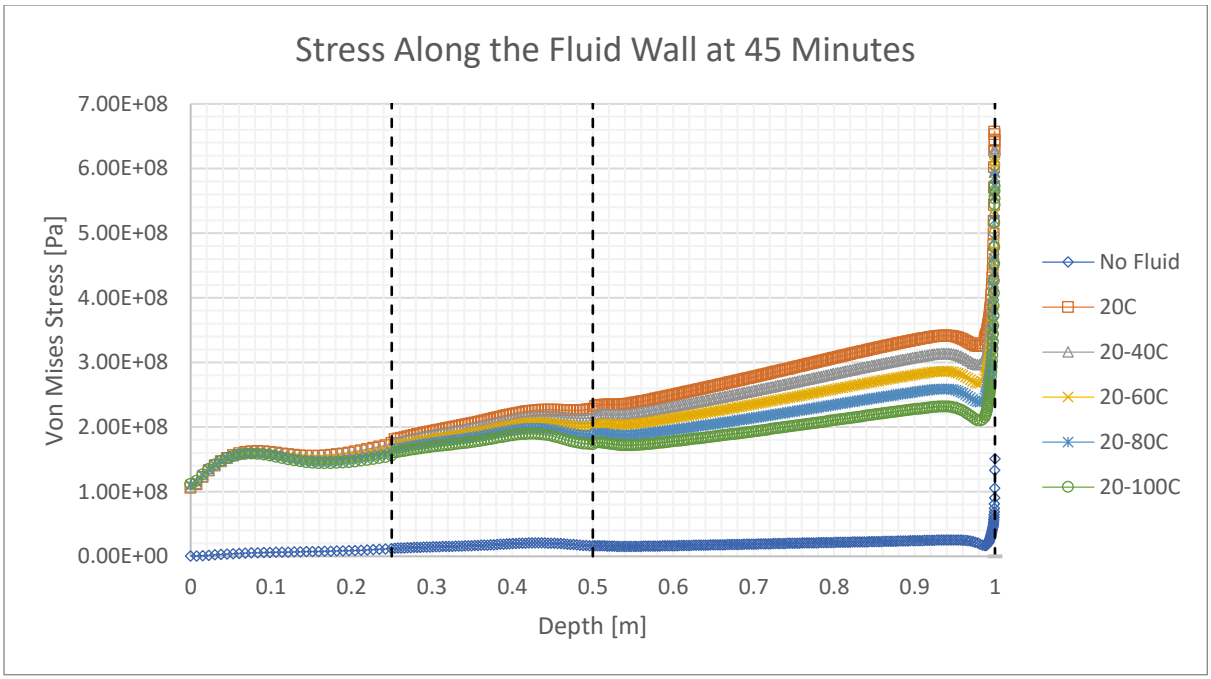

Figure 24: Stress along the fluid wall path at 45 minutes

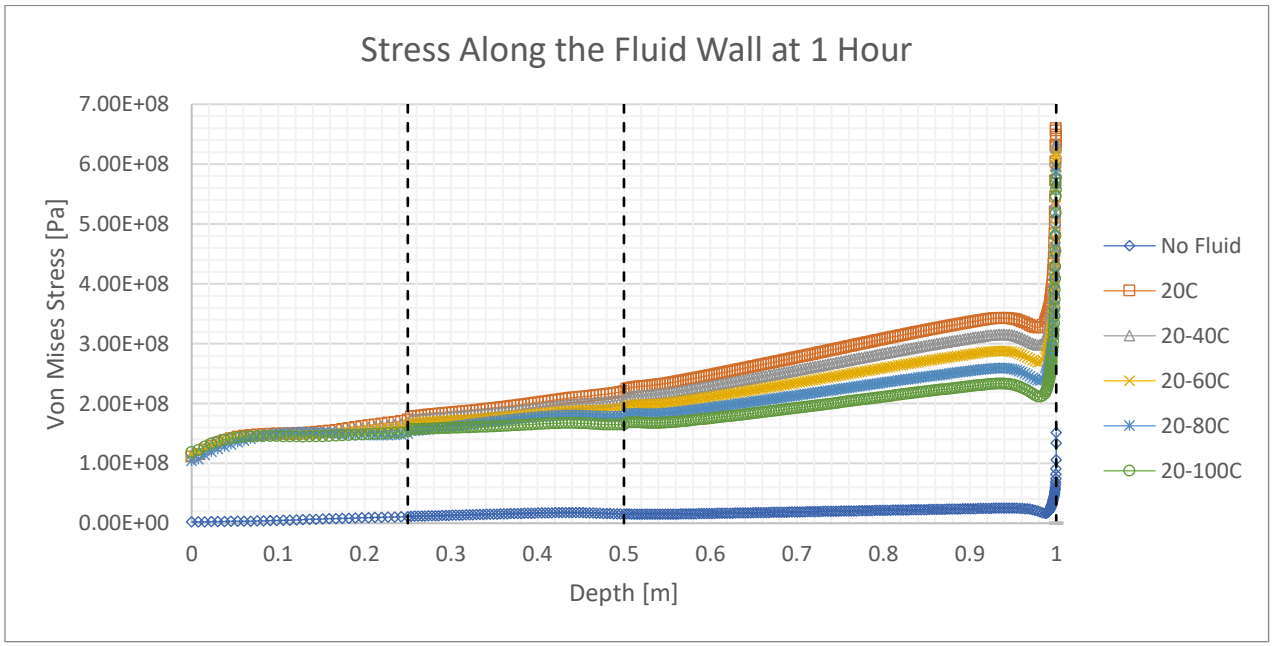

Figure 25: Stress along the fluid wall path at 1 hour

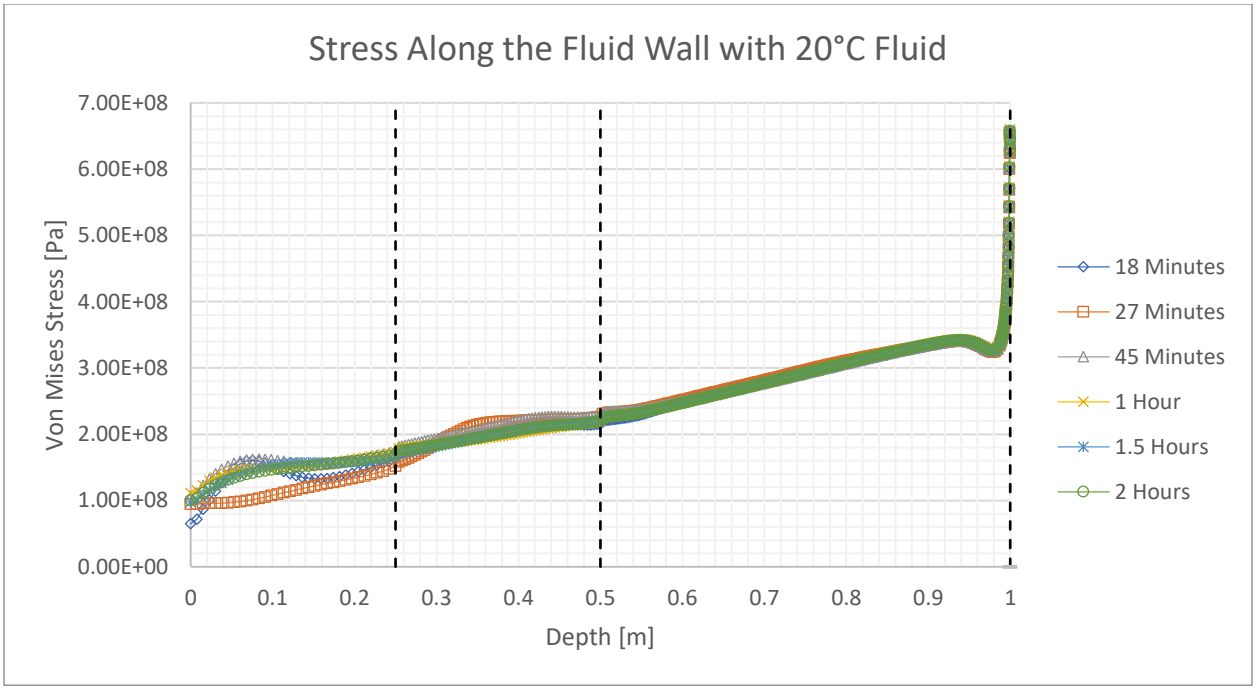

Figure 26: Stress along the fluid wall over time with 20°C fluid

Like the strain graphs, the stress seems to fluctuate as time passes. Additionally, as the depth increases, when a casing string ends, which occurs at a depth of 0.25 and at 0.5 meters, when the outer and middle casing stops, respectively, the slope of the line changes. The region with the steepest slopes relatively happens when there's only one layer between the production casing and the surrounding geomaterial. When comparing the five test scenarios to the control simulation that has no fluid, the cause of this may not be because of the earth pressure, but because of the thermal loading's effect on the structure. The upper area of the structure has little difference in temperature between the fluid and the well body, but the bottom half of the structure, 0.5 meters to 1 meter, is in a more volatile environment. With less material between the geomaterial and fluid, the graphs demonstrate a steeper slope no matter the fluid temperature. However, the fluid with a constant of 20°C shows the highest values, while the fluid that has been allowed to gather heat while being injected shows relatively lower stress values.

Inner-Middle-Outer Transition Path

Once the fluid wall was examined, the next path that was investigated was the transition from the Inner-Middle-Outer path, which can be seen in the previously mentioned Figure 8. This path is located at a depth of 0.25 meters from the surface. In this region, the temperature of the fluid also plays a more significant role in the stress and strain values. The first casing string is intended to help provide zonal isolation from the fluid and the surrounding environment, as many countries have requirements to prevent contamination in the environment, especially if there is underground safe drinking water. This zonal isolation was also helpful in isolating the heat of the fluid, as the temperature of the fluid quickly approaches the temperature of the well body, which can be seen in Figure 27. It can also be seen that Titanium wasn't as good of an insulation material compared to the cement sheath which can be seen in the steepness of the slopes when the material is metal relative to the titanium.

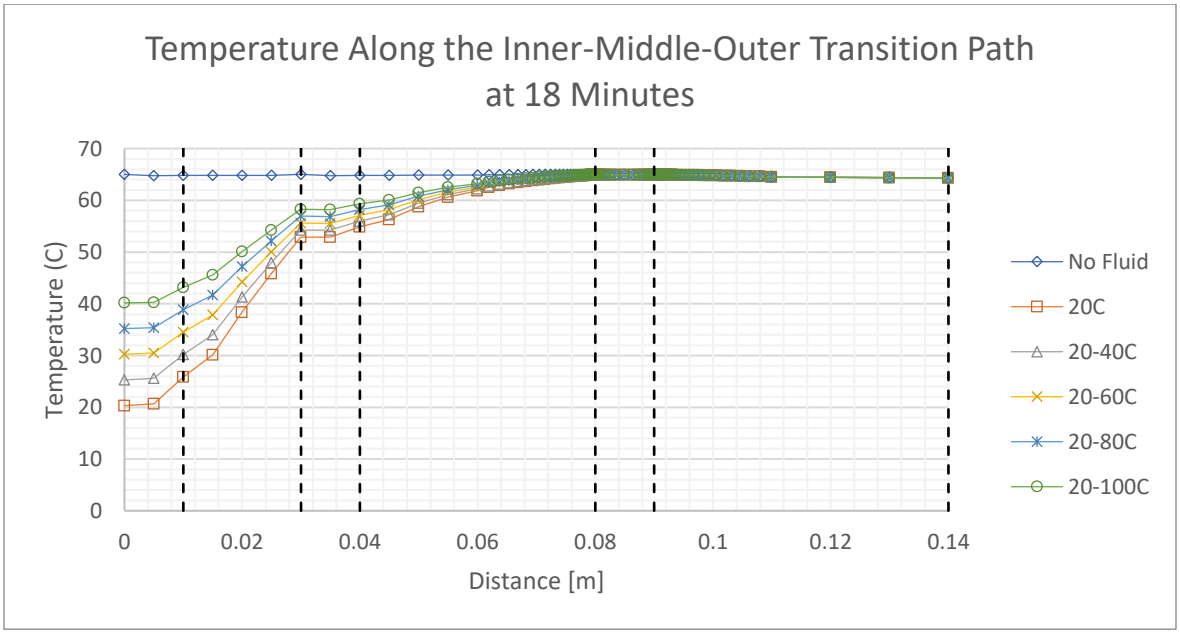

Figure 27: Temperature along the IMO casing string transition path when time is 18 minutes

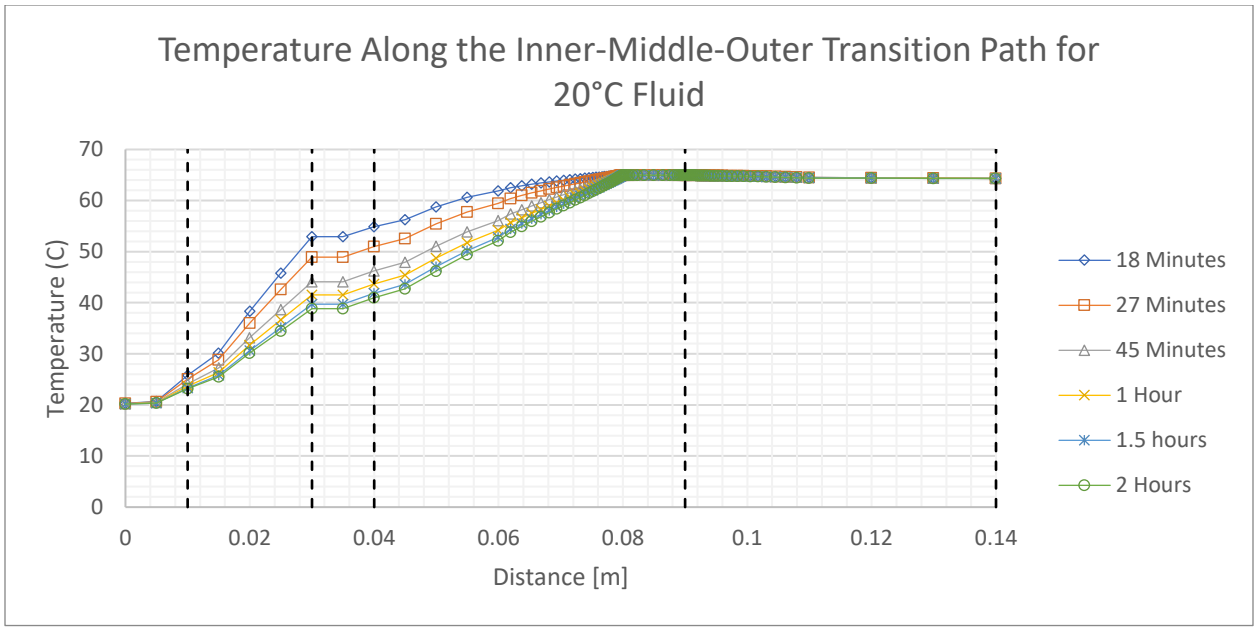

Figure 28: Temperature along the IMO casing string transition path over time for a 20°C working fluid

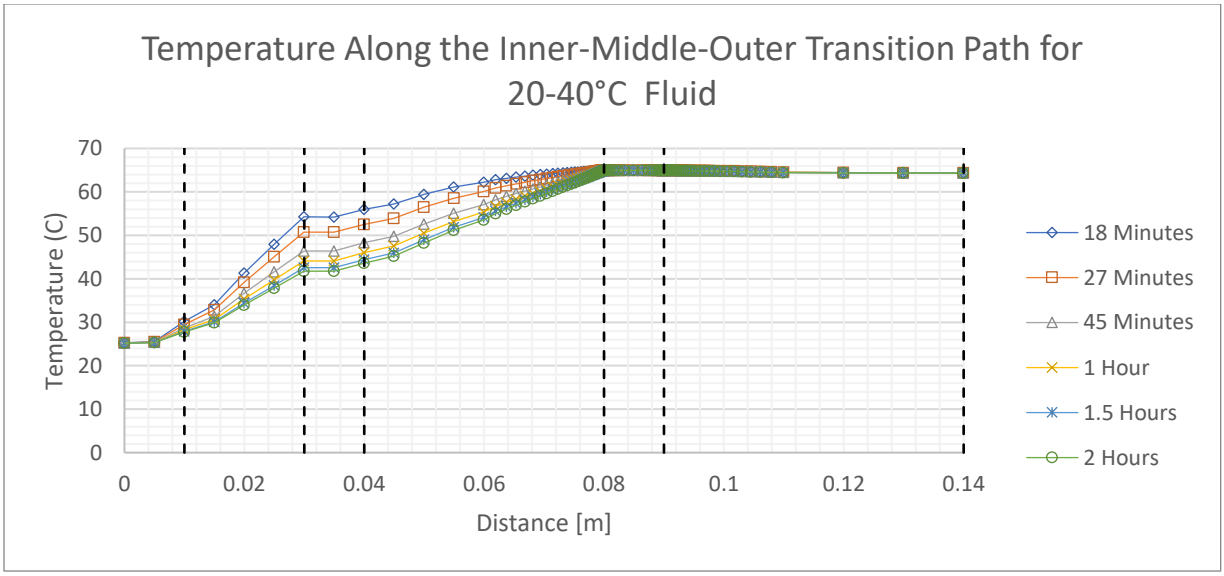

Figure 29: Temperature along the IMO casing string path over time for a 20-40°C working fluid

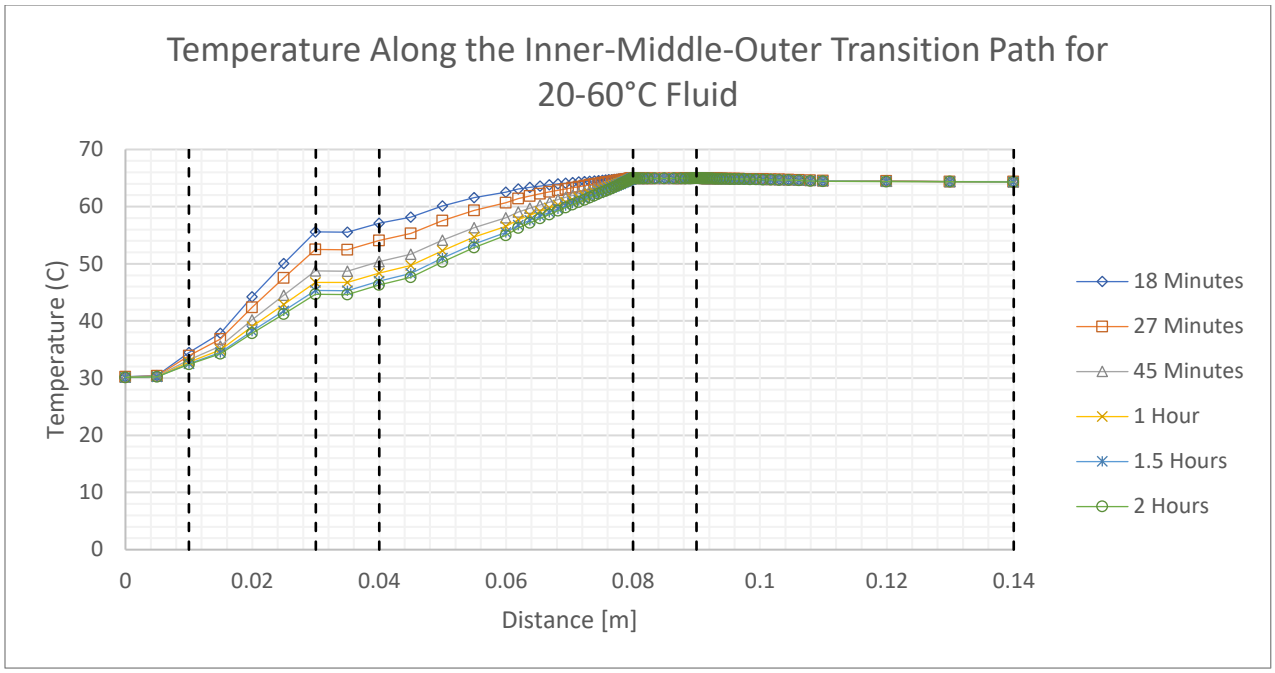

Figure 30: Temperature along the IMO casing string path over time for a 20-60°C working fluid

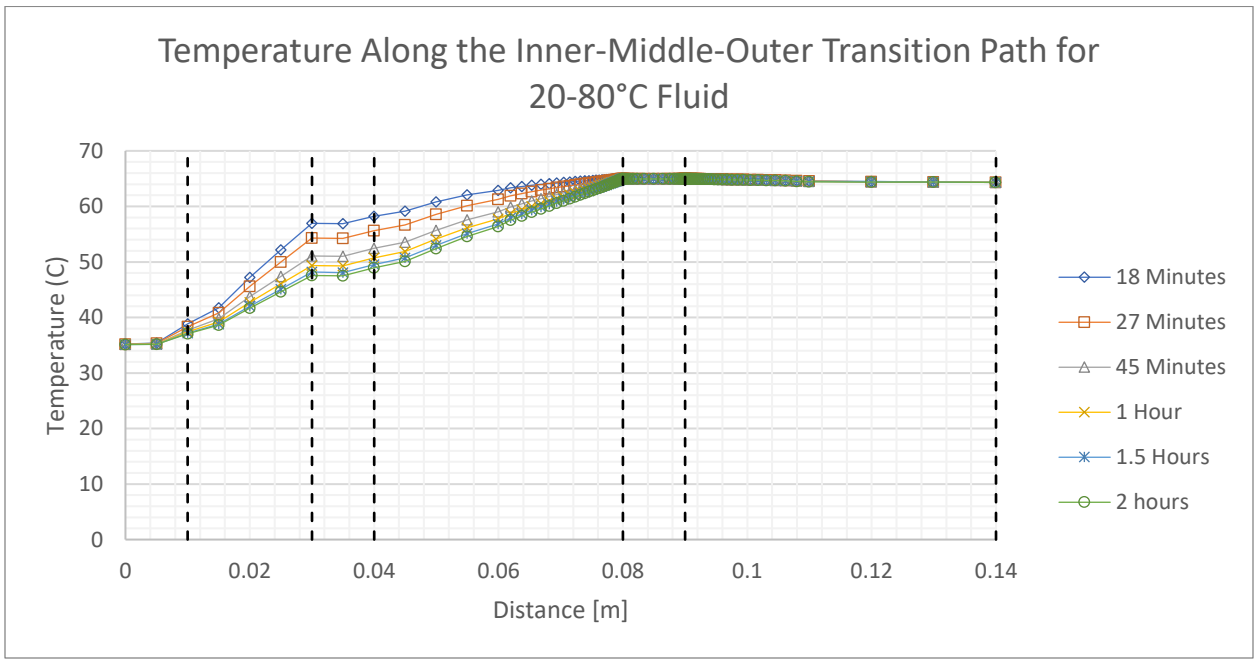

Figure 31: Temperature along the IMO casing string path over time for a 20-80°C working fluid

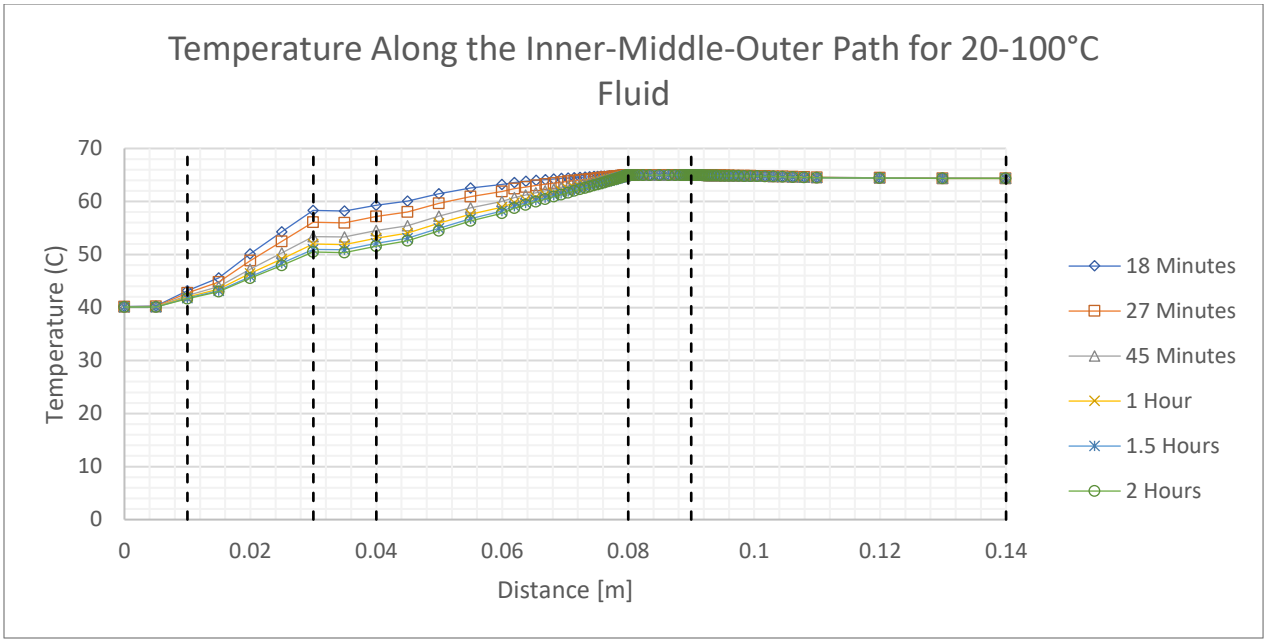

Figure 32: Temperature along the IMO casing string transition path over time for a 20-100°C fluid

Due to the temperatures varying more at the section closer to the fluid wall, the amount of stress and strain experienced by the model was different per loading condition scenario. When considering the strain over time, a similar behavior was seen in the fluid wall was also seen along this path where the strain would fluctuate over time, but would slowly approach a certain slope, the closer the model got to a steady state, which can be seen in the following series of figures.

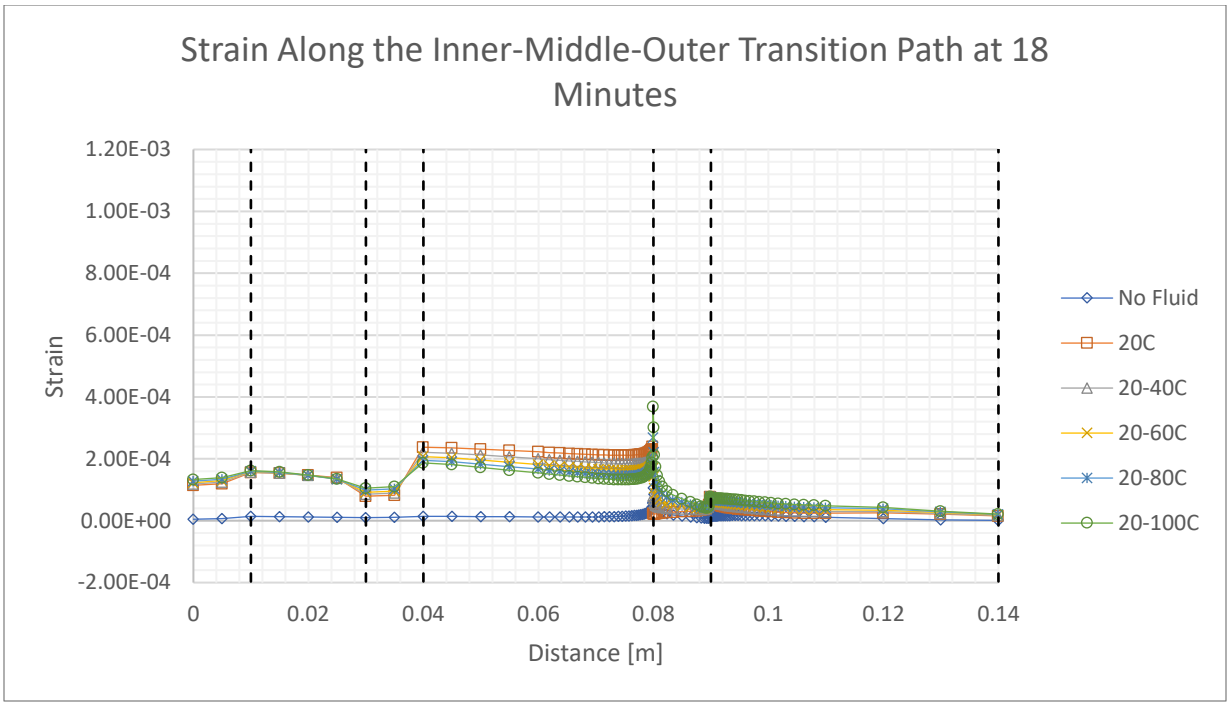

Figure 33: Strain along the Inner-Middle-Outer casing string transition path when time is 18 minutes

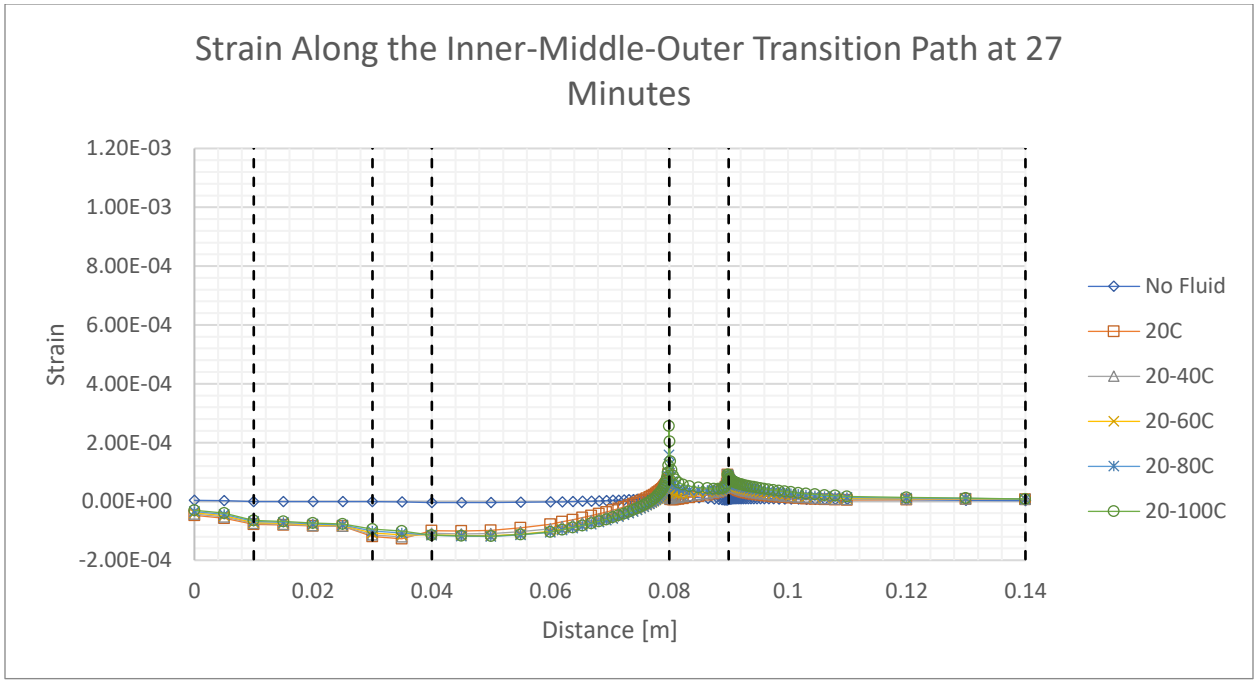

Figure 34: Strain along the Inner-Middle-Outer casing string transition path when time is 27 minutes

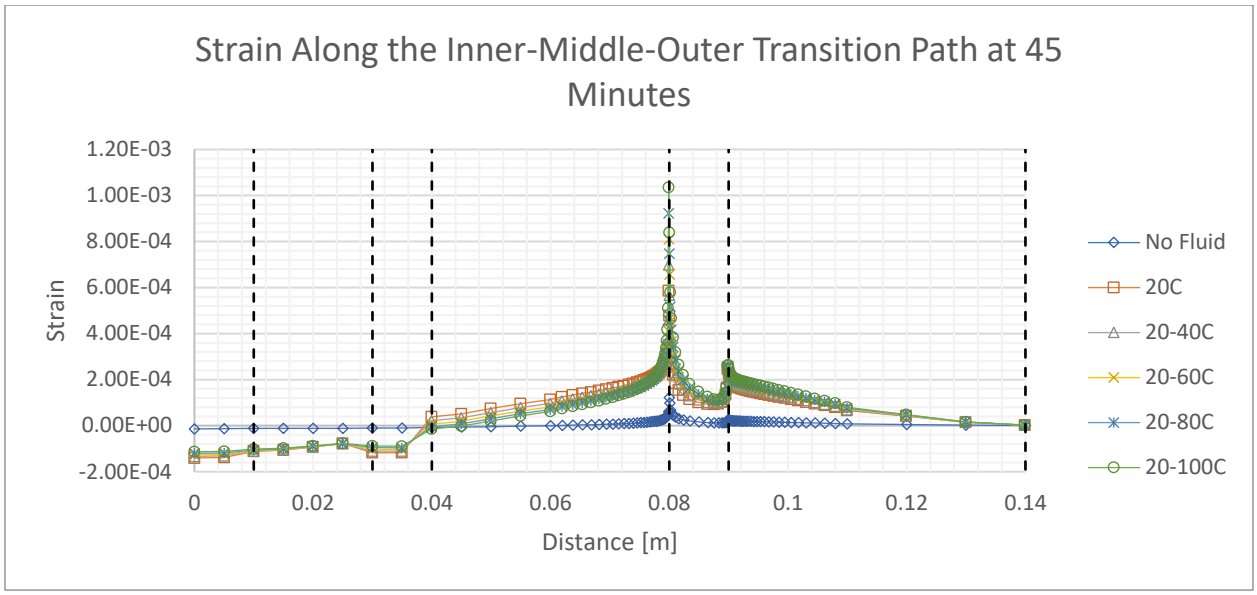

Figure 35: Strain along the Inner-Middle-Outer casing string transition path when time is 45 minutes

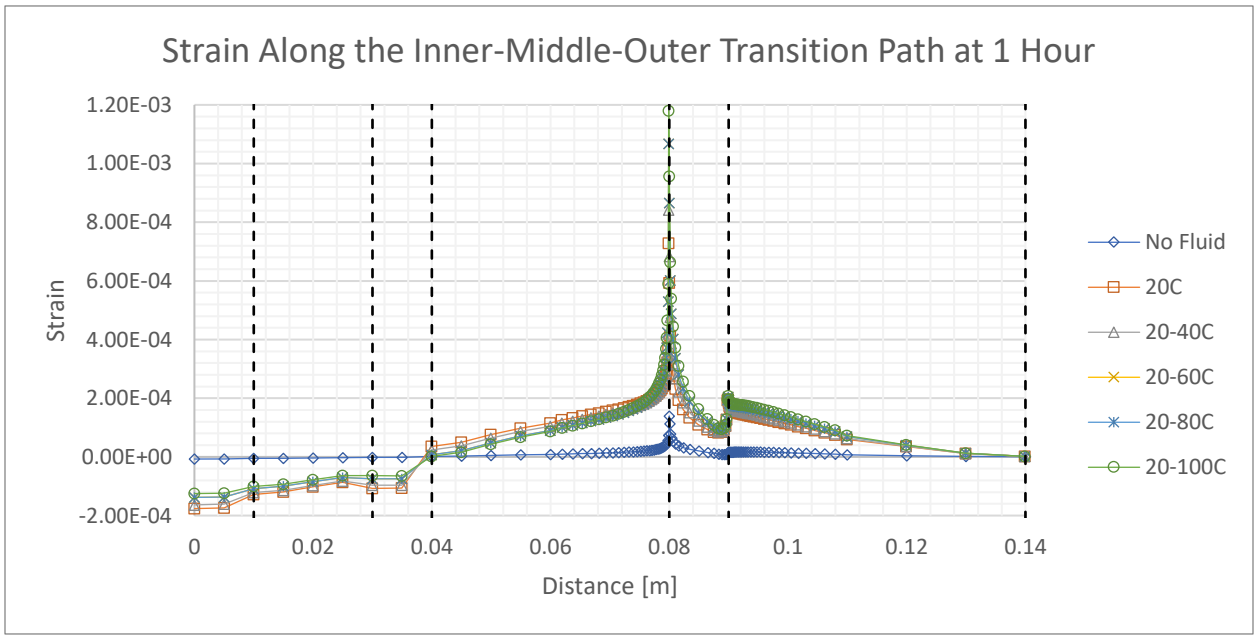

Figure 36: Strain along the Inner-Middle-Outer casing string transition path when time is 1 hour

Furthermore, at 0.8 m from the fluid wall, the strain increases drastically over time. This location is where the outer or surface casing ends. Additionally, the higher-temperature fluid scenarios showed higher peaks at this point compared, such as the 20-100°C having an

approximate value of 1.20E-3 Pa, while the 20-80°C only reached an approximate value of 1.08E-3 Pa. This trend is more noticeable when considering the stress of this region.

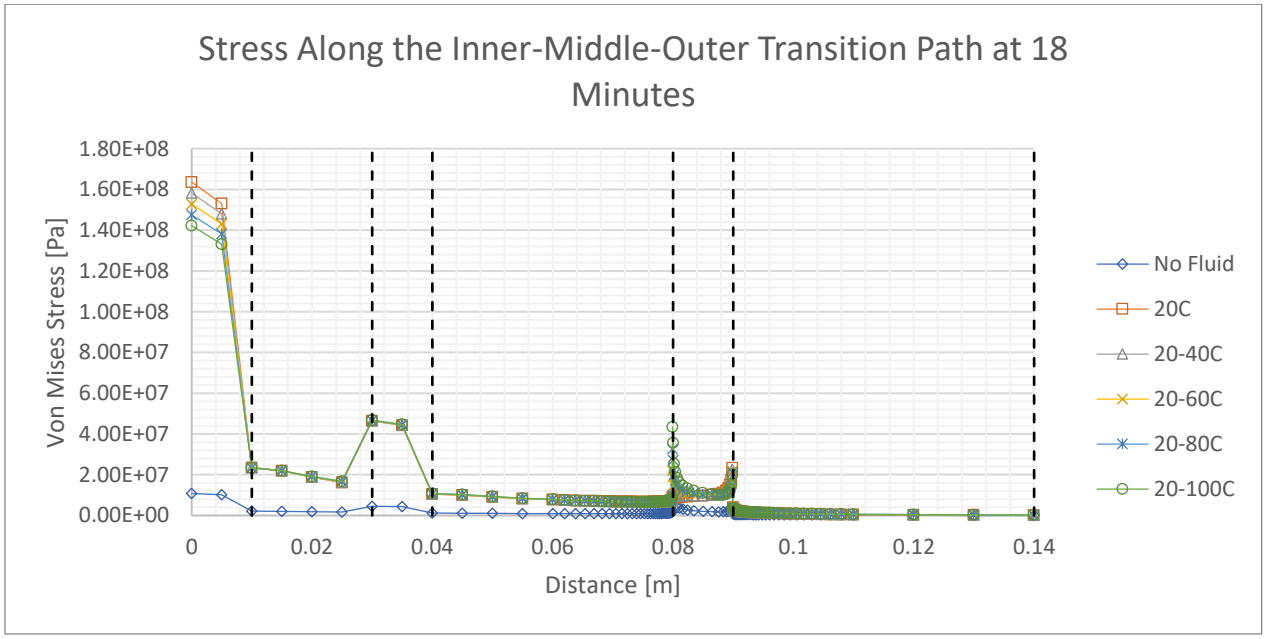

Figure 37: Stress along the IMO casing string transition path when time is 18 minutes

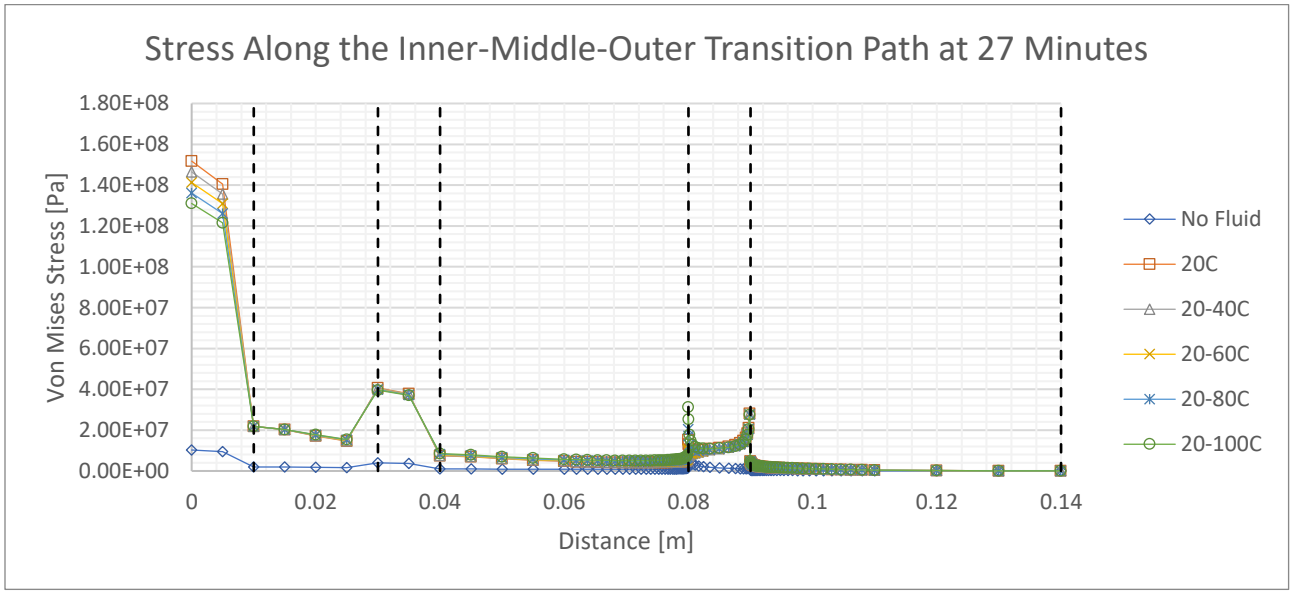

Figure 38: Stress along the Inner-Middle-Outer casing string transition path when time is 27 minutes

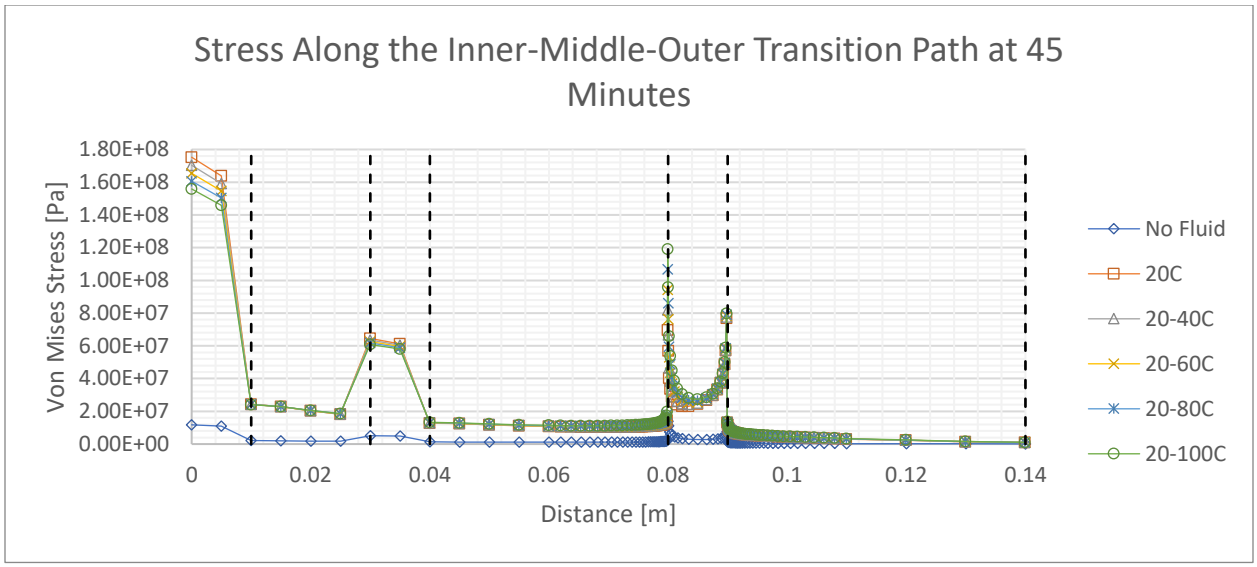

Figure 39: Stress along the Inner-Middle-Outer casing string transition path when time is 45 minutes

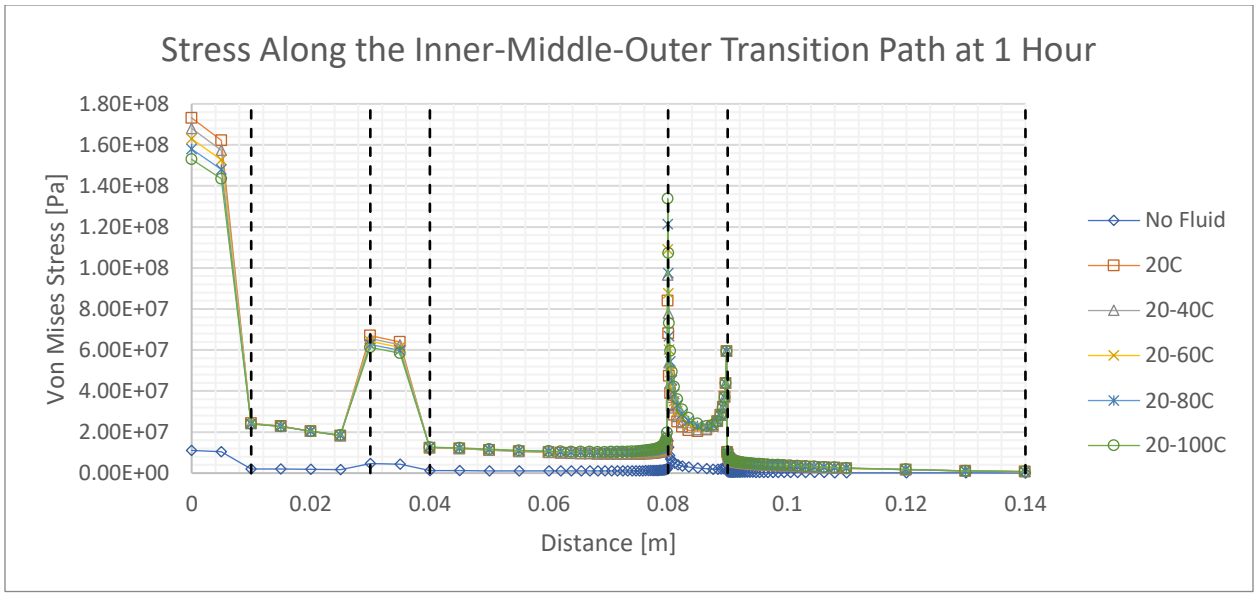

Figure 40: Stress along the Inner-Middle-Outer casing string transition path when time is 1 hour

In these figures shown above, the trends previously mentioned are more discernible, where the cement and metal casings carry the stress and strain differently the further away from the fluid wall. Additionally, the fluid wall area, where the first metal casing is, shows a greater value of stress compared to the rest of the structure, but slowly decreases. The fluid as shown in previous

sections in this chapter, shows that the temperature of the fluid plays a major role in the structure, more than the lateral earth pressure does. Furthermore, as seen with the strain graphs, as time increases, the stress at the bottom of the outer metal casing that contacts the intermediate casing increases. Similarly, the higher-temperature fluid scenario experiences a higher peak in comparison to the lower-temperature fluids, such as the 20-100°C with a peak of approximately 1.38E8 Pa and the 20-40°C having a peak of approximately 9.8E7 Pa at 1 hour. However, after the 1-hour mark the relatively higher peak at 1.5 and 2 hours, the peaks start decreasing in height over time, this can be seen in the figures below.

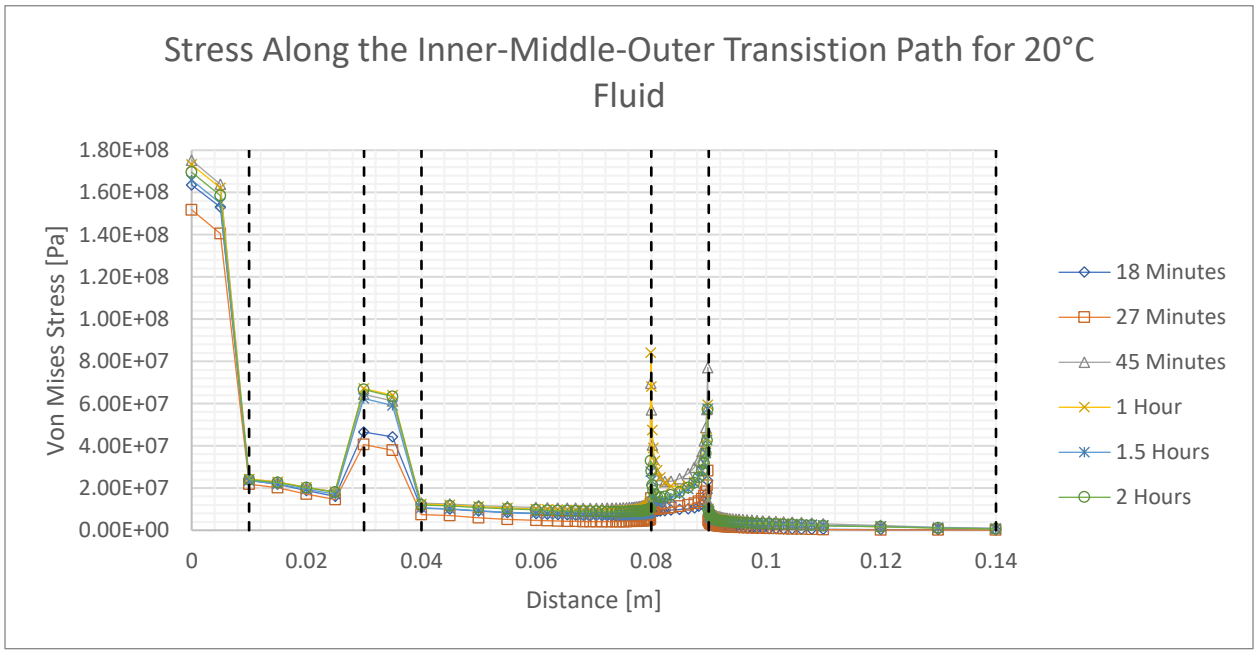

Figure 41: Stress along the Inner-Middle-Outer transition path over time for a 20°C fluid

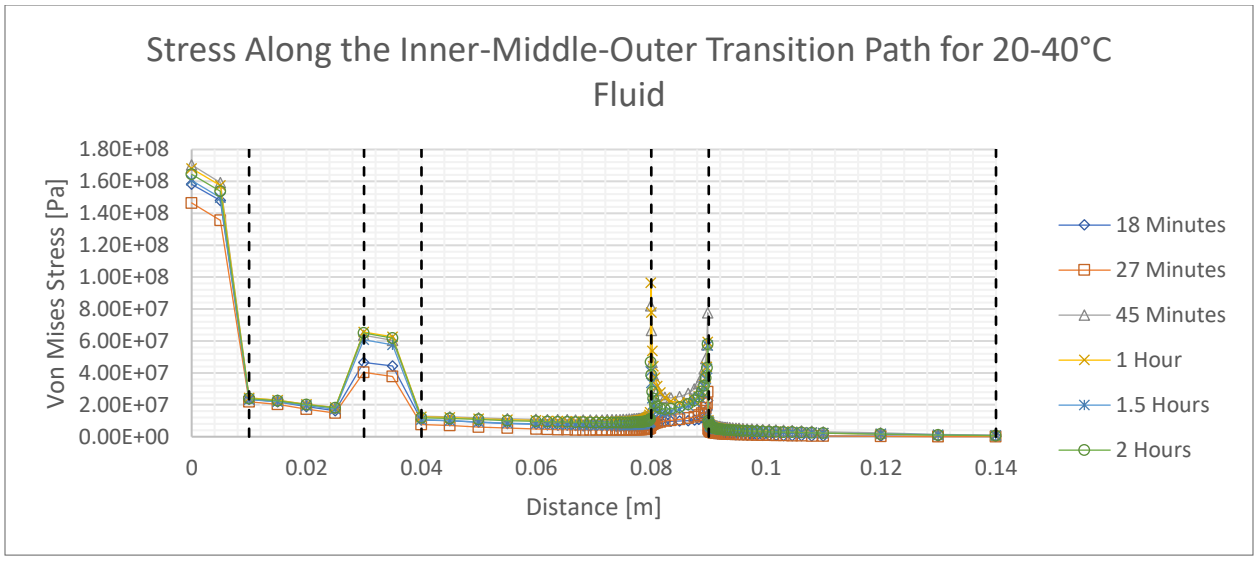

Figure 42: Stress along the Inner-Middle-Outer transition path over time for a 20-40°C fluid

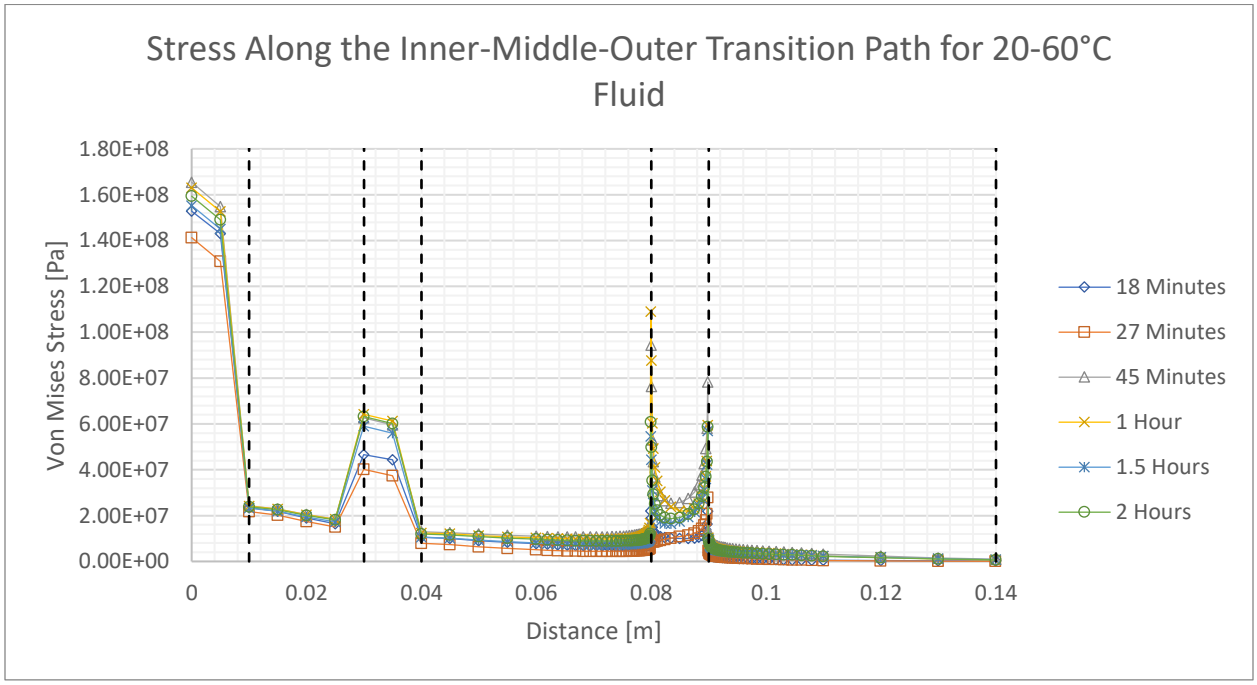

Figure 43: Stress along the Inner-Middle-Outer transition path over time for a 20-60°C fluid

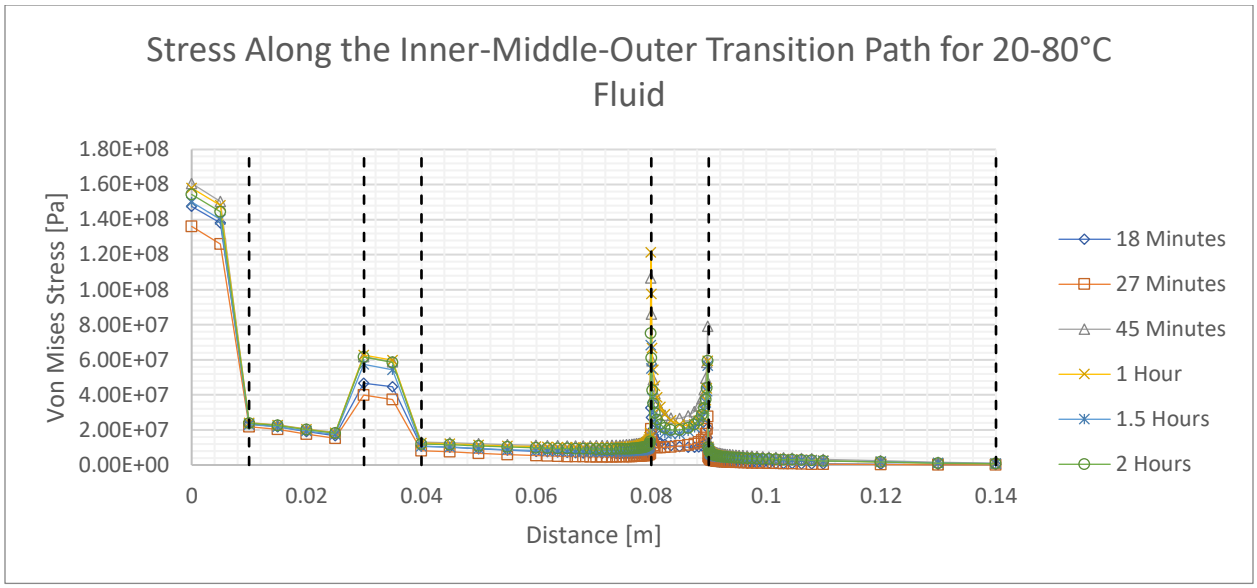

Figure 44: Stress along the Inner-Middle-Outer transition path over time for a 20-80°C fluid

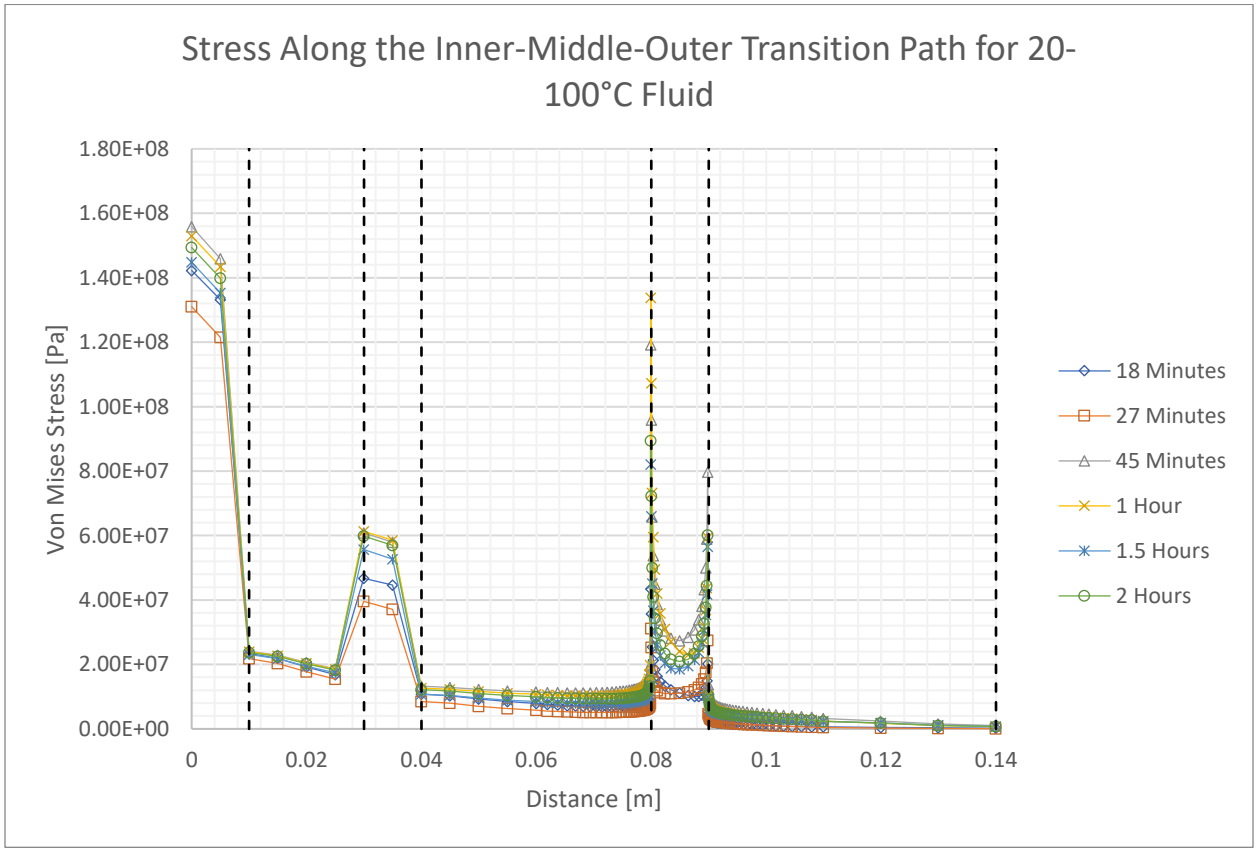

Figure 45: Stress along the Inner-Middle-Outer transition path over time for a 20-100°C fluid

Just like the strain graphs, there is a fluctuation in the amount of stress the path experiences over time, where the initial value is high, then at the 27-minute mark, there is a relatively lower amount. After this period, at the 45-minute mark, the highest amount of stress is seen at a section of the well that contacts the fluid wall (0-0.01 m) and then slowly decreases over time, as the well reaches a steady state. This can also be seen in the metal casing section for the intermediate casing that lies from 0.02-0.04 m area in the graph.

Inner-Middle Transition Path

This region is where the intermediate casing string ends, and is located 0.5 m below the surface, which can be seen in the previously mentioned figure. Since this is deeper into the subsurface, the conditions are relatively more volatile than the last path, where there is a slightly higher lateral earth pressure and temperature. With less material in this section, a steady state was also seen to have occurred at a faster rate in this region, to where it was achieved before the 18-minute mark which can be seen in the following graphs.

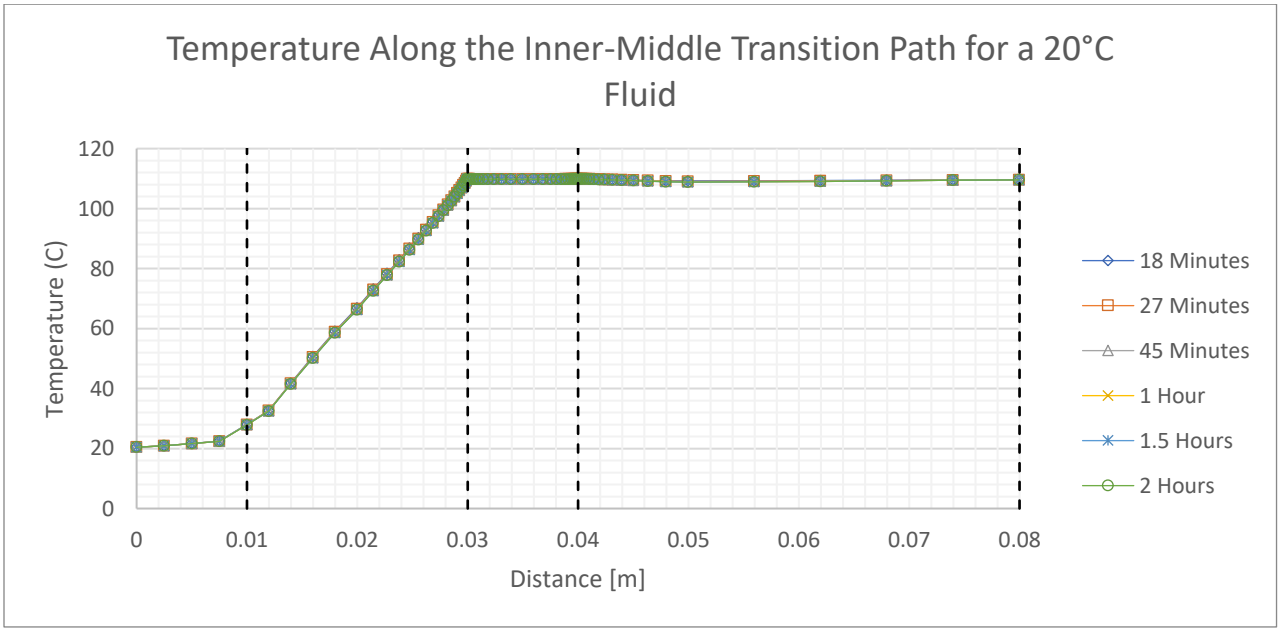

Figure 46: Temperature along the Inner-Middle path over time for a 20°C fluid

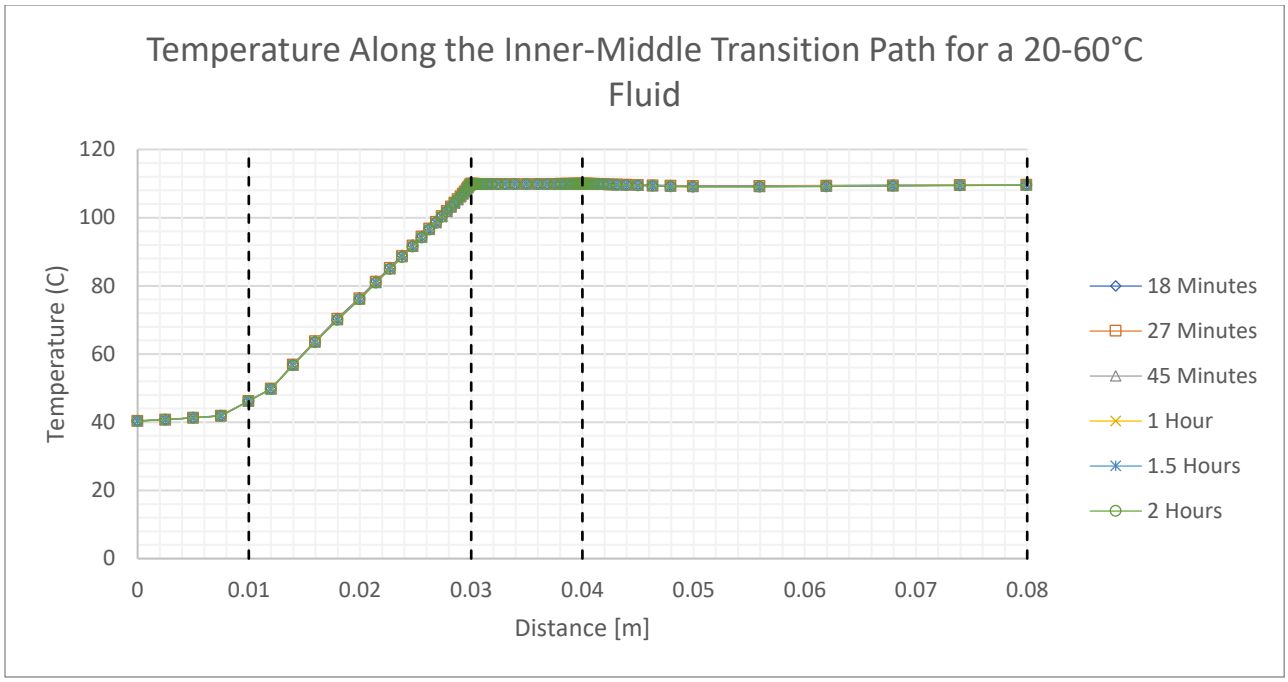

Figure 47: Temperature along the Inner-Middle path over time for a 20-60°C fluid

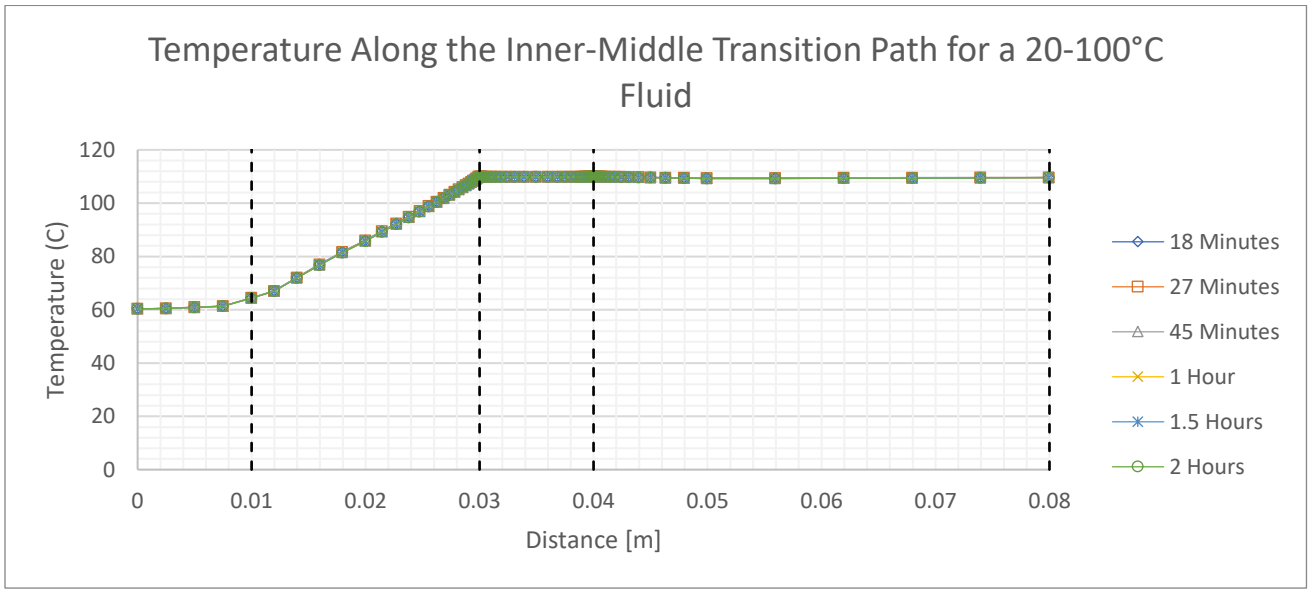

Figure 48: Temperature along the Inner-Middle path over time for a 20-100°C fluid

While the steady state in each of the temperature scenarios was achieved at a faster rate, each fluid temperature condition had varying steepness in the slopes following the path to the

subsurface material. A comparison of the temperature inside the well body structure at a time of 18 minutes can be seen below.

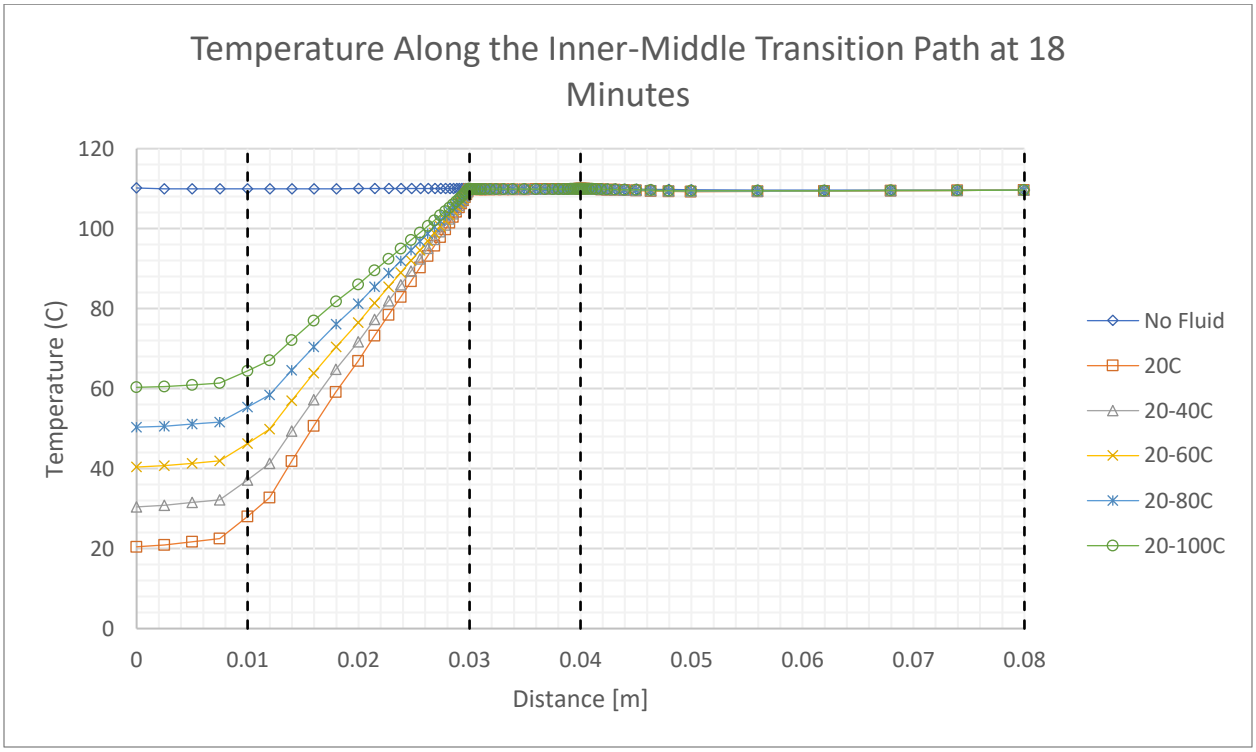

Figure 49: Temperature along the Inner-Middle transition path at 18 minutes

Just like the Inner-Middle-Outer Casing path, the Inner-Middle casing shows that the thermal loads played a larger role in applying stress and strain to the structure than the lateral earth and fluid pressure does, while also showing that the bottom of the metal casing is a vulnerable point of concern due to an increasing amount of stress and strain at this point. The intense drop-off or increase when going across the path of the well is commonly seen at the contact point between the metal casing and cement sheath surfaces. Over time, as seen in Figures 50, 51, 52, and 53, the same fluctuating behavior can be seen again, showing that an interesting phenomenon is occurring as the stress and strain are continuously changing even after a steady state is achieved within the region.

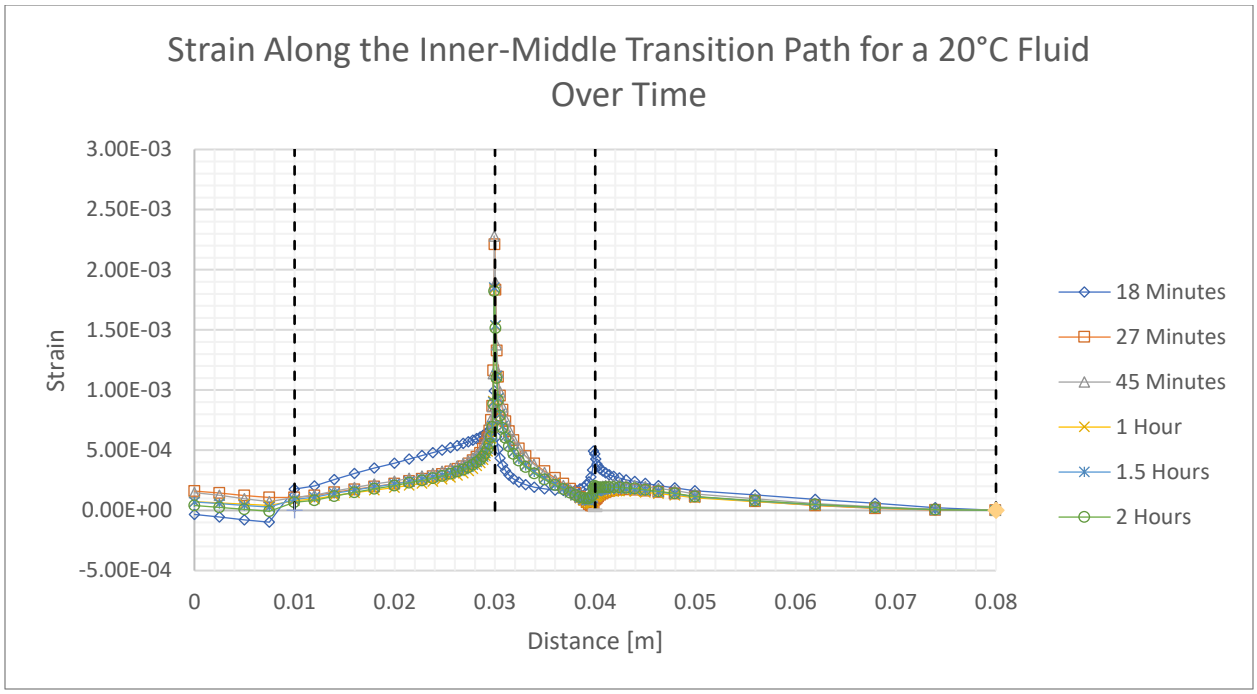

Figure 50: Strain along the Inner-Middle Transition Path for a 20°C fluid

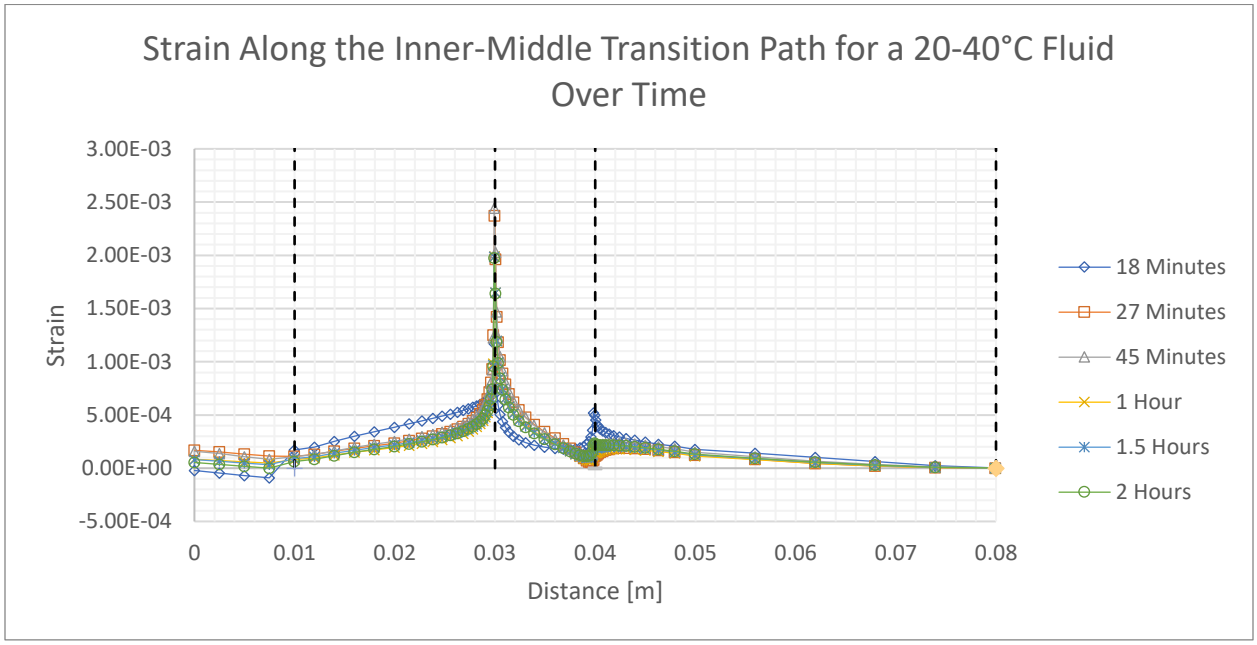

Figure 51: Strain along the Inner-Middle Transition Path for a 20-40°C fluid

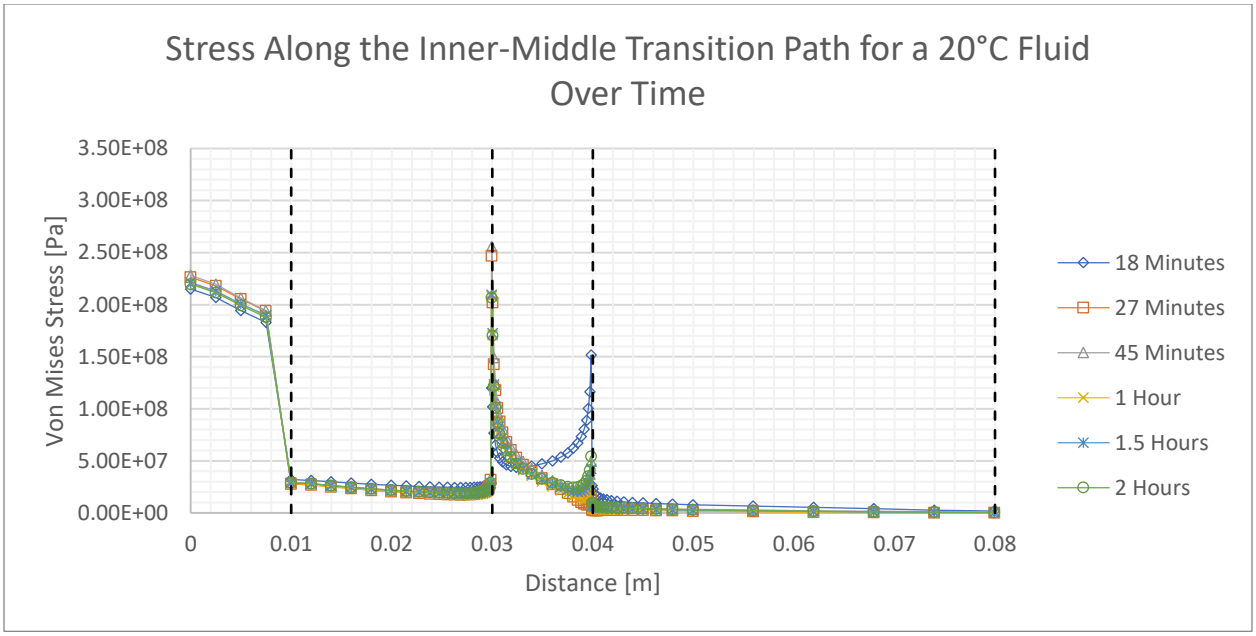

Figure 52: Stress along the Inner-Middle Transition Path for a 20°C fluid

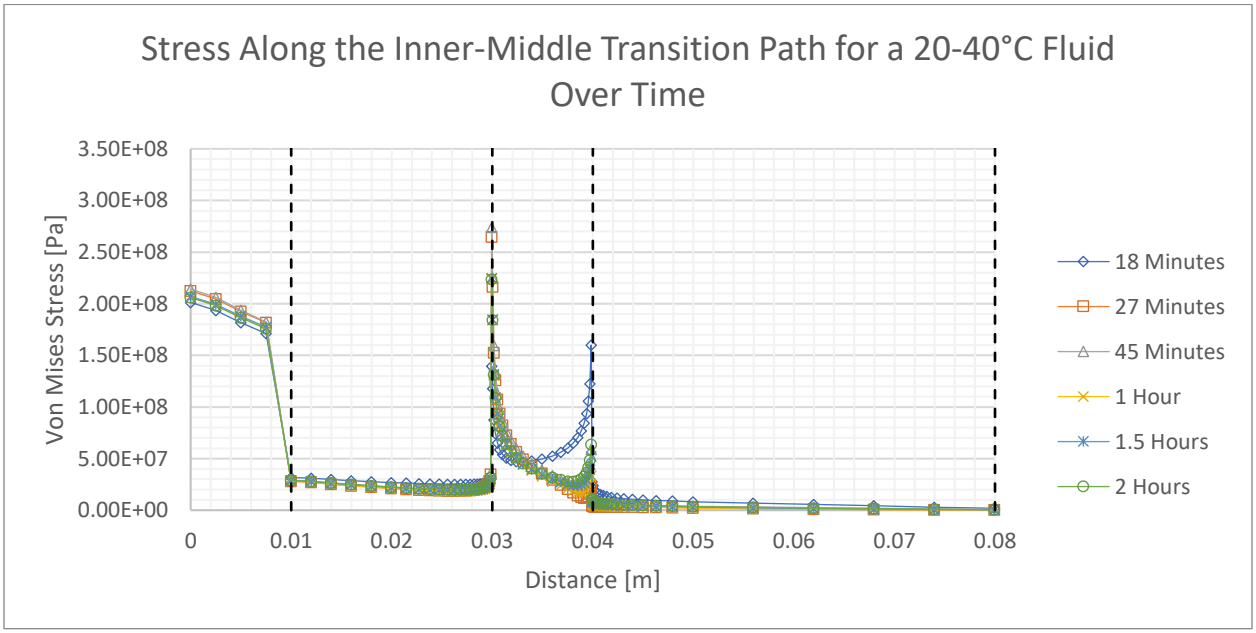

Figure 53: Stress along the Inner-Middle Transition Path for a 20-40°C fluid

Additionally, the colder fluid doesn't have as large of a peak in the stress or strain at the 0.03 and 0.04 m mark relative to the higher temperature scenarios. Also, it does show that a colder

fluid temperature will experience a substantially larger amount of stress and a smaller amount of strain at the region that is in contact with the fluid wall, or the 0-0.01 m area on the graph.

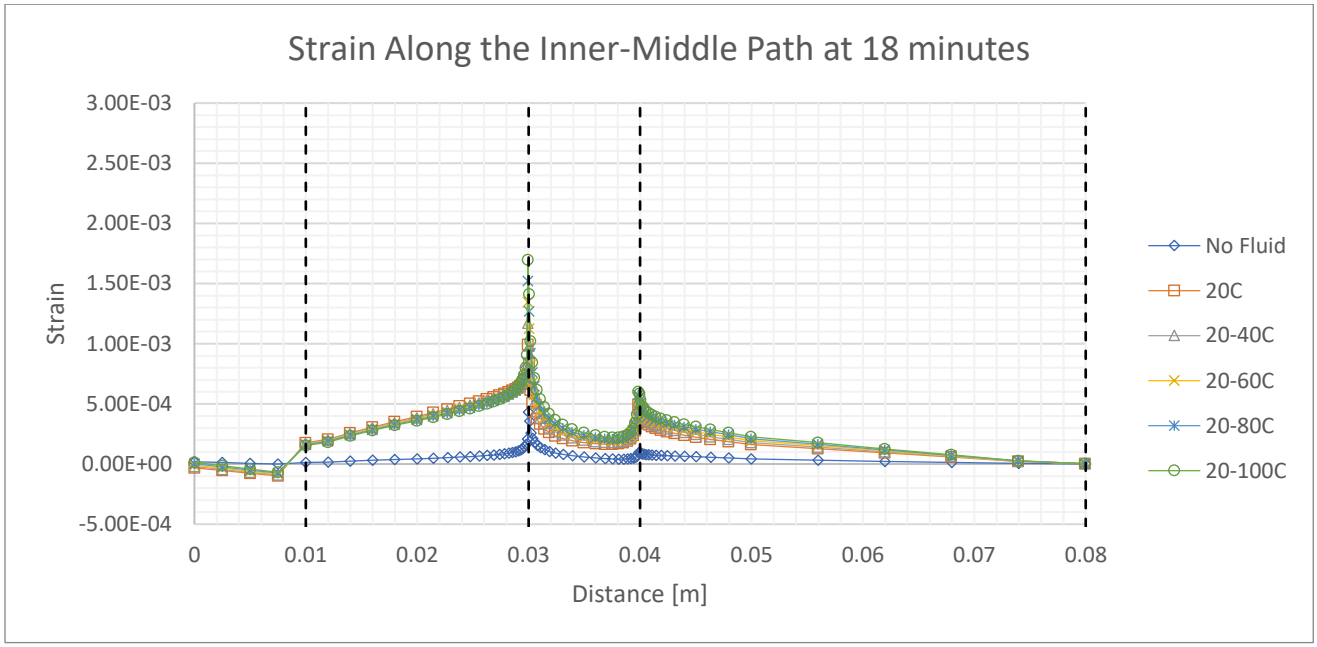

Figure 54: Strain along the Inner-Middle path at 18 minutes

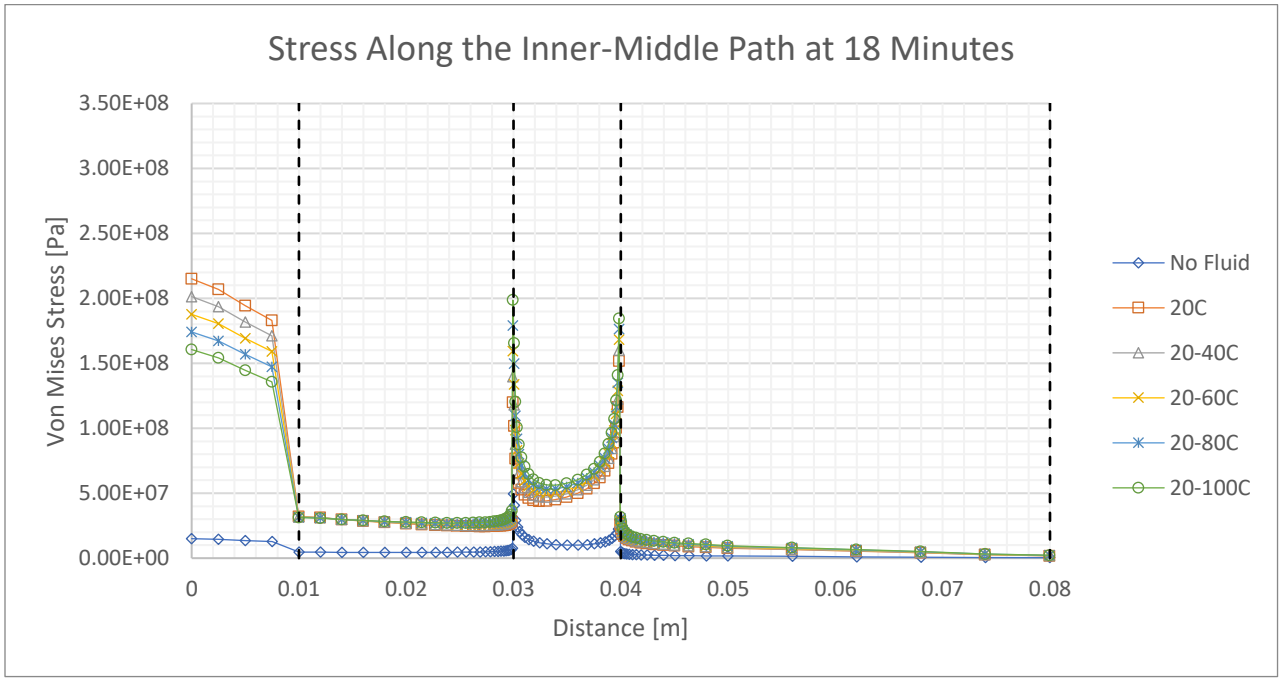

Figure 55: Stress along the Inner-Middle path at 18 minutes

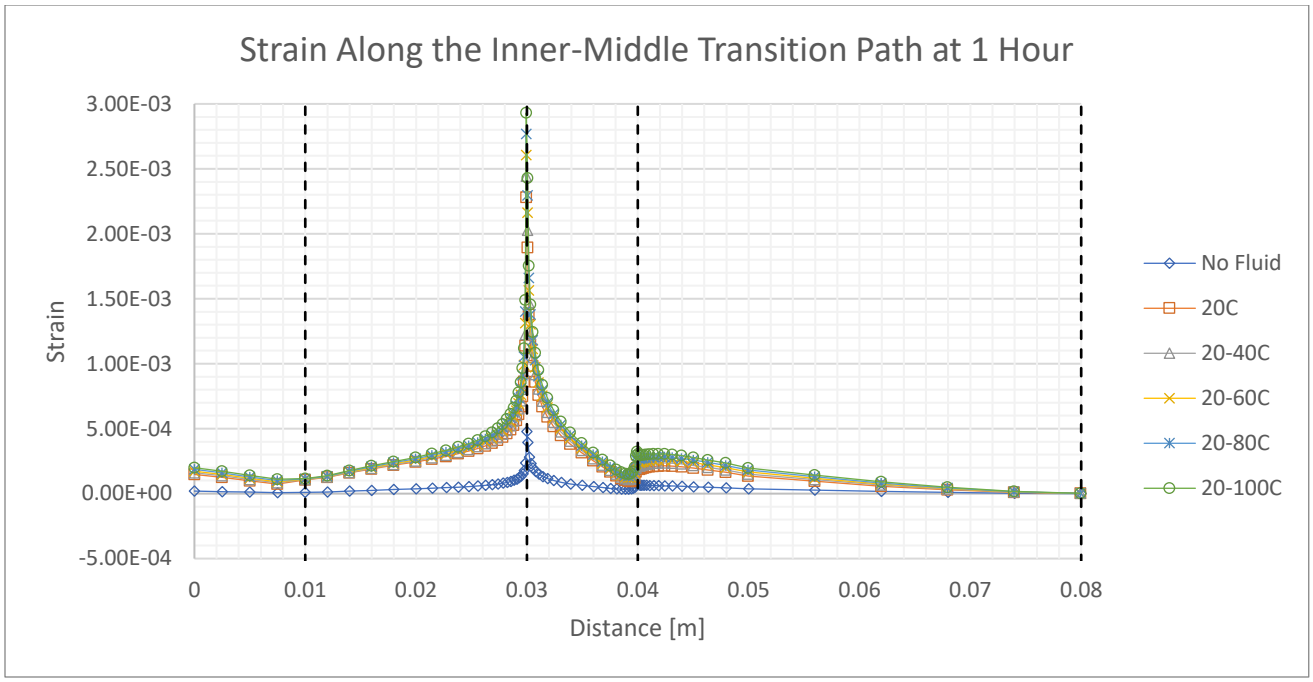

Figure 56: Strain along the Inner-Middle Path at 1 Hour

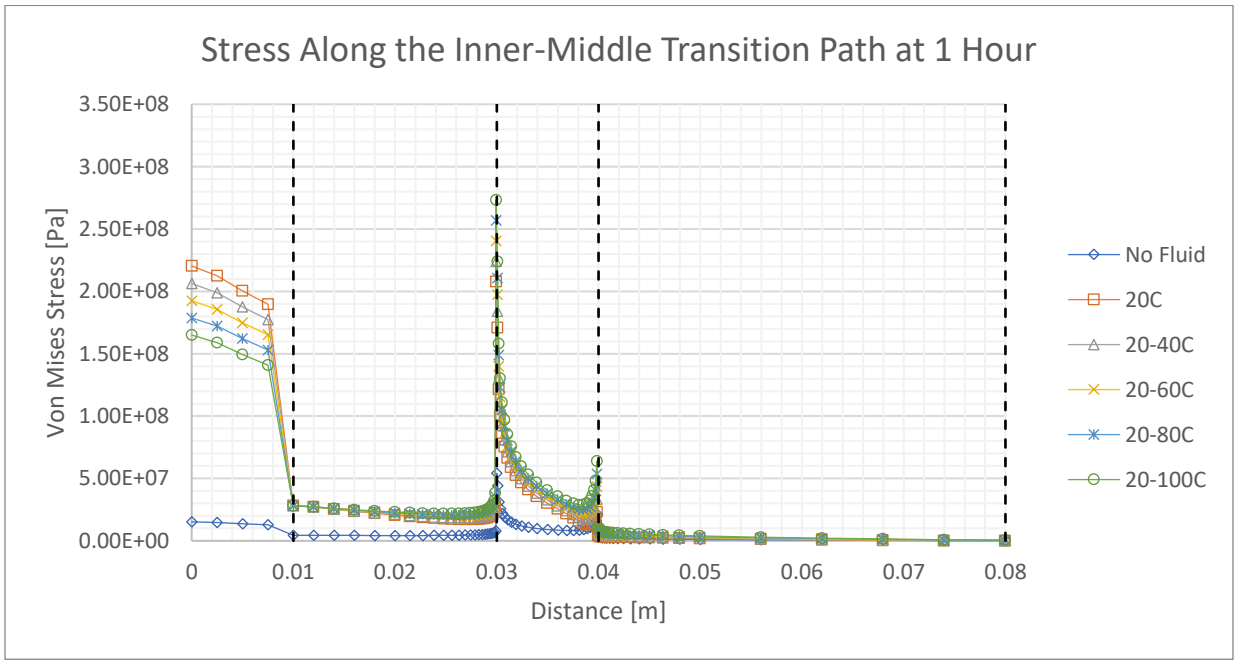

Figure 57: Stress along the Inner-Middle path at 1 hour

Hot Rock Zone Path

In this region, compared to the IMO and IM, and the entirety of the rest of the structure, the HRZ path exists in the most volatile conditions for this model, where the temperature and pressure are at their highest at the bottom of the production casing is right outside the target reservoir. Here, a steady state was achieved extremely quickly, but the large temperature difference between the fluid and the well body showed extremely high levels of stress and strain in the structure in all five thermal conditions.

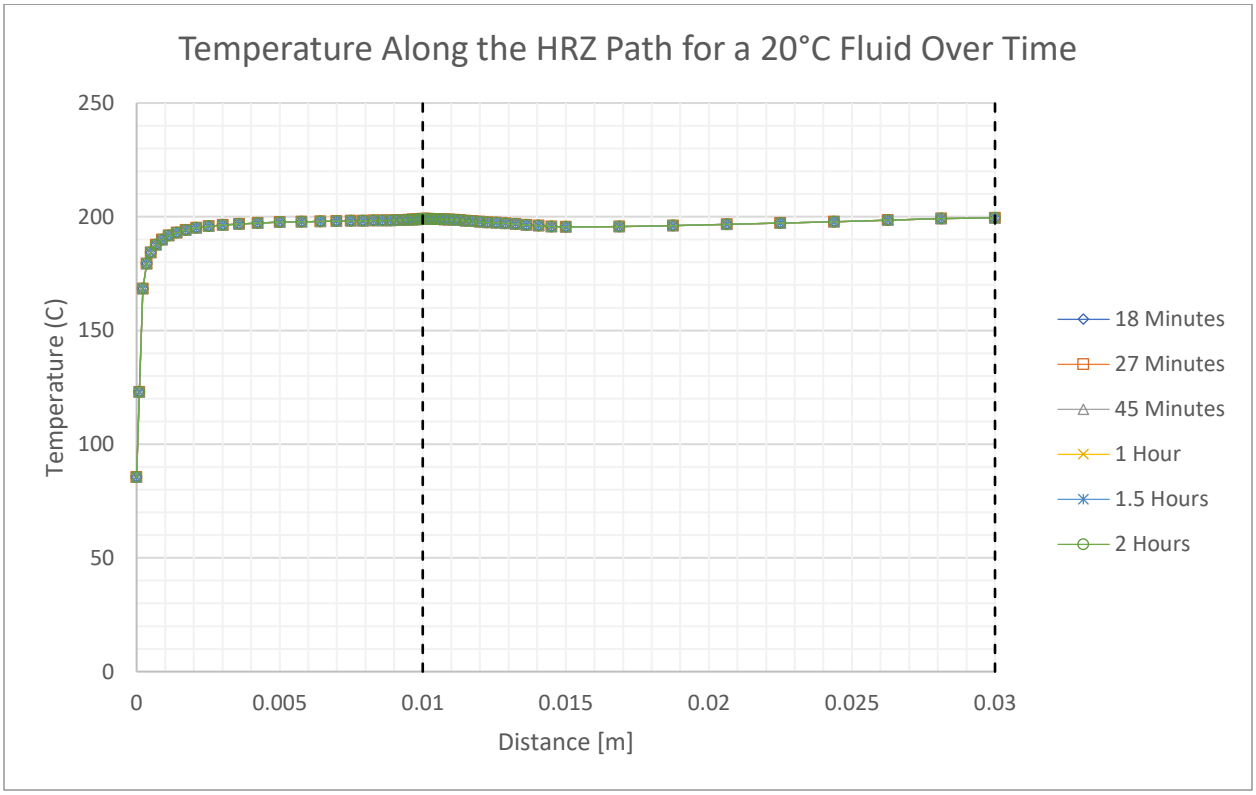

Figure 58: Temperature along the HRZ path for a 20°C fluid over time

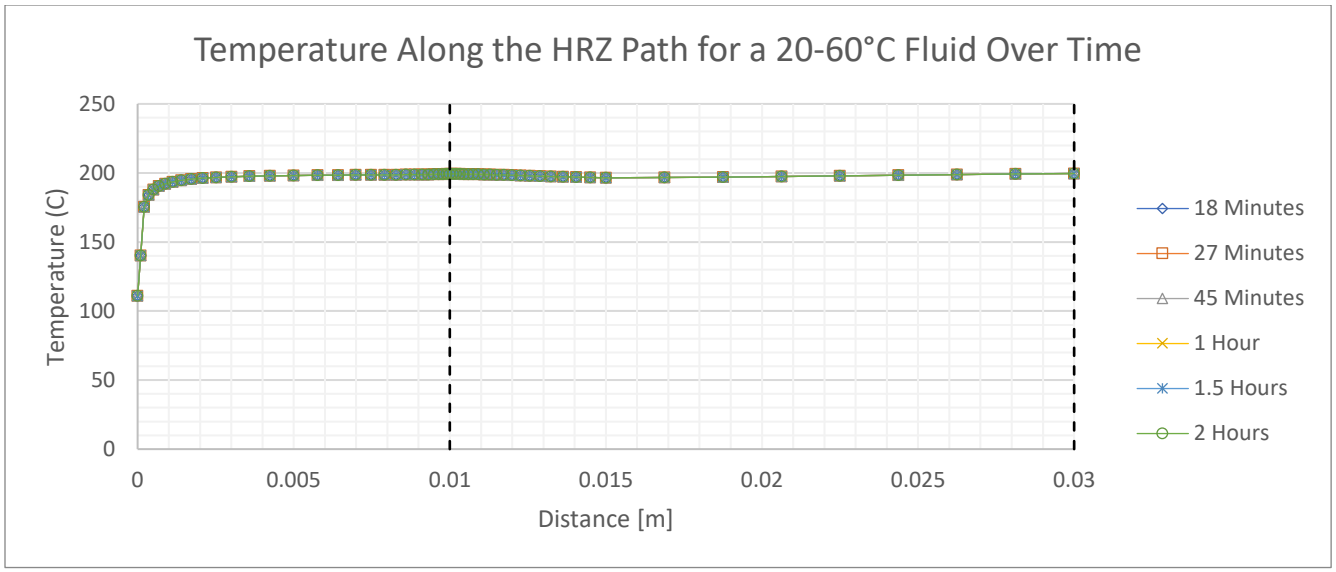

Figure 59: Temperature along the HRZ path for a 20-60°C fluid over time

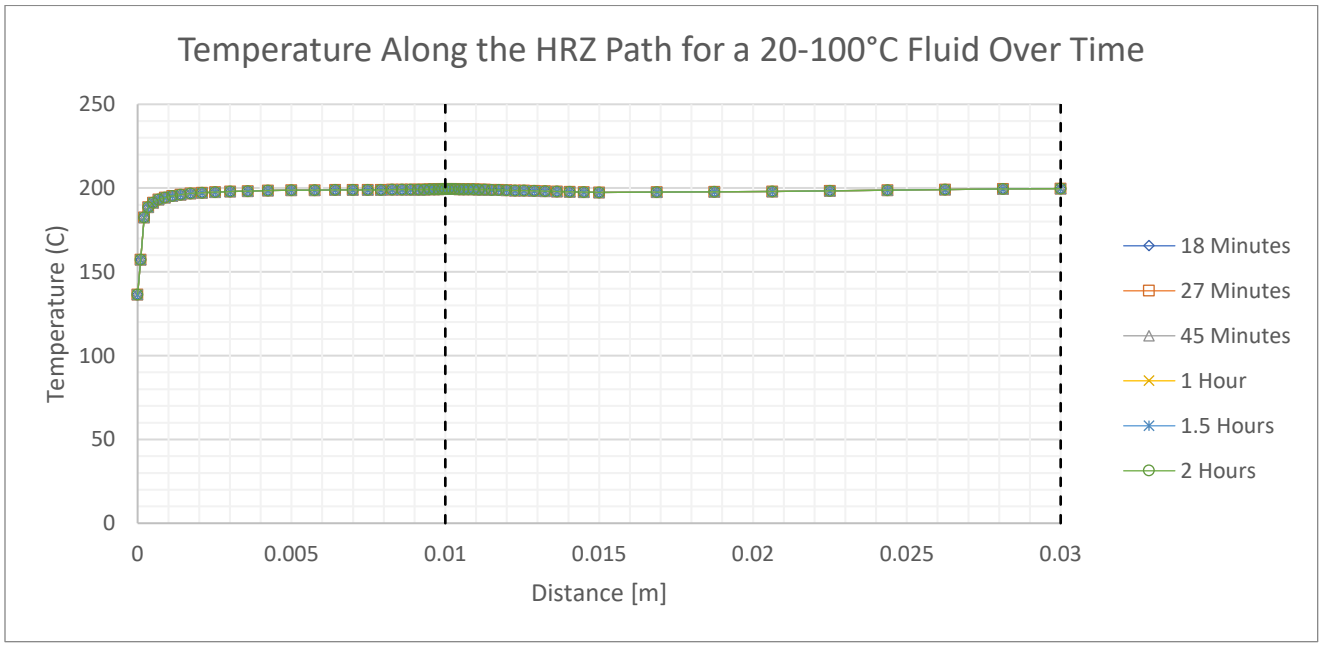

Figure 60: Temperature along the HRZ path for a 20-100°C fluid over time

While a steady state was achieved quickly, in contrast to the other regions, the shear and stress of the path experienced minimal changes as time passed, as seen in some of the figures below.

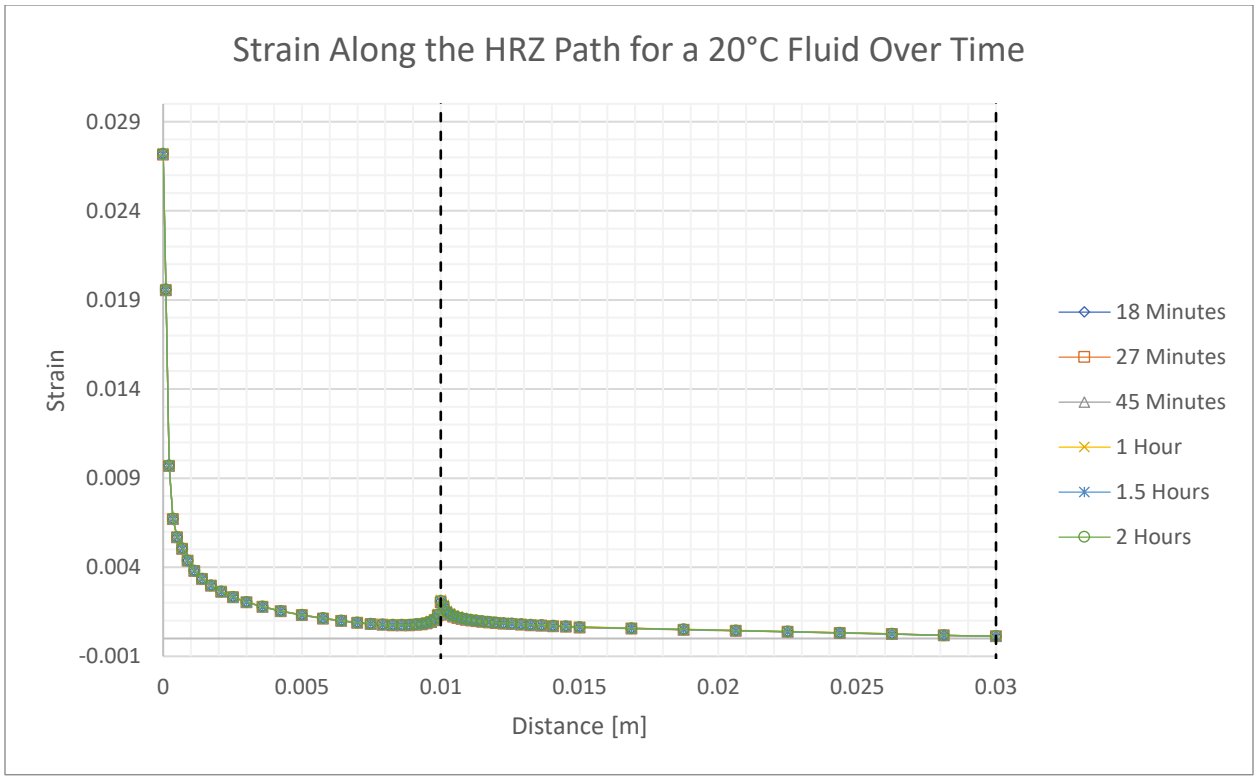

Figure 61: Strain along the HRZ path for a 20°C fluid over time

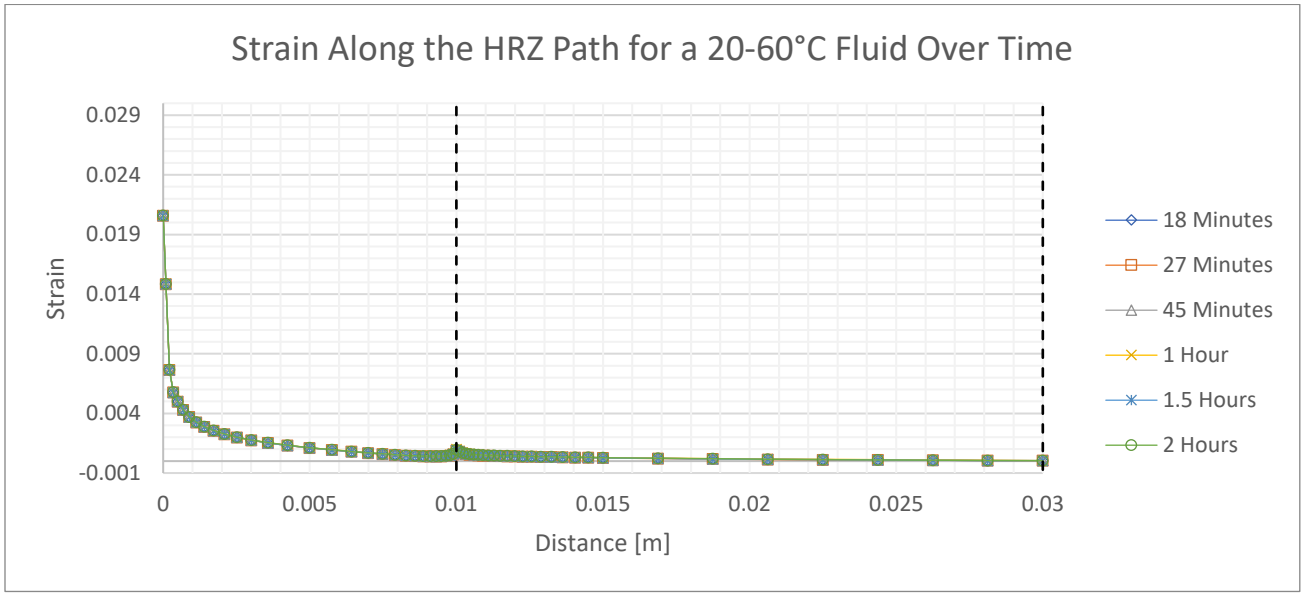

Figure 62: Strain along the HRZ path for a 20-60°C fluid over time

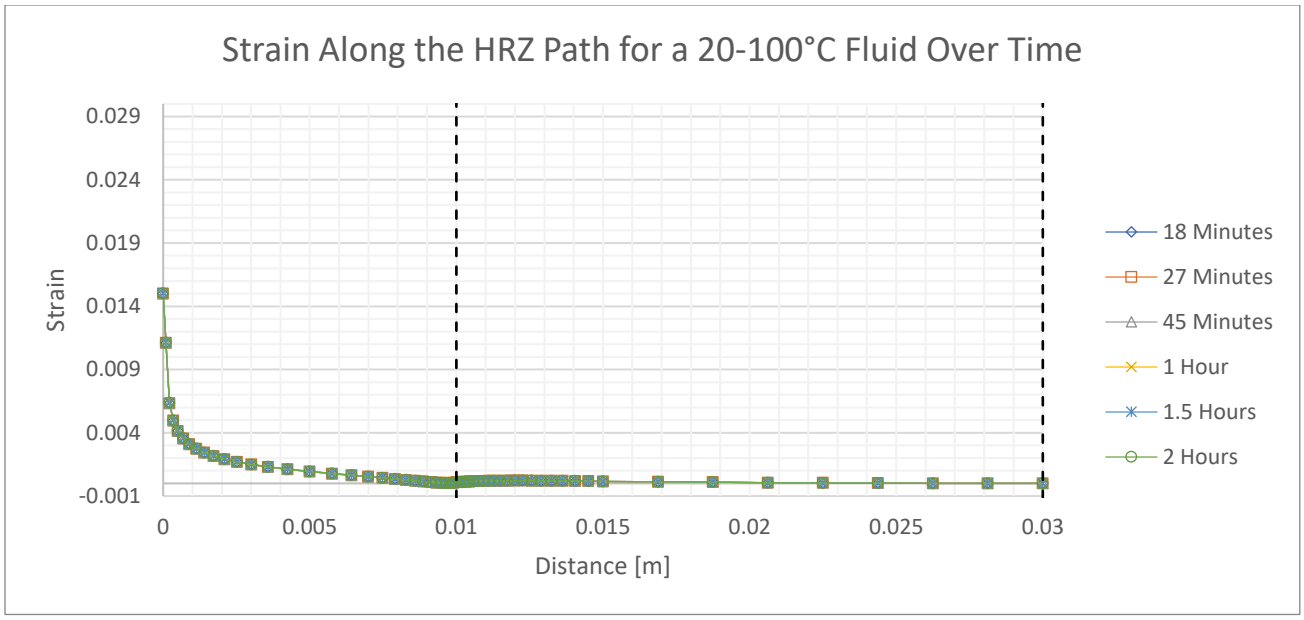

Figure 63: Strain along the HRZ path for a 20-100°C fluid over time

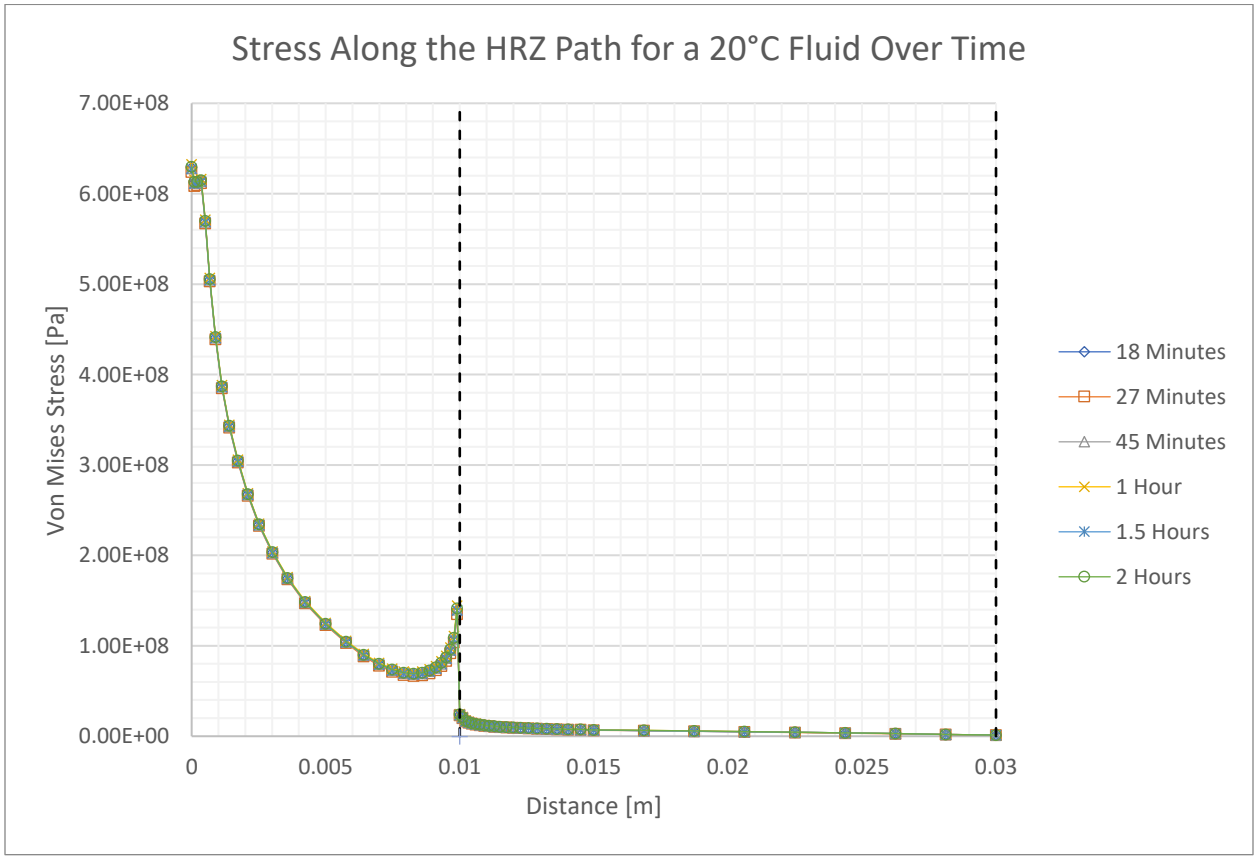

Figure 64: Stress along the HRZ path for a 20°C fluid over time

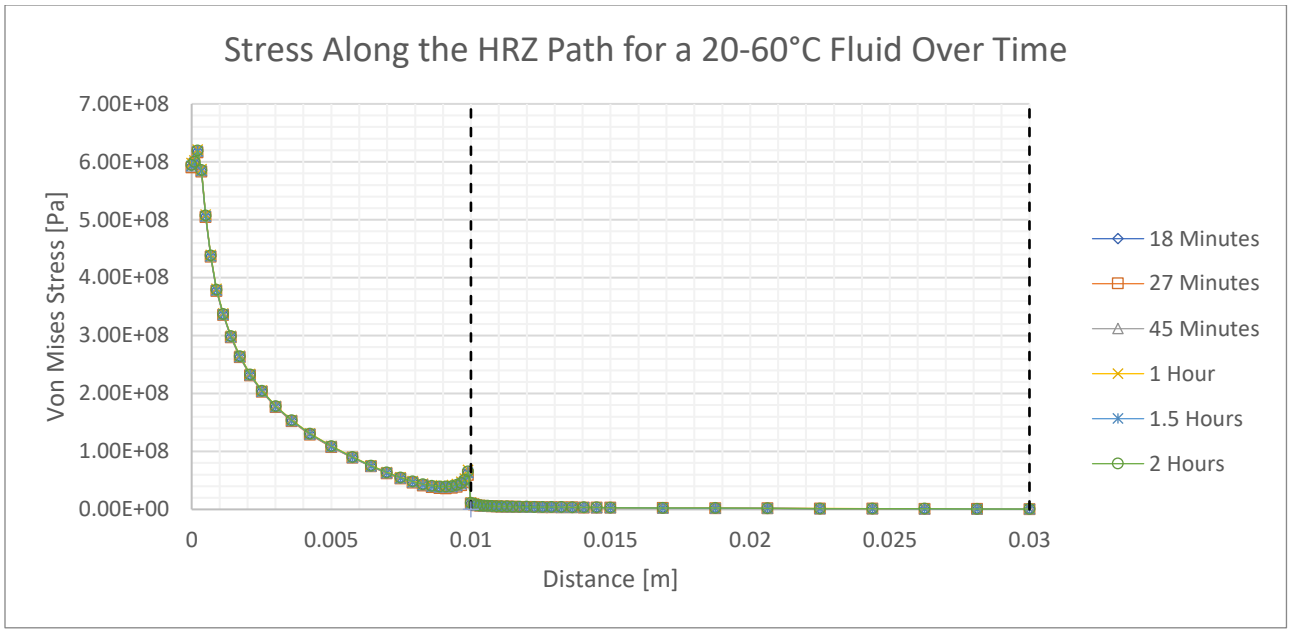

Figure 65: Stress along the HRZ path for a 20-60°C fluid over time

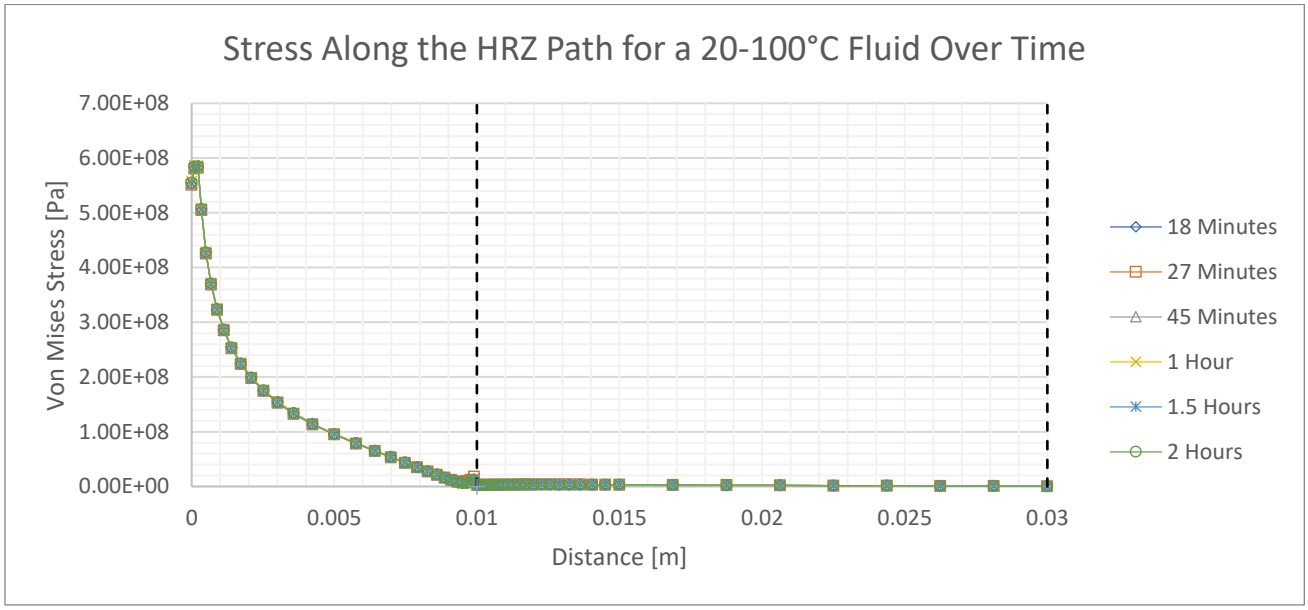

Figure 66: Stress along the HRZ path for a 20-100°C fluid over time

However, as previously mentioned, since the well structure temperature in this region before the fluid is approximately 200°C, the temperature of the working fluid determines how much stress and strain this region will experience. This is especially true since there is little zonal isolation from the surrounding subsurface material and the well.

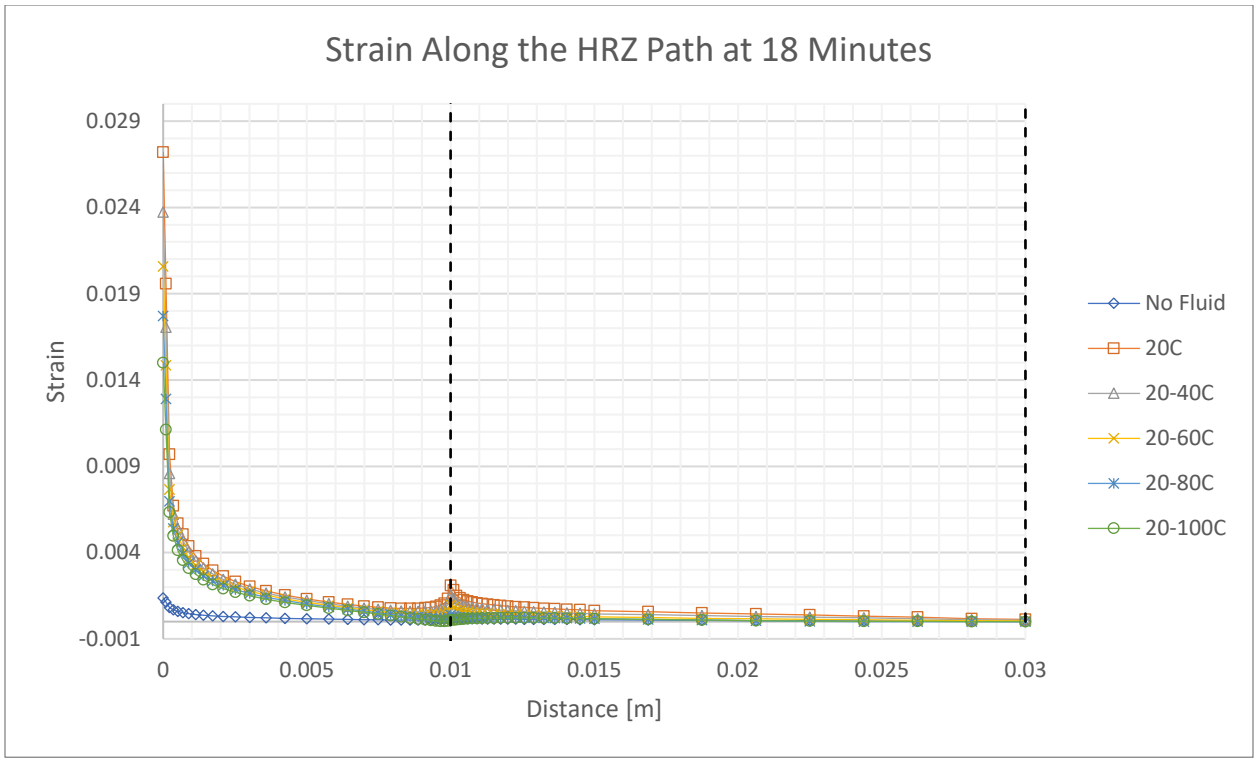

Figure 67: Strain along the HRZ path at 18 minutes

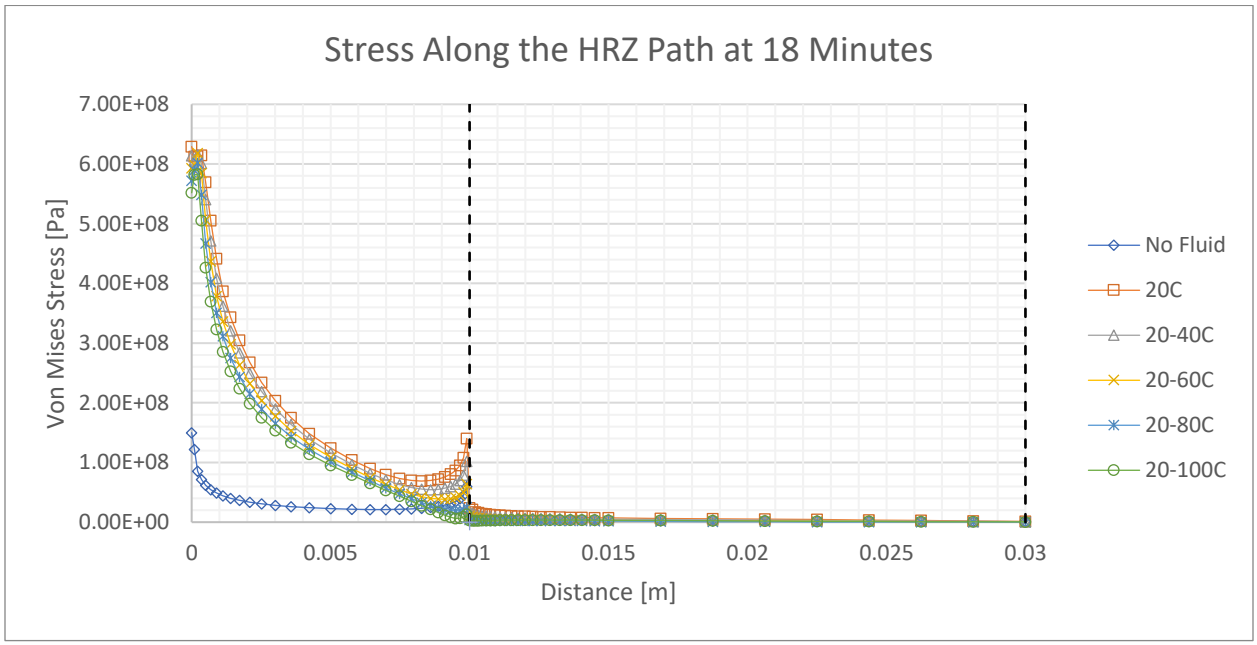

Figure 68: Stress along the HRZ path at 18 minutes

Comparing the fluid temperature being at 20°C and at 100°C the metal material experiences higher amounts of both stress and strain with lower temperature fluids, which varies

from the previously mentioned paths where the lower temperature fluid would experience a higher stress but smaller strain. Furthermore, it should be noted that the metal material experiences more stress and strain in comparison to the cement sheath, where there is a peak that has an immediate drastic drop-off once the metal material ends along the path.

CHAPTER V

CONCLUSION AND FUTURE WORKS

A thermos-mechanical heat transfer analysis was conducted using a commercial code, ABAQUS. An EGS well structure having an elevating temperature with the depth was modeled, and then the variations of stress and strain as working fluid were added. To accomplish this several loading and boundary conditions were considered for the numerical model. Firstly, the designed structure surface was given an encastre boundary condition to ensure that the outermost surface of the well was restricted in movement to represent contact with the subsurface. Next, a lateral earth pressure load was applied to the structure in the form of a linearly increasing distributed load. Additionally, a temperature condition was given to represent the subsurface geothermal heat gradient and well body temperature. To better understand the structure's response during operation, several parameter conditions to represent the fluid were considered. While the fluid pressure was consistent per scenario, different temperatures to represent the working fluid were chosen. One with no fluid present to represent the control group, another where the fluid was at a constant temperature of 20°C, and cases that consider if the fluid temperature increases linearly with depth where the maximum temperature was either 40, 60, 80, or 100°C. As a result, the following was observed.

From the fluid wall path across the well towards the subsurface, the overall amount of stress in the metal material is higher than the stress values of the cement sheath. Stress risers are observed at the interface between metal and concrete. The peak stress values are higher at the metal part of the interface than at the concrete part because of the different Young's modulus. In the

metal casing, there is a notable change in the slope of stress risers depending on the location of the material. If the casing string continues, the degree of stress concentration decreases in a relatively linear fashion along the thickness of the pipe. This behavior is not shared if the metal material is at the shoe/bottom of the casing. In this case, after the peak value experienced at the beginning of the metal casing, the stress decreases and then increases again as it approaches the casing's designated cement sheath. At the bottom of a casing, if the titanium is in direct contact with another surface, a high-stress concentration is likely to occur due to having differing modulus of elasticities than the surrounding material.

The variations in both the stress and strain are the results of the structure expanding due to temperature at different rates since the degrees of the stress concentrations increase with depth, i.e. increasing temperature and pressure approaching the subsurface target reservoir, and hydrostatic fluid pressure and temperature, for this model. When the metal material starts expanding at higher temperatures, it can cause the upper section of the well to increase in strain since the titanium isn't as deformed due to minimal temperature difference and is subjected to some tension. As a result, the well has a high stress concentration due to the high initial temperature because of the expansion of the different material layers pressing into each other, but since the material deforms more at the bottom of the well, and is nonuniform throughout the entirety of the structure, the stress and strain values start to adjust as the material deforms during the transient state for the middle-to-upper well regions. In the HRZ path, since the path is short, the material quickly deforms and approaches a steady state. The cooler temperature regions are towards the upper part of the structure, this zone is more isolated, it is less likely to experience stress variations than the IMO and IM regions experienced. However, the stress variations in the material over time need to be further investigated to determine the exact cause.

Overall, it is notable that, with just the presence of the fluid, both the temperature change and fluid pressure drastically increase the magnitudes of stress and strain, while the earth pressure constantly affects the structure. The larger the temperature difference between the fluid and the well body, the greater the stress and strain concentrations. Additionally, during the transient stage, the values would constantly change until reaching the steady state.

Further investigation should be considered when the fluid is removed from the structure, as there will be a new thermal equilibrium, possibly causing more stress. It is known already from previous literature that repeated thermal cycling in the model causes failure and fatigue in cement, and the observations from actual projects reported that it could be a potential reason for the metal casing ruptures/failures. On the other hand, the previous work investigating the metal casing ruptures reported that there was also a vast amount of mineral clogging and corrosion, but due to different circumstances such as toxic gases present, the exact cause of failure and severity were difficult to investigate. Furthermore, the cement investigation was done in the laboratory environment, and not on an actual project site. It would be beneficial to consider modeling the structure undergoing various thermal cycling at its effects on the well body structure with appropriate resources. Examples of future investigation topics include the effect of the periods of shut-off and operation times and changing the temperature of the working fluid after resuming the fluid injection. Previous literature has also suggested that using a higher reinjection temperature was beneficial in extracting heat in the target reservoir, and this study suggests that it could also be beneficial in the well integrity, which can in turn, help the project operate longer without frequently shutting off for maintenance or failing earlier than intended.

Additionally, since the metallic material and cement material transfer thermal energy throughout the well body, it is worth considering materials with different heat conductivity and

the thicknesses for the piping or cement mixtures and their responses to the thermal loading, which are not included in this study due to time limitations. The thickness and heat conductivity of the materials in either the metal casing or cement sheath could drastically affect the production cost of implementing the well and will be the major contributors to the cost of the project. The use of the real field data such as the temperature and earth pressure profiles would increase the accuracy of the future analysis. Additionally, since the type of material does play a role in the zonal isolation of the working fluid and the subsurface in both the temperature and material, optimizing this should be considered for future investigations. Considering different design choices in the intermediate and surface casing strings to address the stress concentrations at their shoe should also be investigated.

REFERENCES

Akbar, S., Fathianpour, N., & Al Khoury, R. (2016). A finite element model for high enthalpy two-phase flow in geothermal wellbores. *Renewable Energy*, *94*, 223-236. https://doi.org/https://doi.org/10.1016/j.renene.2016.03.034

Akerley, J., Robertson-Tait, A., Zemach, E., Spielman, P., & Drakos, P. S. (2019). Near-Field EGS: A Review and Comparison of the EGS Demonstration Projects at Desert Peak and Brady.

Ang, T.-Z., Salem, M., Kamarol, M., Das, H. S., Nazari, M. A., & Prabaharan, N. (2022). A comprehensive study of renewable energy sources: Classifications, challenges and suggestions. *Energy Strategy Reviews*, *43*, 100939. https://doi.org/https://doi.org/10.1016/j.esr.2022.100939

API. (2018). 5L, Line Pipe 46th Edition. In: American Petroleum Institute.

API. (2019). 5CT, Casing and Tubing 10th Edition. In: American Petroleum Institute.

Axelsson, G., Egilson, T., & Gylfadóttir, S. S. (2014). Modelling of temperature conditions near the bottom of well IDDP-1 in Krafla, Northeast Iceland [Article]. *Geothermics*, *49*, 49-57. https://doi.org/10.1016/j.geothermics.2013.05.003

Barbier, E. (2002). Geothermal energy technology and current status: an overview. *Renewable and Sustainable Energy Reviews*, *6*(1), 3-65. https://doi.org/https://doi.org/10.1016/S1364-0321(02)00002-3

Baujard, C., Rolin, P., Dalmais, É., Hehn, R., & Genter, A. (2021). Soultz-sous-Forêts Geothermal Reservoir: Structural Model Update and Thermo-Hydraulic Numerical Simulations Based on Three Years of Operation Data. *Geosciences*, *11*(12), 502. https://doi.org/10.3390/geosciences11120502

Benato, S., Hickman, S., Davatzes, N. C., Taron, J., Spielman, P., Elsworth, D., Majer, E. L., & Boyle, K. (2016). Conceptual model and numerical analysis of the Desert Peak EGS

project: Reservoir response to the shallow medium flow-rate hydraulic stimulation phase [Article]. *Geothermics*, *63*, 139-156. https://doi.org/10.1016/j.geothermics.2015.06.008

Blöcher, G., Reinsch, T., Henninges, J., Milsch, H., Regenspurg, S., Kummerow, J., Francke, H., Kranz, S., Saadat, A., Zimmermann, G., & Huenges, E. (2016). Hydraulic history and current state of the deep geothermal reservoir Grob Schonebeck [Article]. *Geothermics*, *63*, 27-43. https://doi.org/10.1016/j.geothermics.2015.07.008

Breede, K., Dzebisashvili, K., Liu, X., & Falcone, G. (2013). A systematic review of enhanced (or engineered) geothermal systems: past, present and future. *Geothermal Energy*, *1*(1), 4. https://doi.org/10.1186/2195-9706-1-4

Budiono, A., Suyitno, S., Rosyadi, I., Faishal, A., & Ilyas, A. X. (2022). A Systematic Review of the Design and Heat Transfer Performance of Enhanced Closed-Loop Geothermal Systems. *Energies*, *15*(3), 742. https://www.mdpi.com/1996-1073/15/3/742

Calvert, D. G., & Smith, D. K. (1990). API Oilwell Cementing Practices. *Journal of Petroleum Technology*, *42*(11), 1364-1373. https://doi.org/10.2118/20816-pa

Carter, J. P., & Cramer, S. D. (1992). Materials of construction for high-salinity geothermal brines [Report]. https://stacks.cdc.gov/view/cdc/10189 (Report of investigations (United States. Bureau of Mines) ; 9402)

Cladouhos, T. T., Petty, S., Swyer, M. W., Uddenberg, M. E., Grasso, K., & Nordin, Y. (2016). Results from Newberry Volcano EGS Demonstration, 2010-2014 [Article]. *Geothermics*, *63*, 44-61. https://doi.org/10.1016/j.geothermics.2015.08.009

Company, R. T. (2000). Titanium Alloy Guide. In.

Dincer, I., & Demir, M. E. (2018). 4.7 Gas Turbine Cycles. In I. Dincer (Ed.), *Comprehensive Energy Systems* (pp. 209-263). Elsevier. https://doi.org/https://doi.org/10.1016/B978-0-12-809597-3.00408-9

Finger, J. T., & Blankenship, D. A. (2012). *Handbook of Best Practices for Geothermal Drilling*. https://www.osti.gov/biblio/1325261 https://www.osti.gov/servlets/purl/1325261

Frick, S., Regenspurg, S., Kranz, S., Milsch, H., Saadat, A., Francke, H., Brandt, W., & Huenges, E. (2011). Geochemical and Process Engineering Challenges for Geothermal Power Generation [Review]. *Chemie Ingenieur Technik*, *83*(12), 2093-2104. https://doi.org/10.1002/cite.201100131

Friðleifsson, G. Ó., Elders, W. A., Zierenberg, R. A., Fowler, A. P. G., Weisenberger, T. B., Mesfin, K. G., Sigurðsson, Ó., Níelsson, S., Einarsson, G., Óskarsson, F., Guðnason, E. Á., Tulinius, H., Hokstad, K., Benoit, G., Nono, F., Loggia, D., Parat, F., Cichy, S. B., Escobedo, D., & Mainprice, D. (2020). The Iceland Deep Drilling Project at Reykjanes: Drilling into the root zone of a black smoker analog. *Journal of Volcanology and Geothermal Research*, *391*, 106435. https://doi.org/10.1016/j.jvolgeores.2018.08.013

Friðleifsson, G. Ó., Pálsson, B., Stefánsson, B., Albertsson, A., Gíslason, Þ., Gunnlaugsson, E., Thorsteinsson, H. H., Ketilsson, J., Sæther, S., Sörlie, C., Elders, W. A., & Zierenberg, R. A. (2021). *The IDDP Success Story - Highlights* World Geothermal Congress, https://www.geothermal-energy.org/pdf/WGC/papers/WGC/2020/37000.pdf

Garcia, J., Hartline, C., Walters, M., Wright, M., Rutqvist, J., Dobson, P. F., & Jeanne, P. (2016). The Northwest Geysers EGS Demonstration Project, California Part 1: Characterization and reservoir response to injection. *Geothermics*, *63*, 97-119. https://doi.org/10.1016/j.geothermics.2015.08.003

Gischig, V., & Preisig, G. (2015). *HYDRO-FRACTURING VERSUS HYDRO-SHEARING: A CRITICAL ASSESSMENT OF TWO DISTINCT RESERVOIR STIMULATION MECHANISMS*. https://doi.org/10.13140/RG.2.1.4924.3041

Gruben, G., Dillingh, B., Kaldal, G. S., Hoang, N.-H., Wollenweber, J., Rørvik, G., Thorbjornsson, I., & Nyhus, B. (2021). Thermo-mechanical tensile testing of geothermal casing materials. *Geothermics*, *89*, 101944. https://doi.org/https://doi.org/10.1016/j.geothermics.2020.101944

Häring, M. O., Schanz, U., Ladner, F., & Dyer, B. C. (2008). Characterisation of the Basel 1 enhanced geothermal system [Article]. *Geothermics*, *37*(5), 469-495. https://doi.org/10.1016/j.geothermics.2008.06.002

Hartline, C., Walters, M., Wright, M., Rawal, C., Garcia, J., & Farison, J. (2019). *The Northwest Geysers Enhanced Geothermal System Demonstration Project, The Geysers, California. Final Report*. https://dx.doi.org/10.2172/1523288

Hijriawan, M., Pambudi, N. A., Biddinika, M. K., Wijayanto, D. S., Kuncoro, I. W., Rudiyanto, B., & Wibowo, K. M. (2019). Organic Rankine Cycle (ORC) in geothermal power plants. *Journal of Physics: Conference Series*, *1402*(4), 044064. https://doi.org/10.1088/1742-6596/1402/4/044064

Hogarth, R., & Holl, H.-G. (2017). Lessons Learned from the Habanero EGS Project. *Geothermal Resources Council Transactions*, *41*, 865-877.

Huenges, E., Holl, H.-G., Bruhn, D., Brandt, W., Saadat, A., Moeck, I., & Zimmermann, G. (2007). Current state of the EGS project Groß Schönebeck-Drilling into deep sedimentary geothermal reservoirs. European Geothermal Congress-EGC (Unterhaching, Germany 2007),

Ikeuchi, K., Doi, N., Sakagawa, Y., Kamenosono, H., & Uchida, T. (1998). High-temperature measurements in well WD-1A and the thermal structure of the Kakkonda geothermal system, Japan [Article]. *Geothermics*, *27*(5-6), 591-+. https://doi.org/10.1016/s0375-6505(98)00035-2

Iverson, B., Maxson, J., & Bour, D. (2010). Strength Retrogression in Cements Under High-Temperature Conditions. 35th Workshop on Geothermal Reservoir Engineering,

Kaldal, G. S., Jonsson, M. T., Palsson, H., & Karlsdottir, S. N. (2015). Structural modeling of the casings in high temperature geothermal wells. *Geothermics*, *55*, 126-137. https://doi.org/https://doi.org/10.1016/j.geothermics.2015.02.003

Kaldal, G. S., Jonsson, M. T., Palsson, H., & Karlsdottir, S. N. (2016). Structural modeling of the casings in the IDDP-1 well: Load history analysis [Article]. *Geothermics*, *62*, 1-11. https://doi.org/10.1016/j.geothermics.2016.02.002

Kalousek, G. L., & Adams, M. Hydration Products Formed in Cement Pastes at 25 to 175 C. *ACI Journal Proceedings*, *48*(9). https://doi.org/10.14359/11872

Karlsdottir, S. N., Ragnarsdottir, K. R., Thorbjornsson, I. O., & Einarsson, A. (2015). Corrosion testing in superheated geothermal steam in Iceland. *Geothermics*, *53*, 281-290. https://doi.org/https://doi.org/10.1016/j.geothermics.2014.06.007

Kasai, K., Hishi, Y., Fukuda, D., Kato, O., Doi, N., Akaku, K., Ominato, T., & Tosha, T. (2000). The Fluid Geochemistry and Reservoir Model for the Kakkonda Geothermal System, Obtained by NEDO's Deep-Seated Geothermal Reservoir Survey, Japan. World Geothermal Congress, Kyushu - Tohoku, Japan.

Kaya, E., Zarrouk, S. J., & O'Sullivan, M. J. (2011). Reinjection in geothermal fields: A review of worldwide experience. *Renewable and Sustainable Energy Reviews*, *15*(1), 47-68. https://doi.org/https://doi.org/10.1016/j.rser.2010.07.032

Koelbel, T., & Genter, A. (2017). Enhanced Geothermal Systems: The Soultz-sous-Forêts Project. In (pp. 243-248). Springer International Publishing. https://doi.org/10.1007/978-3-319-45659-1_25

Krauss, G. (2017). 4 - Physical metallurgy of steels: An overview. In R. Rana & S. B. Singh (Eds.), *Automotive Steels* (pp. 95-111). Woodhead Publishing. https://doi.org/https://doi.org/10.1016/B978-0-08-100638-2.00004-3

Kruszewski, M., & Wittig, V. (2018). Review of failure modes in supercritical geothermal drilling projects. *Geothermal Energy*, *6*(1). https://doi.org/10.1186/s40517-018-0113-4

Kurnia, J. C., Shatri, M. S., Putra, Z. A., Zaini, J., Caesarendra, W., & Sasmito, A. P. (2022). Geothermal energy extraction using abandoned oil and gas wells: Techno-economic and policy review. *International Journal of Energy Research*, *46*(1), 28-60. https://doi.org/10.1002/er.6386

Laloui, L., & Rotta Loria, A. F. (2020). Chapter 1 - Energy and geotechnologies. In L. Laloui & A. F. Rotta Loria (Eds.), *Analysis and Design of Energy Geostructures* (pp. 3-23). Academic Press. https://doi.org/https://doi.org/10.1016/B978-0-12-816223-1.00001-1

Lamy-Chappuis, B., Yapparova, A., & Driesner, T. (2023). Simulations of the IDDP-2 well, Reykjanes, Iceland, and its behavior in different operation scenarios [Article]. *Geothermics*, *114*, 11, Article 102790. https://doi.org/10.1016/j.geothermics.2023.102790

Ledésert, B. A., Hébert, R. L., Mouchot, J., Bosia, C., Ravier, G., Seibel, O., Dalmais, É., Ledésert, M., Trullenque, G., Sengelen, X., & Genter, A. (2021). Scaling in a Geothermal Heat Exchanger at Soultz-Sous-Forêts (Upper Rhine Graben, France): A XRD and SEM-EDS Characterization of Sulfide Precipitates. *Geosciences*, *11*(7), 271. https://www.mdpi.com/2076-3263/11/7/271

Liu, X. (2020). An Overview of EGS Development and Management Suggestions. *Frontiers Research of Architecture and Engineering*, *3*, 6. https://doi.org/10.30564/frae.v3i3.2452

Lutz, S. J., Moore, J. N., Jones, C. G., Suemnicht, G. A., & Robertson-Tait, A. (2009). GEOLOGICAL AND STRUCTURAL RELATIONSHIPS IN THE DESERT PEAK GEOTHERMAL SYSTEM, NEVADA: IMPLICATIONS FOR EGS DEVELOPMENT. Thirty-Fourth Workshop on Geothermal Reservoir Engineering, Stanford University, Stanford, California.

MacDonald, W. D., & Grauman, J. S. (2018). Exposure Testing of UNS R53400, R56404 and N06625 in Simulated Salton Sea Geothermal Brine. CORROSION 2018,

MacDonald, W. D., & Grauman, J. S. (2019). Development of New Titanium Alloys for Use in Aggressive Geothermal Environments. CORROSION 2019,

Madhlopa, A. (2022). Chapter 5 - Characteristics of heat transfer media. In A. Madhlopa (Ed.), *Solar Receivers for Thermal Power Generation* (pp. 113-149). Academic Press. https://doi.org/https://doi.org/10.1016/B978-0-323-85271-5.00005-7

Marbun, B. T. H., Ridwan, R. H., Nugraha, H. S., Sinaga, S. Z., & Purbantanu, B. A. (2020). Casing setting depth and design of production well in water-dominated geothermal system with 330 °C reservoir temperature. *Energy Reports*, *6*, 582-593. https://doi.org/https://doi.org/10.1016/j.egyr.2020.02.013

Mills, T., & Humphreys, B. (2013). Habanero Pilot Project - Australia's First EGS Power Plant. 35th New Zealand Geothermal Workship: 2013 Proceedings, Rotorua, New Zealand.

Milsch, H., Spangenberg, E., Raab, S., Schepers, A., Blocher, G., Bruhn, D., Kristindottir, L., Flovenz, O., & Huenges, E. (2010). *Effects of Pressure, Temperature, Fluid-Rock Interactions, and Phase Changes on the Physical Properties of Geothermal Reservoir Rocks: The Experimental Perspective* World Geothermal Congress, Bali, Indonesia.

Moska, R., Labus, K., & Kasza, P. (2021). Hydraulic Fracturing in Enhanced Geothermal Systems-Field, Tectonic and Rock Mechanics Conditions-A Review. *Energies*, *14*(18). https://doi.org/ARTN 5725 10.3390/en14185725

Muela Maya, S., García-Gil, A., Garrido Schneider, E., Mejías Moreno, M., Epting, J., Vázquez-Suñé, E., Marazuela, M. Á., & Sánchez-Navarro, J. Á. (2018). An upscaling procedure for the optimal implementation of open-loop geothermal energy systems into hydrogeological models. *Journal of Hydrology*, *563*, 155-166. https://doi.org/https://doi.org/10.1016/j.jhydrol.2018.05.057

Muraoka, H., Asanuma, H., Tsuchiya, N., Ito, T., Mogi, T., & Ito, H. (2014). The Japan Beyond-Brittle Project. *Scientific Drilling*, *17*, 51-59. https://doi.org/10.5194/sd-17-51-2014

Olasolo, P., Juárez, M. C., Morales, M. P., D'Amico, S., & Liarte, I. A. (2016). Enhanced geothermal systems (EGS): A review. *Renewable & Sustainable Energy Reviews*, *56*, 133-144. https://doi.org/10.1016/j.rser.2015.11.031

Pálsson, B., Hólmgeirsson, S., Gudmundsson, A., Bóasson, H. A., Ingason, K., Sverrisson, H., & Thórhallsson, S. (2014). Drilling of the well IDDP-1 [Article]. *Geothermics*, *49*, 23-30. https://doi.org/10.1016/j.geothermics.2013.08.010

Pang, X., Qin, J., Sun, L., Zhang, G., & Wang, H. (2021). Long-term strength retrogression of silica-enriched oil well cement: A comprehensive multi-approach analysis. *Cement and*

Concrete Research, *144*, 106424. https://doi.org/https://doi.org/10.1016/j.cemconres.2021.106424

Pernites, R. B., & Santra, A. K. (2016). Portland cement solutions for ultra-high temperature wellbore applications [Article]. *Cement & Concrete Composites*, *72*, 89-103. https://doi.org/10.1016/j.cemconcomp.2016.05.018

Potter, R. M., Robinson, E. S., & Smith, M. C. (1974). *Method of extracting heat from dry geothermal reservoirs* (United States Patent No. https://www.osti.gov/biblio/4304847

Pyatina, T., & Sugama, T. (2018). Cements for High-Temperature Geothermal Wells. In H. M. Saleh & R. O. A. Rahman (Eds.), *Cement Based Materials*. InTech. https://doi.org/10.5772/intechopen.74108

Rutqvist, J., Jeanne, P., Dobson, P. F., Garcia, J., Hartline, C., Hutchings, L., Singh, A., Vasco, D. W., & Walters, M. (2016). The Northwest Geysers EGS Demonstration Project, California - Part 2: Modeling and interpretation. *Geothermics*, *63*, 120-138. https://doi.org/10.1016/j.geothermics.2015.08.002

Sakuma, S., Naganawa, S., Sato, T., Ito, T., & Yoshida, Y. (2021). Evaluation of High-Temperature Well Cement for Supercritical Geothermal Drilling. *Geothermal Resources Council Transactions*, *45*, 268-283.

Silva, J. C., & Milestone, N. B. (2018a). Cement/rock interaction in geothermal wells. The effect of silica addition to the cement and the impact of CO enriched brine. *Geothermics*, *73*, 16-31. https://doi.org/10.1016/j.geothermics.2018.01.004

Silva, J. C., & Milestone, N. B. (2018b). Cement/rock interaction in geothermal wells. The effect of silica addition to the cement and the impact of CO₂ enriched brine. *Geothermics*, *73*, 16-31. https://doi.org/10.1016/j.geothermics.2018.01.004

Smith, M. (2023). *Oil and Gas Technology and Geothermal Energy Development* (R47405). C. R. Service.

Stefánsson, A., Friðleifsson, G. Ó., Sigurðsson, Ó., & Gíslason, Þ. (2021). The IDDP-2 DEEPEGS Drilling Experience and Lesson Learned. World Geothermal Congress, Reykjavik, Iceland.

Stober, I., & Bucher, K. (2013). Geothermal energy. *Germany: Springer-Verlag Berlin Heidelberg. doi*, *10*, 978-973.

Stober, I., Ladner, F., Hofer, M., & Bucher, K. (2022). The deep Basel-1 geothermal well: an attempt assessing the predrilling hydraulic and hydrochemical conditions in the basement of the Upper Rhine Graben. *Swiss Journal of Geosciences*, *115*(1). https://doi.org/10.1186/s00015-021-00403-8

Sugama, T., & Pyatina, T. (2022). Cement Fomulations for Super-Critical Geothermal Wells. Workshop on Geothermal Reservoir Engineering, Standford University, Standford, California.

Suzuki, Y., Akatsuka, T., Yamaya, Y., Watanabe, N., Okamoto, K., Osato, K., Kajiwara, T., Ogawa, Y., Mogi, T., Tsuchiya, N., & Asanuma, H. (2022). Estimation of an ultra-high-temperature geothermal reservoir model in the Kakkonda geothermal field, northeastern Japan [Article]. *Geothermics*, *105*, 18, Article 102525. https://doi.org/10.1016/j.geothermics.2022.102525

Sveinbjornsson, B. M., & Thorhallsson, S. (2014). Drilling performance, injectivity and productivity of geothermal wells. *Geothermics*, *50*, 76-84. https://doi.org/https://doi.org/10.1016/j.geothermics.2013.08.011

Swayze, M. (1954). Effects of high pressures and temperatures on strength of oil-well cements. *Drilling and Production Practice*, 72.

Tayactac, R. G., & Manuel, M. C. (2022). *Understanding Material Selection Challenges in Geothermal Well and Systematic Qualification Approach* IOP Conderence Series: Earth and Environmental Science, https://dx.doi.org/10.1088/1755-1315/1046

Teodoriu, C. (2013). Why and When does Casing Fail in Geothermal Wells [Article]. *Oil Gas-European Magazine*, *39*(1), 38-40. <Go to ISI>://WOS:000318193100012

Thomas, R. (2003). Titanium in the geothermal industry. *Geothermics*, *32*(4), 679-687. https://doi.org/https://doi.org/10.1016/j.geothermics.2003.08.004

Thorbjornsson, I. O., Kaldal, G. S., Krogh, B. C., Palsson, B., Markusson, S. H., Sigurdsson, P., Einarsson, A., Gunnarsson, B. S., & Jonsson, S. S. (2020). Materials investigation of the high temperature IDDP-1 wellhead [Article]. *Geothermics*, *87*, 15, Article 101866. https://doi.org/10.1016/j.geothermics.2020.101866

Thórhallsson, S., Pálsson, B., Hólmgeirsson, S., Ingason, K., Matthíasson, M., Bóasson, H. A., & Sverrisson, H. (2014). Well design for the Iceland Deep Drilling Project (IDDP) [Article]. *Geothermics*, *49*, 16-22. https://doi.org/10.1016/j.geothermics.2013.08.004

Verma, M. P. (1997). Thermodynamic classification of vapor and liquid dominated reservoir and fluid geochemical parameter calculations. *Geofísica Internacional*, *36*(3), 181-189. https://doi.org/10.22201/igeof.00167169p.1997.36.3.643

Wolterbeek, T. K. T., & Hangx, S. J. T. (2023). The thermal properties of set Portland cements – a literature review in the context of CO2 injection well integrity. *International Journal of Greenhouse Gas Control*, *126*, 103909. https://doi.org/https://doi.org/10.1016/j.ijggc.2023.103909

Wood, P. (2017). *Corrosion review and Materials Selection for Geothermal Wells*.

Xu, C. S., Dowd, P., & Li, Q. (2016). Carbon sequestration potential of the Habanero reservoir when carbon dioxide is used as the heat exchange fluid. *Journal of Rock Mechanics and Geotechnical Engineering*, *8*(1), 50-59. https://doi.org/10.1016/j.jrmge.2015.05.003

Xu, H., Peng, N., Ma, T., & Yang, B. (2018). Investigation of Thermal Stress of Cement Sheath for Geothermal Wells during Fracturing. *Energies*, *11*(10), 2581. https://doi.org/10.3390/en11102581

Yuan, W., Chen, Z., Grasby, S. E., & Little, E. (2021). Closed-loop geothermal energy recovery from deep high enthalpy systems. *Renewable Energy*, *177*, 976-991. https://doi.org/https://doi.org/10.1016/j.renene.2021.06.028

Zarrouk, S. J., & McLean, K. (2019). Chapter 2 - Geothermal systems. In S. J. Zarrouk & K. McLean (Eds.), *Geothermal Well Test Analysis* (pp. 13-38). Academic Press. https://doi.org/10.1016/B978-0-12-814946-1.00002-5

Zealand, S. N. (2015). Code of practice for deep geothermal wells. In *NZS* (Vol. 2403, pp. 116).

Zemach, E., Drakos, P., Spielman, P., & Akerley, J. (2013). *Desert Peak East Enhanced Geothermal Systems (EGS) Project*. https://dx.doi.org/10.2172/1373310

Zeng, Y. C., Su, Z., & Wu, N. Y. (2013). Numerical simulation of heat production potential from hot dry rock by water circulating through two horizontal wells at Desert Peak geothermal field [Article]. *Energy*, *56*, 92-107. https://doi.org/10.1016/j.energy.2013.04.055

Zheng, J., Li, P., Dou, B., Fan, T., Tian, H., & Lai, X. T. (2022). Impact research of well layout schemes and fracture parameters on heat production performance of enhanced geothermal system considering water cooling effect [Article]. *Energy*, *255*, 17, Article 124496. https://doi.org/10.1016/j.energy.2022.124496

Zheng, S., Li, S. B., & Zhang, D. X. (2021). Fluid and heat flow in enhanced geothermal systems considering fracture geometrical and topological complexities: An extended embedded discrete fracture model [Article]. *Renewable Energy*, *179*, 163-178. https://doi.org/10.1016/j.renene.2021.06.127

Zhiliang, H., Zhang, Y., Feng, J., Ding, Q., & Pengwei, L. (2018). An EGS Site Evaluation Method for Geothermal Resources Based on Geology , Engineering and Economic Considerations.

VITA

John Alfred Ganal Acevedo was a master's student at the University of Texas at Rio Grande Valley. He obtained a bachelor's degree from this university in May 2022 and will have his master's as of August 2024, both of which were in Civil Engineering. He plans on taking the Material Sciences and Engineering PhD Program during the fall 2024 semester at the University of Texas at Rio Grande Valley. If there are any questions or concerns the author can be reached at johnalfred.acevedo01@utrgv.edu and at john.alfredacevedo@hotmail.com.